University of Alberta

Influence of Bubble Size on an Effervescent Atomization

by

Johana Gomez I.

A thesis submitted to the Faculty of Graduate Studies and Research
in partial fulfillment of the requirements for the degree of

Master of Science

Department of Mechanical Engineering

Fall 2010
Edmonton, Alberta

Examining Committee

Dr. Brian A. Fleck, Mechanical Engineering

Dr. Jason Olfert , Mechanical Engineering

Dr. David Nobes , Mechanical Engineering

Dr. Sean Sanders, Chemical and Materials Engineering

To my parents and ”mi hermanita”

Abstract

An experimental investigation was performed to study the influence of the bubble size on an effervescent atomization. Experiments were conducted in horizontal facility using water and air as the working fluids, which were premixed to create a two-phase flow before entering a horizontal feeding conduit, with a 25.4 mm diameter. Then, the mixture was sprayed through an effervescent nozzle. Water flow rates from 113 to 189 kg/min and air to liquid mass ratios from 1 % to 4 % were selected. High speed photographs, of the bubbles in the feeding conduit and of the resulting droplets on the spray, were taken to use the particle projected areas to estimate their sizes.

A small portion of the feeding pipe was replaced with a transparent conduit to acquired images of the images of the two-phase flow. Shadowgraphy, an imaged-based technique, was employed to determine the droplet sizes, droplet size distributions, centricity and velocity of the resulting droplets.

A characterization of the spray was done to investigate the behavior and evolution in the near field region, select a representative control volume and finally correlate the size between bubbles in the feeding conduit and the atomized droplets. Measurements were done at different locations along the axial and radial directions of the spray and their droplet size distribution analyzed. An impact probe was used to find the location with maximum momentum defined as the control volume most representative of the

spray.

A bubble breaker was installed in the feed conduit to mechanically change the bubble size. The observed bubble size was reduced as a consequence of the insertion of the bubble breakers. A droplet size reduction was also observed.

A monotonic positive correlation was found between the size of the bubbles in the flow upstream and the droplet size in the spray, in a fairly narrow range of feed flow void fractions. A bubble size sensitivity parameter was defined. Knowledge of the droplet behavior in the spray provides data to enhance the design and operating conditions of the atomization process and a means to control droplet size.

Acknowledgements

I would like to express my sincere gratitude to my supervisor Dr. Brian Fleck for giving me the opportunity to work in this research project. Thanks for the supervision, encouragement and support provided during this investigation. I would also like to thank Dr. Jason Olfert for his support, guidance and valuable suggestions.

I would like to manifest my gratitude to the staff at the Syncrude Canada - Edmonton Research Centre, Jennifer McMillan and Eb Mueller, for the opportunity work in the facility and their willingness to help me when I approached to them. Special thanks to Doug Appelt for his significant support, technical expertise, discussions, ideas and time during the different stages of this research. Thanks Doug!

The financial support from the Syncrude, Department of Mechanical Engineering and NSREC is also gratefully acknowledge.

Finally, I would like to thank my family and friend whose unconditional support, positive attitude and encouragement helped me through all this program.

Table of Contents

List of Tables

List of Figures

List of Symbols

A	Area [m^2]
d	Nozzle exit diameter [m]
D	Particle diameter [m]
D_{32}	Sauter mean diameter [μm]
$D_{32,\mathrm{B}}$	Bubble Sauter mean Diameter [μm]
$D_{32,\mathrm{D}}$	Droplet Bubble Sauter mean Diameter [μm]
g	gravitational acceleration [m/s^2]
N	Experimental sample number
P	Pressure [kPa]
P_D	Delivery pressure [kPa]
Q	Flow rate [kg/min]
r	Radial coordinate [cm]
S	Standard Deviation
U	Velocity of the flow [m/s]
U^{S}	Superficial velocity [m/s]
V	Velocity of the droplet [m/s]
$\widetilde{V}$	Volume of the particle
We	Weber number
x	Axial coordinate [cm]

Subscripts

ave	Average
B	Bubbles

c	Continuos
$crit$	Critic
D	Droplets
d	Dispersed
g	Geometric
G	Gas
i	Injection
L	Liquid
m	Mixture
max	Maximun
min	Minimum

Greek Letters

α	Void fraction
Δt	Time interval
γ	Air liquid ratio [%]
σ	Standard deviation of a population
Φ	Bubble size sensitivity

Abbreviations

ALR	Air to liquid mass ratio
GLR	Gas to liquid mass ratio
SMD	Sauter mean diameter

Chapter 1

Introduction

1.1 Introduction and background

Atomization is used in a wide range of industrial applications such as combustion, gasification, evaporative cooling and agriculture. For instance, atomization is used in the fluid cooking process where bitumen is sprayed with the assistance of an atomizing steam to thermally convert it into lighter products and coke. Therefore, it is essential to have a good understanding of the variables that affect the atomization process in order to operate the system with a high bitumen recovery. Particularly, for effervescent atomization the quality of the spray has been reported to be principally a function of two parameters: the inlet pressure and amount of gas injected [Lefebvre, 1989]. However the influence of other parameters such as the bubble size, bubble distribution and bubble concentration in the mixture upstream of the nozzle has not been covered in the literature.

1.1.1 Atomization in the Fluid Coking process

Petroleum produced from oil sands must be upgraded to extract usable products. One upgrading technology is to process the bitumen in a fluidized bed coker, where bitumen together with steam are heated to obtain low-boiling petroleum products. It has been well established that the efficiency of the coking process is a function of the heat transfer between the fluidized bed of hot coke particles to the bitumen [Lefebvre, 1989; Baukal, 2001; Babisnky and Sojka, 2002]. An enhancement to the heat transfer process is produced by increasing the surface area of the bitumen, which means transforming the bitumen into small diameter droplets, augmenting their contact to a large number of coke particles. As a consequence, the resulting liquid products are maximized and undesired by-products minimized. On the other hand, if a nozzle is not operating properly, atomizing only a portion of the liquid phase, the contact between the sprayed droplets and fluidized particles will be poor, obtaining less liquid products, and potentially creating large agglomerates.

Among all types of atomizers, effervescent atomizers are used because of their ability to produce good atomization with a relatively small droplet size at a relatively low injection pressure [Lefebvre, 1989]. In this atomization process, an atomizing gas is injected into the liquid upstream of the nozzle to form a two-phase flow in the feeding conduit. The atomization is enhanced by the rapid expansion of bubbles at the nozzle exit that shatter the liquid stream into ligaments and then into droplets.

Many parameters are involved in the atomization analysis to obtain a uniform spray with droplets within a desired size range. It has been well established that the mixture upstream of the nozzle, a two-phase flow, affects the spray quality and with it the efficiency of the process [Whitlow and Lefebvre, 1993; Tafreshi et al., 2002]. Depending on the phase flow rates, different flow patterns might appear at the nozzle inlet and as a consequence create some unsteady fluctuation in the spray quality. It is thought that the dispersed bubble flow, characterized by small roughly spherical bubbles, tends to generate a more uniform spray with a nearly constant droplet size [Sovani, 2001]. Bubbles expand rapidly because of the pressure drop, shattering the liquid phase in droplets. However, when an intermittent flow is feeding the nozzle, with a variation in time of the gas to liquid mass ratio, the liquid may also break by gas slugs, and a pulsated spray is produced with a wide droplet size distribution [Maldonado, 2006]. Though flow regime has been shown to influence atomization, the bubble size has not been conclusively shown to influence droplet size in the spray. Bubble size of the dispersed phase in the feeding conduit appears to be a parameter that influences the atomization process.

In summary, the efficiency of the coking process depends on proper atomization. This is subject to the characteristics of the mixture flowing upstream of the nozzle. The scope of this project is limited to determine the influence of the bubble size in the two-phase flow entering the nozzle in effervescent atomization, particularly the droplet size and droplet size distribution.

1.1.2 Objectives of the thesis

The main objective of this thesis is to investigate the influence of the bubble size in the upstream flow on the droplets produced through an effervescent nozzle in an horizontal conduit. Bubble distributions were altered by installing a bubble breaker, a plate with perforated holes, to change their size and radial distribution. Specific objectives were established to have a better understanding of the atomizing process and techniques available for sizing particles:

- Characterization of the spray. Establish a methodology to investigate the evolution of the spray in a near field area. This process should include the definition of parameters and the appropriate control volume which represents the whole spray.

- Bubble sizing. Experimentally evaluate different schemes to visualize and measure bubble size in the flow.

- Alteration of the bubble size. Design and experimentally evaluate a system or accessories to influence the bubble size in the feeding conduit. This design should be simple to install and work at similar operating conditions for comparison purposes.

- Characterize droplet size as a function of the bubble size for the different configurations. For this, establish as the standard configuration the assembly without any alteration of the bubble size and compare the data with the results for the modified configurations.

This project is designed to provide information about the influence of bubble size distribution on the atomization. Chapter 2 introduces fundamental definitions used in this study including superficial velocity, size distributions, and type of flows. Chapter 3 covers the experimental set up and the procedure followed to run experiments. Chapter 4 addresses the characterization of the spray and discussion of a representative sample. The bubble analysis and the influence of the bubble breakers on bubble size and pressure measured are covered in Chapter 5. Chapter 6, the final chapter in the thesis, summarizes the conclusions and recommendations. The appendix shows detailed information of the operating conditions used, drawings of the components, settings used in the software and the regression analysis done between droplet size and the dependent variables such as bubble size.

References

Babisnky, E. and Sojka, P. (2002). Modeling drop size distribution. *Progress in Energy and Combustion Science*, 28:303–329.

Baukal, C. (2001). *The John Zink Combustion Handbook*. CRC Press.

Lefebvre, A. H. (1989). *Atomization and Sprays*. Hemisphere.

Maldonado, S. (2006). Improving the stability of gas-liquid spray. Master's thesis, University of Alberta.

Sovani, S. D. (2001). High pressure gas-liquid flow inside an effervescent diesel injector ans its effect on spray characteristics. Master's thesis, Purdue University.

Tafreshi, Z. M., Kirpalani, D., Bennett, A., and McCracken, T. W. (2002). Improving the efficiency of fluid cokers by altering two-phase feed characteristics. *Powder Technology*, 125(2-3):234–241.

Whitlow, J. D. and Lefebvre, A. H. (1993). Effervescent atomizer operation and spray characteristics. *Atomization and Sprays*, 3:137–155.

Chapter 2

Atomization of a Two-phase Flow in Horizontal Pipes

The pattern of the upstream two-phase flow has a major influence in the atomization process. Different flow patterns upstream of the nozzle generate sprays with different characteristics [Sovani, 2001]. Operationally, it has been found that annular flow is the most desirable flow pattern to obtain small droplets, though this requires high gas rates that may not always be possible or desirable in industrial facilities.

The dispersed bubble flow pattern, with a uniform distribution of smaller near-circular shaped bubbles in the flow appears to enhance the atomization process downstream, compared to slug flow pattern, with the explosion of a larger number of bubbles shattering the liquid phase. In this section some of the fundamental definitions of the two-phase flow, flow patterns and atomization are presented.

2.1 Fundamentals definitions in a two phase flow

In this study, several flow patterns are discussed. Before continuing certain terminology is introduced for a better understanding of the terms used in this work.

2.1.1 Void fraction

Void fraction, α, of the dispersed phase refers to the portion of the pipe cross-section occupied by the phase. In a gas-liquid flow, the gas void fraction is defined by the expression:

$$\alpha_{\mathrm{G}} = \frac{A_{\mathrm{G}}}{A} \tag{2.1}$$

Where A_{G} is the cross-sectional area occupied by the gas phase and A is the cross sectional area of the pipe. For the continuous phase, usually a liquid, the void fraction commonly is named liquid hold up, α_{L}. By definition, the sum of all void fractions must be one.

$$\alpha_{\mathrm{G}} + \alpha_{\mathrm{L}} = 1 \tag{2.2}$$

For the homogeneous case, where the velocity of the phases are assumed to be same (no-slip condition), the void fraction is estimated by:

$$\alpha_{\mathrm{HOM}} = \frac{Q_{\mathrm{G}}}{Q_{\mathrm{G}} + Q_{\mathrm{L}}} \tag{2.3}$$

where Q_{G} and Q_{L} are the volumetric flow rates of the gas and liquid, respectively.

The homogenous model is usually used for the dispersed bubbles flow [Andreussi et al. (1999)].

2.1.2 Phase and superficial velocities

For multiphase flow in a pipe, the phase velocity is the actual velocity of the phase moving through the pipe cross-sectional area occupied by it. Meanwhile, the superficial velocity refers to the velocity of the fluid as if it was the only fluid presented in the entire pipe cross sectional area, A.

To obtain the phase velocity of the gas, U_{G}, and the phase velocity of the liquid, U_{L}, the following expressions are used:

$$U_{\mathrm{G}} = \frac{Q_{\mathrm{G}}}{A_{\mathrm{G}}} \tag{2.4}$$

$$U_{\mathrm{L}} = \frac{Q_{\mathrm{L}}}{A_{\mathrm{L}}} \tag{2.5}$$

Where A_G is the area occupied by the gas phase, A_{L} the area of the liquid phase, Q_{G} and Q_{L} are the volumetric flow rates of the gas and liquid, respectively.

Gas superficial velocity, $U_{\mathrm{G}}^{\mathrm{S}}$, and liquid superficial velocity, $U_{\mathrm{L}}^{\mathrm{S}}$, are given by:

$$U_{\mathrm{G}}^{\mathrm{S}} = \frac{Q_{\mathrm{G}}}{A} \tag{2.6}$$

$$U_{\mathrm{L}}^{\mathrm{S}} = \frac{Q_{\mathrm{L}}}{A} \tag{2.7}$$

2.1.3 Gas to liquid mass ratio

The gas to liquid mass ratio (GLR) refers to the ratio of the gas to the liquid mass flow, according to:

$$\mathrm{GLR} = \frac{\dot{m}_{\mathrm{G}}}{\dot{m}_{\mathrm{L}}} \tag{2.8}$$

where $\dot{m}_{\mathrm{G}}$ and $\dot{m}_{\mathrm{L}}$ are the mass flow rates of gas and liquid, respectively. If air is the gas phase this parameter is known as air to liquid mass ratio (γ).

2.2 Two phase flow in horizontal pipe

Two-phase flow in a circular pipe is common in many engineering processes and industrial applications, such as petroleum production where gas and liquid are the predominant phases involved. Understanding the operation of a two-phase flow system, to optimize the performance and increase its efficiency, is only possible through the comprehension of the flow patterns and its mechanism for transition.

The establishment of a particular flow pattern is a function of several parameters of the flow such as superficial and actual velocities, void fraction, interaction of gravitational, inertial and surface tension forces, properties of the fluids involved and the characteristics of the pipe. Several flow pattern maps have been proposed in the last decades to help readers predict the flow regime given some characteristics of the flows involved. One of the pioneers of two-phase flow pattern map for horizontal pipes is O. Baker, who developed empirical flow map for small tubes, [Baker, 1954]. The flow pattern could be predicted knowing the flow rates and the fluid properties of each phase in the pipe. Gregory et al. (1974) suggested the use of the phase superficial velocities of the phases as the parameters for comparison. The use of these parameters, as the axis for a two dimensional plot to depict the data acquired experimentally, was also reported by other researchers [Mandhane et al., 1974; Taitel and Dukler, 1976].

Most of the literature reports experimental observations for vertical flow, based on the model developed by Barnea et al. (1980). However, for horizontal multiphase flow several authors have proposed different designations for the patterns observed. The model proposed by Taitel and Dukler (1976) has been validated by other researchers [Barnea et al., 1980] and presently it has become a standard map in the oil and gas industry. Based on that, this model was selected in this study to determine the regime flow of the experimental conditions.

Taitel and Dukler (1976) suggested and explained five flow regimes that are: Smooth Stratified (SS), Wavy stratified (WS), Intermittent (I), Annular Dispersed (AD) and Dispersed bubble (DB). Barnea et al., 1980 grouped the SS and WS flows in the Stratified flow (S) for their four basic horizontal flow patterns.

In a horizontal pipe, the S pattern flow is found at relatively low superficial liquid and gas velocities. A complete separation of the two phases occurs, with the liquid flowing at the bottom of the pipe and gas above it, separated by an undisturbed horizontal interface. This represents one of the principal characteristics of this pattern.

An increase of the gas flow generates a slug flow with the liquid been pushed by the gas accompanied by a high pressure drop, with the front of the slug creating a highly turbulent mixing zone with a high void fraction. Increasing the liquid velocity causes the waves to grow resulting in intermittent plugs of liquid flowing between gas pockets, which it is known as I pattern.

At high gas velocities the AD is observed. It is characterized by liquid film flowing along the pipe wall with the gas core in the central, with the presence of droplets entrained in it. The transition from I to AD was revised by Barnea et al. (1980).

DB is characterized by the distribution of the gas phase as discrete bubbles within the continuous liquid phase. DB occurs at relatively high liquid flow rates causing the bubbles, located at the top of the pipe during the transition, to relocate more uniformly in the cross section of the pipe.

In a vertical or inclined pipe different transitions occur with an increase in the velocity of any phase due to the gravitational force. Gravity plays an important role in the resulting pressure drop, which also depends on the direction of the flow, upward or downward.

In this study, according to the definitions given by Taitel and Dukler (1976), two flow patterns are encountered: dispersed bubble and intermittent. As it was mentioned before, flow pattern maps use superficial velocities as coordinates. Thus, the transition lines strongly depend on the pipe diameter, working pressure and fluid properties. Figure 2.1 shows the transition lines for intermittent, dispersed bubble and annular flow regimes according to the work proposed by Taitel and Dukler (1976) for different working pressures.

2.3 Bubbles in horizontal pipes

In addition to the complexity of the analysis of the two-phase flow in a horizontal pipe, the analysis of the DB flow pattern adds the presence of the bubbles and the interaction between them. This affects the mixture pressure, velocity and turbulence structure of the flow. Usually two processes are dominant and determine the bubble size distribution: coalescence and breakup. A local dynamic equilibrium between these two phenomena is found for a long residence time of the bubbles [Liu and Li, 1999; Razzaque et al., 2003].

The equilibrium is limited by two diameters; a minimum diameter, $D_{\min}$ and a maximum diameter, $D_{\max}$. Breakup occurs for bubbles with diameter larger than $D_{\max}$; meanwhile coalescence occurs for bubbles with diameter smaller than $D_{\min}$. In the latter process, the liquid film trapped between two colliding bubbles drains out and

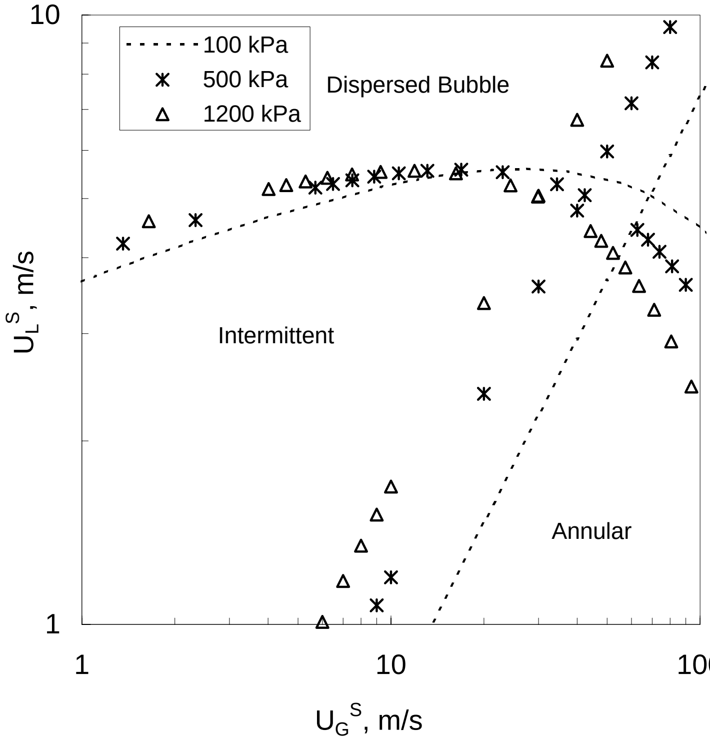

Figure 2.1: Flow patterns transition map based on the work proposed by Taitel and Dukler [Taitel and Dukler, 1976] for water-air, pipe diameter 2.54 cm, 20°C and different working pressures

ruptures; it usually plays a predominant role when the liquid velocity is small and there are not enough shear forces to produce the breakup.

Limited data are available about the characteristics of the bubbles in a horizontal multiphase flow. Experimental investigations of the size, shape and velocity of the bubbles in the flow mainly refer to vertical flow, where the gravity effects influence the flow pattern, pressure drop and void fraction. Other works are focused on a single bubble, where there is no interaction between bubbles.

Most of the literature published about predicting bubble size is based on the models suggested by Kolmogorof (1949) and then adopted by Hinze (1955) as reported by Andreussi et al. (1999). This model proposed that the breakup of the bubbles occurs when the Weber number, We, is larger than a critical value. We is a dimensionless number which is the ratio of the momentum forces of the fluid compared to its surface tension as shown in Eq. (2.9), where ρ_d is the dispersed gas density, ΔU is the relative gas-liquid velocity, ϕ is the characteristic dimension and σ is the surface stress coefficient.

$$\text{We} = \frac{\rho_d \Delta U \phi}{\sigma} \tag{2.9}$$

For the breakup process, the critical Weber number, We_{crit}, is usually defined according to the Eq. (2.10).

$$\text{We} = \frac{\tau_c}{\sigma / D_{\text{max}}} \tag{2.10}$$

where τ_c is the shear stress acting on the bubble and D_{max} the maximum bubble size. Levich, 1962 suggested a critical Weber number, $\text{We}^*_{\text{crit}}$, based on the balance between the internal pressure force and the surface force, considering the densities of the phases involved.

$$\text{We}^*_{\text{crit}} = \frac{\tau_c}{\sigma / D_{\text{max}}} \Big(\frac{\rho_d}{\rho_c}\Big)^{1/3} \tag{2.11}$$

where ρ_c is the density of the continuous phase. Combining Eq. (2.10) and Eq. (2.11) Hesketh et al. (1987) suggested the following two equations to estimate D_{max}. A bubble with a diameter larger than D_{max}, exceeds the We_{crit} and tends to break up.

$$D_{\text{max}} = \Big(\frac{\text{We}_{\text{crit}}}{2}\Big)^{0.6} \Big(\frac{\sigma}{\rho_c}\Big)^{0.6} \epsilon^{-0.4} \tag{2.12}$$

$$D_{\text{max}} = \Big(\frac{\text{We}^*_{\text{crit}}}{2}\Big)^{0.6} \Big(\frac{\sigma^{0.6}}{(\rho_c^2 \rho_d)^{0.2}}\Big)^{0.6} \epsilon^{-0.4} \tag{2.13}$$

Where D_{max} is the maximum possible diameter of a bubble in a turbulent flow field; σ is the interfacial tension, ρ_c density of the continuous phase, ρ_d is dispersed phase density and τ is the shear stress on the bubble caused by the turbulence of the continuous phase. The variable ε is the energy dissipation rate defined by Hinze (1955) as a function of the density of the mixture, ρ_{m}, and the velocity of the mixture U_{m}, according to the following expression:

$$\varepsilon = \Big(\frac{dP}{dx}\Big) \frac{U_{\text{m}}}{\rho_{\text{m}}} \tag{2.14}$$

Besides the consideration of the bubble size, coalescence and breakups, a horizontal two-phase flow analysis must also consider the concentration or distribution of the bubbles across a sectional area of the pipe or void fraction. In horizontal flows, bubbles tend to migrate to the upper wall because of the density difference. However, at high gas rates bubbles tend to relocate to the centreline. Thus, different flow patterns have different void fraction radial distributions.

For slug flow, Andreussi et al. (1999) reported mean radial void profile in a cylindrical pipe with inner diameter 53 mm. The measurements were done with a probe located at different vertical positions along the diameter. At low gas superficial velocity ($U_G^S = 2.0$ and 4.0 m/s) the void fraction increases in the radial direction with a maximum value near the upper wall pipe, indicating bubbles tends to migrate to the ceiling; meanwhile at higher U_G^S (6 and 9 m/s) the radial distributions is parabolic and symmetric to the centerline in both locations, in front and in the tail of the slugs. Similar results for the void fraction, interfacial area concentration and bubble frequency were reported by Kocamustafaogullari and Wang (1991).

In summary, most of the literature regarding the behavior of the bubbles in a two-phase flow refer to vertical cases. Some models have been developed for particular conditions. Thus, all these experimental results are limited to a narrow range of applications. Extrapolating the conclusions requires an analysis of the underlaying physics. For this study, experimental data were acquired to analyze bubble size.

2.4 Effervescent atomization

Atomization of liquid consists in the production of small droplets by forcing the liquid through a nozzle. In this study, effervescent atomization is considered. This type of atomizer was first discussed by Lefebvre (1989). It is characterized by the injection of air into the liquid flow at some point in the feeding conduit to create a two-phase mixture entering the nozzle. Here, the gas phase is not intended to transfer its kinetic energy to the liquid phase, instead it is injected at low velocities to form bubbles that squeeze the liquid through the nozzle, breaking it into ligaments and later into small droplets.

Droplet size distribution is an important factor to characterize the spray and its effectiveness and stability. The final droplet size is obtained after radical changes of the two-phase flow through the nozzle. Two steps can be identified: the primary breakup, where the instabilities or perturbation generate dense sheets, converting the liquid into ligaments and ending with the creation of the droplets; and a secondary breakup, where the final droplet size is defined. In this step, a balance between the internal forces of the droplets, due to viscosity and surface tension, and external forces is achieved [Lasheras and Hopfinger, 2000]. Thus, the resulting droplets are a function of the characteristics of the mixture upstream of the nozzle [Lefebvre, 1989].

The influence of the the nozzle geometry on the effervescent atomization has been extensively studied. Several experimental studies have been published to show the improvement on the spray by changing the design of the nozzle [Sutherland et al., 1997; Bush, 1993]. Recently, Jedelsky et al. (2009) proposed a procedure for the design of effervescent atomizers and the study of key geometrical parameters for comparison reasons.

In brief, the final size distribution depends on physical properties of the fluids (density, viscosity and superficial tension), working conditions (flow rates and pressure) and atomizer geometry. A variation on one of these may affect the final droplet size.

Many methods have been developed to predict a representative droplet diameter, considering an analysis of the transport of mass, momentum and heat of the two phase flow. As mentioned, the analysis of a two phase flow is complex and it is even more intricate when the mixture flows through a nozzle. There, some mechanisms might take place to produce droplets at their final size. Several models have been proposed for the instabilities to produce the break up, such as the Rayleigh model and Taylor model. Reitz and Bracco (1982) reported a review of of the break up studies of the atomization process.

The Rayleigh instability suggests the break up results from the hydrodynamic instability caused by surface tension. This phenomena explains that any perturbation appears as a wave and a differential pressure is created between the crest and the trough of the wave. Eventually, this pressure difference will make the wave grow large enough that the stream is pinched off and spherical droplets are formed, finding a more stable low energy form. Later, Weber 1931 concluded that liquid viscosity has a stabilizing effect on the break up process. Break up occurs when the surface tension is overcome by the shear forces, turbulence forces or the collision of bubbles.

A detailed study involves many parameters making the analysis intricate. Babisnky and Sojka (2002) highlighted two analytical models: the maximum entropy principle, and the Discrete Probability Function (DPF). The former needs at least two diameters parameters (arithmetic diameter, Sauter mean diameter, surface mean diameter or volume mean diameter), which generally are calculated experimentally. Meanwhile DPF requires the assumption of a breakup model.

Therefore, the most common methods to predict size distribution are empirical, [Lefebvre, 1989; Babisnky and Sojka, 2002]. A curve is fit to the diameter range of droplets atomized, collected experimentally for a given operating condition. For atomization, the data are usually presented as a mathematical distribution, such as: normal, log-normal, root-normal, log-hyperbolic, Rosin-Rammler or Nukiyama-Tanasawa.

The limitation of an empirical model is that each model is attached and limited to the conditions of the experiments under which the data were obtained. The extrapolations to other working conditions outside the specific validated range might yield to significant error and erroneous conclusions. However, the most common methods to predict size distribution are empirical.

For these reasons, the characterization of the spray is not a standardized procedure. Operating conditions, working fluids, geometry and measurement technique affect the final droplet size measured.

2.5 Shadowgraphy - an image visualization technique

Many techniques have been used to measure bubbles in a flow and the resulting droplets of a spray [Malot and Blaisot, 2000]. In recent years, optical methods have become more common due to their non-intrusive nature and wide size operating range. They are mainly divided in Imaging and Non Imaging [Schick, 2006]. Imaging involves photography and holography, evaluating a control volume in an instant time. Non-imaging consists of analyzing the light diffracted or scattered by the particles, which is assumed to be proportional to their size. The techniques used most often are based on diffraction and light scattering. However, for an effervescent spray, these techniques are limited because of the multi-scattering effect, high droplet velocity, high concentration and the presence of non-spherical droplets. The use of these techniques may lead to error in the estimation of the characteristic diameter by not including non-spherical or elongated particles.

As a consequence, an imaged-based method is more suitable to evaluate a spray with particles that have arbitrary shapes [Ariyapadi et al., 2005; Kashdan et al., 2003; Zama et al., 2004]. The principal drawback of these techniques is the consideration of out of focus particles, and over sizing the results. This effect can be reduced by selecting the appropriate group of settings [Lee and Kim, 2004 Blaisot and Yon, 2005].

Basically, an image technique consists of using a camera as a detector to record an image of the flow illuminated with a source of light (stroboscope or laser). The image is analyzed and particles are sized individually. The image collected is one projection of the particle area, perimeter and orientation. Since the third dimension is not obtained in the images, a precise volume calculation is not possible. However, a good estimation is obtained by assuming spherical particles. From the projected area, an equivalent diameter is obtained as the diameter of a sphere with the same projected area. The spherical particle assumption is widely used in the particle sizing field, with more accurate results for small, rigid and near-spherical bubbles or droplets.

Some factors to be considered while using a optical technique are the blurring caused by the motion of the flow and reduced by a pulse light, depth of field variations, selection of the location and size of the volume control. If the particles are flowing inside a transparent conduit, the test section is required to have polished faces. External rounded pipe will deform the image of the shape of the bubbles detected.

When backlighting is used the technique is known as Shadowgraphy. A high resolution camera collects the refracted light coming through the measurement volume from a source of light. All components, camera, object and illumination must be aligned in one line. The light usually is proportioned by a flash lamp or a pulse laser, depending on the flow velocity, to freeze the flow and reduce the blurring on the images.

Typically, a light source from a laser beam is passing through a diffuser to evenly illuminate the measurement volume. The focal plane and the depth of field define the volume control. By changing the focus of the lens, the sharpness as seen by the camera can be adjusted.

For this study, due to presence of numerous gas bubbles in the conduit and to the dense spray obtained, an inclined illumination of about 45° respect to the pipeline and Shadowgraphy were selected to size bubbles on the conduit and droplets in the spray, respectively.

References

Andreussi, P., Paglianti, A., and Sanchez, F. (1999). Dispersed bubble flow in horizontal pipes. *Chemical Engineering Science*, 54:1101–1107.

Ariyapadi, S., Berruti, F., Briens, C., Knapper, B., Skwarok, R., and Chan, E. (2005). Stability of horizontal gas-liquid sprays in open-air and in a gas-solid fluidized bed. *Powder Technology*, 155(3):161–174.

Babisnky, E. and Sojka, P. (2002). Modeling drop size distribution. *Progress in Energy and Combustion Science*, 28:303–329.

Baker, O. (1954). Simultaneous flow of oil and gas. *Oil and Gas Journal*, 53(12):185–190.

Barnea, D., Shoham, O., Taitel, Y., and Dukler, A. E. (1980). Flow pattern transition for gas-liquid flow in horizontal and inclined pipes. *International Journal of Multiphase Flow*, 6(3):217–226.

Blaisot, J. and Yon, J. (2005). Droplet size and morphology characterization for dense sprays by image processing: application to the diesel spray. *Experiments in Fluids*, 39(6):977–994.

Bush, S. G.; Sojka, P. E. (1993). Entrainment by effervescent sprays at low mass flowrates. *Fluid Mechanics and Heat Mass Transfer in Sprays*, pages 117–121.

Gregory, G., Nicholson, M., and Aziz., K. (1974). Correlation of the liquid volume fraction in the slug for horizontal gas-liquid slug flow. *International Journal of Multiphase Flow*, 4:33–39.

Hesketh, R., Fraser, T., and Etchell, A. (1987). Bubble size in horizontal pipe. *American Institute of Chemical Engineers Journal*, 33(4).

Hinze, O. (1955). Fundamentals of the hydrodynamic mechanism of splitting dispersion processes. *American Institute of Chemical Engineers Journal*, 1:289.

Jedelsky, J., Jicha, M., Slama, J., and Otahal, J. (2009). Development of an effervescent atomizer for industrial burners. *Energy Fuels*, 23(12):6121–6130.

Kashdan, J., Shrimpton, J., and Whybrew, A. (2003). Two-phase flow characterization by automated digital image analysis. part 1: Fundamental principles and calibration of the technique. *Particle and Particle Systems Characterization*, 20:387–397.

Kocamustafaogullari, G. and Wang, Z. (1991). An experimental study on local interfacial parameters in a horizontal bubble twp-phase flow. *International Journal Multiphase Flow*, 17(5).

Kolmogorof, A. (1949). Sizing of spray particles using image processing techniques. *Dokl. Akad. Nauk. SSSR*, 66:825.

Lasheras, J. and Hopfinger, E. (2000). Liquid jet instability and atomization in coaxial gas streams. *Annual Review of Fluids Mechanics*, 32:275–308.

Lee, S. and Kim, Y. (2004). Sizing of spray particles using image processing techniques. *KSME International Journal*, 18:879–894.

Lefebvre, A. H. (1989). *Atomization and Sprays*. Hemisphere.

Levich, V. (1962). *Physiochemical Hydrodynamics*. Prentice Hall, Englewood Cliffs, NJ, 464.

Liu, S. and Li, D. (1999). Drop coalescence in turbulent dispersions. *Chemical Engineering Science*, 32:195–202.

Malot, H. and Blaisot, J. (2000). Droplet size distribution and sphericity measurements of low-density sprays through image analysis. *Part. Part. System Characteristic*, 17:146–158.

Mandhane, J. M., Gregory, G. A., and Aziz, K. (1974). A flow pattern map for gas-liquid flow in horizontal pipes. *International Journal of Multiphase Flow*, 1:537–553.

Razzaque, M., Afacan, A., Liu, S., Nandakumar, K., Masliyah, J., and Sean, S. (2003). Bubble size in coalescence dominant regime of turbulent air-water flow through horizontal pipes. *International Journal of Multiphase Flow*, 29:1451–1471.

Reitz, R. and Bracco, F. (1982). Mechanism of atomization of a liquid jet. *Physics of Fluids*, 25(10):1730–1742.

Schick, R. (2006). Spray technology reference guide: Understanding drop size. *Spraying System Co.*

Sovani, S. D. (2001). High pressure gas-liquid flow inside an effervescent diesel injector ans its effect on spray characteristics. Master's thesis, Purdue University.

Sutherland, J., Sojka, P., and Plesniak, M. (1997). Ligament controlled effervescent atomization. *Atomization Sprays*, 7(4):383–406.

Taitel, Y. and Dukler, A. (1976). A model for predicting flow regime transitions in horizontal and near horizontal gas-liquid flow. *American Institute of Chemical Engineers Journal*, 22(1):47–55.

Zama, Y., Kawahash, M., and Hirahara, H. (2004). Simultaneous measurement of droplet size and three-components of velocity in spray. *Optical Review*, 11(6):358–364.

Chapter 3

Experimental and Measurement Set Up

Experiments were conducted in the two-phase flow horizontal nozzle test facility of Syncrude Canada Ltd. Edmonton Research Centre, which simulates the conditions of the commercial facility located in Fort McMurray in scale, components and operating ranges. To cover the conditions used in the commercial facility, several water and air flow rates were tested. Images were taken of the flow and the spray to characterize bubbles and droplets, respectively. The same illumination and detection equipment was used for all the measurements taken. A bubble breaker was installed to influence the bubble size. All the data acquired will help in the design and performance of this type of commercial nozzle, without facing scaling-up problems.

3.1 Experimental Set Up

Experiments were performed in a liquid-gas horizontal flow nozzle assembly to investigate droplet size, shape and velocity. Measurements were taken before and after the nozzle to analyze bubbles in the conduit and droplets in spray, respectively. The facility was equipped with components similar to those installed in the commercial facility, and it was operated under a range of liquid rate flows for several values of air to liquid ratio, γ. The experimental data were collected using front illumination for bubbles and shadowgraphy for droplets. DaVis 7.4, a commercial software developed by LaVision, was employed to analyze the data [LaVisionGmbH (2007)].

3.1.1 Nozzle test facility

Experiments were conducted in a commercial scale horizontal nozzle testing facility. A schematic diagram is shown in Figure 3.1. The facility has a compressor and pump arrangement to supply streams of air and water to the mixing device. The mixture flows through a horizontal feeding pipe and sight glass before entering the nozzle. The liquid generated by the spray was collected in a channel and directed to the water tank in a recycle loop.

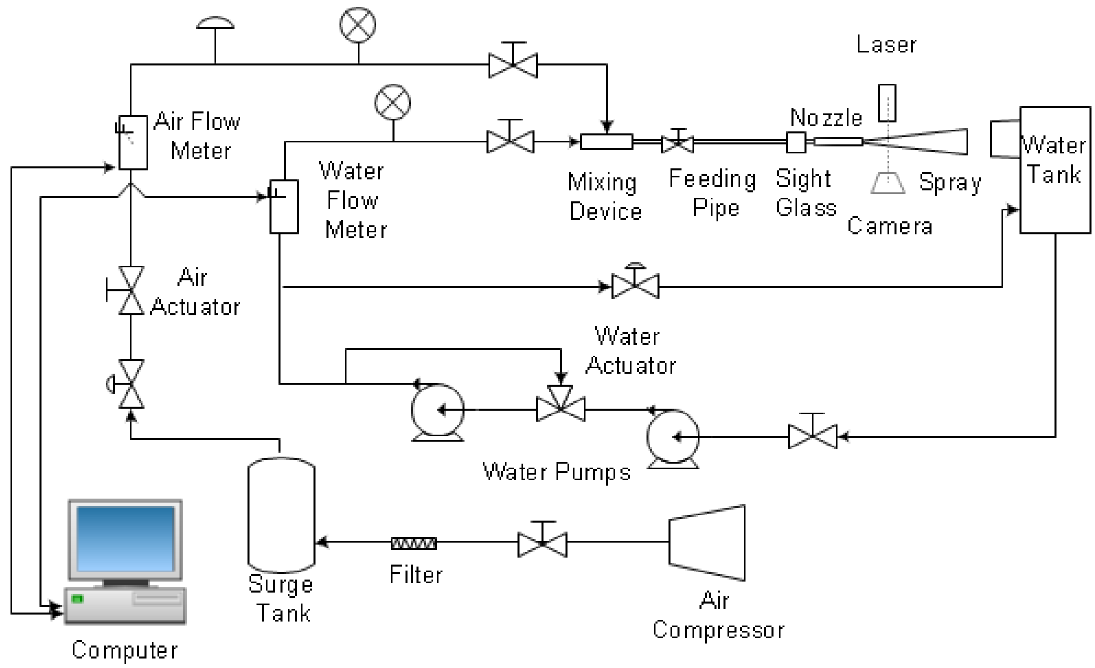

Figure 3.1: Schematic diagram of the experimental setup for the spray generation. Optical components are shown for droplets images acquisition, laser and camera aligned in one line

In order to influence the bubble size, two configurations were tested. The first without altering the bubbles, the standard configuration; and the second with a bubble breaker installed in the feeding pipe before the nozzle. Both configurations are represented in Figure 3.2.

The liquid flow rate was metered by a magnetic flow meter and the air flow was measured using a Coriolis meter. The facility is equipped with a system to control the single-phase flow rates, either manually or automatically. In addition, pressure transducers were installed to record mean and fluctuating pressure.

3.1.2 Horizontal assembly

At the nozzle test facility a horizontal assembly was installed to produce the atomization with components similar to those installed in the commercial facility: a mixing device, valve, feeding pipe, bubble breaker, sight glass and nozzle. A schematic in presented in Figure 3.2 (a).

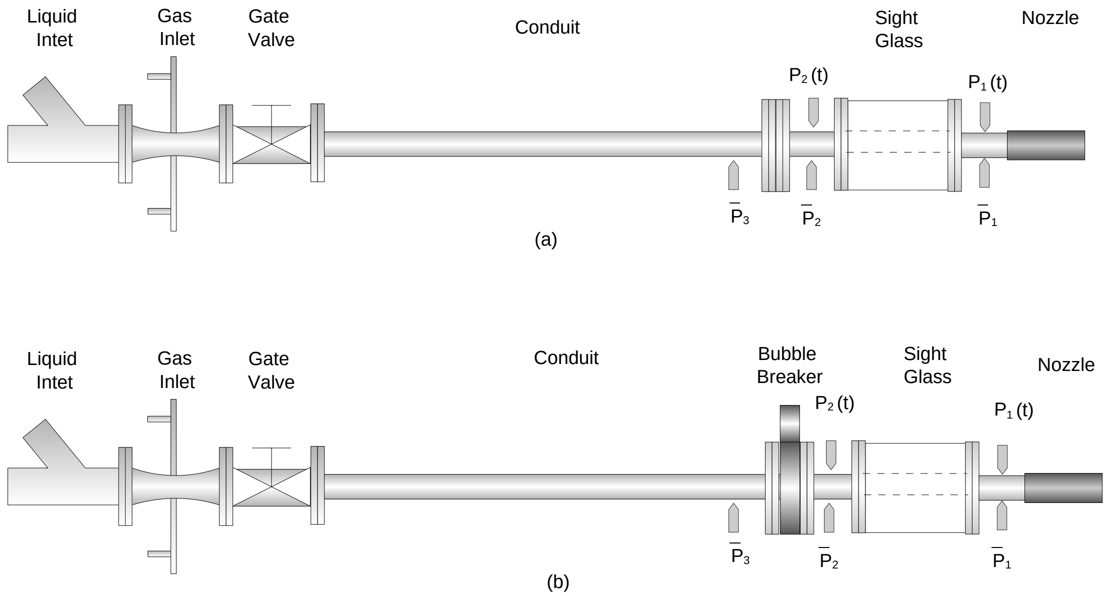

Figure 3.2: Configurations of the horizontal nozzle test facility. Pressure transducers are identified as $\overline{P}_i$ for average pressure, and P_i(t) for pressure fluctuations. (a) Standard configuration and (b) with bubble breaker installed.

Mixing device, valve and feeding pipe

For this study, the mixing device was installed to rapidily establish developed and well mixed bubbly flow and to enhance the formation of bubbles. A 3.81 cm (1 $^1/_2$in.) gate valve was installed to reproduce the conditions at the commercial facility.

The feeding pipe is a horizontal 2.54 cm (1 in.) nominal diameter, schedule 80 steel pipe, with 137.16 cm (54 in) length. Five pressure transducers were installed in the feeding conduit. Three pressure transducers, designated as $\overline{P_1}$, $\overline{P_2}$ and $\overline{P_3}$ in Figure 3.2, measure the average pressure at three different points located at 26, 49 and 67 cm upstream of the nozzle tip and the other two transducers $P_1(t)$ and $P_2(t)$, were installed in the pipe to measure the wall pressure fluctuations. Those transducers were located at 26 and 49 cm from the nozzle tip as shown in Figure 3.2. Specifications of the pressure transducers are presented in Table 3.1 and Table 3.2.

Sight glass

A transparent block of dimensions 10.16 cm×12.38 cm×12.38 cm (4 in× 4 7/8 in×4 7/8 in), with rectangular cross section and an internal circular duct of 2.54 cm (1 in) diameter

Table 3.1: Average pressure transducer specifications.

	$\overline{P_1}$; $\overline{P_2}$; $\overline{P_3}$
Model	Omega PX605–300GI
Range (kPa)	0 – 2068
Accuracy (full scale)	0.4%
Response Time (ms)	5

Table 3.2: Fluctuating pressure transducer specifications.

	$P_1(t)$	$P_1(t)$
Model	PCB113A21	PCB 112A04
Measurement Range (kPa)	1379	690
Maximum Pressure (kPa)	6895	34475
Sensitivity (mV/kPa)	3.6	16
Resolution(kPa)	0.0207	0.0276
Resonant Frequency (Hz)	$\geq$500	$\geq$ 250
Non - lineariaty(% full scale) (Hz)	$\leq$ 1	$\leq$ 1

was connected to the feed pipe. This transparent portion, also called the sight glass, allows for the visualization of the flow within the pipe. It is made of polycarbonate (index of refraction = 1.58) with plane and polished faces. Its location was just upstream of the nozzle, at the end of the feeding pipe, to avoid the entrance effects. The connection to feeding pipes was made with four bolts of 0.625 cm $\times$ 1.4 cm (5/8 in $\times$7.5 in) length studs crossing the sight glass length. An image of the sight glass in presented in Figure 3.3 (a detailed drawing is included in Appendix B.1).

A complete transparent feeding pipe would be ideal to visualize the complete evolution of the flow along the pipe. However, due to the thickness required according to the safety rules at the Nozzle Test Facility only a portion of the feeding pipe was replaced.

Bubble breaker

To influence the bubble size and its distribution in the flow, a bubble breaker (BB) was proposed. It consists of a plate with orifices located circumferentially around the center point. For this study, two bubble breakers were used. Their characteristics are presented in Table 3.3. Images of the bubble breakers employed are shown in Figure 3.4 (a detailed drawing is presented in Appendix B.2).

The bubble breakers were made of stainless steel (SA-182 F316) and installed in the feeding pipe with two threaded flanges. Leaking was avoided by using two gaskets.

The bubble breakers were designed to be changed easily and with different dimensions (hole diameter, distribution of holes and number of holes) in order to vary their influence on the two-phase flow.

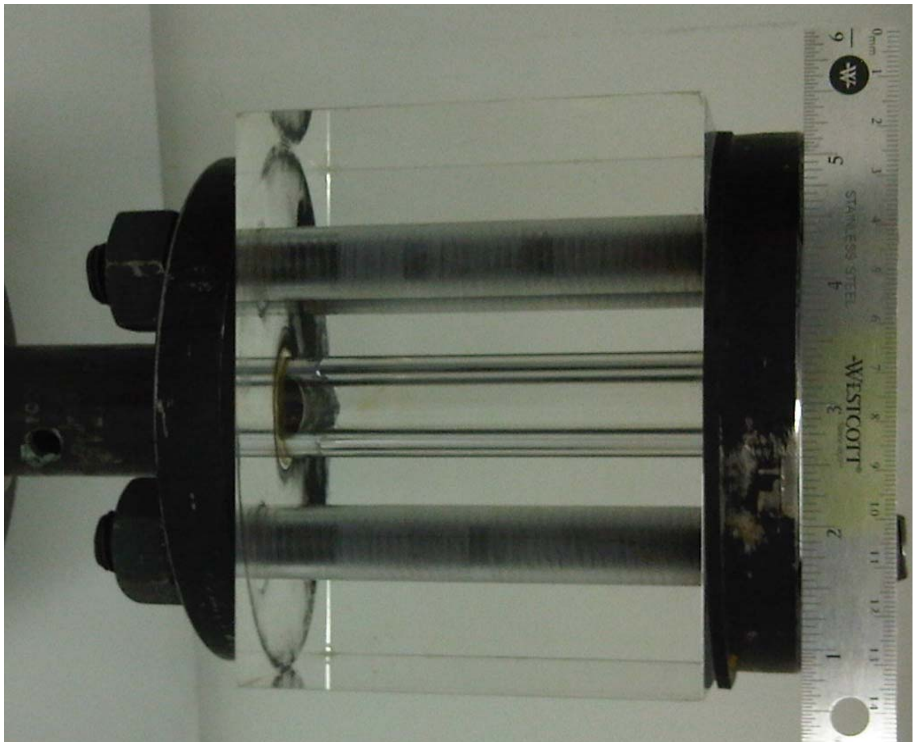

Figure 3.3: An image of the sight glass employed to observe bubbles in the feeding pipe.

Figure 3.4: An image of the bubble breaker employed to influence the bubbles in the feeding pipe. On the left bubble breaker 1 (BB_1) and on the right bubble breaker 2 (BB_2)

Table 3.3: Bubble breaker characteristics.

Description	BB1	BB2
Number of concentric holes	8	8
Concentric holes diameter (cm)	0.95	0.95
Center hole diameter	0.95	1.3
Thickness (cm)	1.25	1.25

As mentioned, this investigation is focused on the evaluation of the bubbles in the feeding conduit and their influence in the atomization process. For this reason, the pre-mixer, nozzle and the length of the duct were the same for all experiments done.

It is important to notice that when a bubble breaker was installed $\overline{P}_2$ and $\overline{P}_3$ measured the pressure drop through this accessory; meanwhile $\overline{P}_1$ always measured the injection pressure, P_i.

Nozzle

The spray was produced by effervescent atomization to create fine liquid droplets. Its geometry consists of a sequence of contraction and diffuser sections before the orifice outlet. These sections were designed to accelerate and decelerate the flow enhancing the droplet formation process. A detailed explanations of its configuration and geometry is found in Patent US 6003789.

3.1.3 Testing fluids

In the present study, air and water were the testing fluids. Recalling that the experiments were done to extrapolate the results to a steam-bitumen system, an analysis of the physical properties of the fluids is required to understand the differences in the air-water and steam-bitumen hydraulics.

As far as flow pattern are concerned, Weisman et al. (1979) conducted experiments to determine the influence of the fluid properties on flow pattern transitions and reported the surface tension and viscosity of the liquid as the properties playing important roles. In comparison to water-air systems, he concluded that for the flow patterns this study deals with, intermittent and dispersed bubble, changes on the liquid viscosity produces a small change in the flow pattern maps at lower liquid and high gas flow rate; surface tension did not produce any significant change, so the transition is unaltered.

With respect to the equivalent mass flow of the bitumen and steam Ejim et al. (2005), reported a procedure for correlate the air-water system to other system. In addition, in Syncrude (2006) report it is explained the steps to estimate the corresponding steam-bitumen droplets sizes considering to the experimental results from air-water system based on a density corrector factor. They also developed a correlation to predict the droplet size based on the fluid properties of the gas and liquid used in the system. Thus, droplet sizes measured in air-water tests are related to a possible droplet size produced in the steam-bitumen system.

The results and conclusions reported in this study using air-water might not be identical to those corresponding to the industrial conditions for a steam-bitumen system. However, there is a reliable and demonstrated similitude that makes the experimental results acquired in this study relevant.

3.1.4 Operating conditions

For this air-water system, the water is supplied by two pumps, while the air is delivered by a reciprocating compressor. A Micro Motion Coriolis flow meter was used to measure the air flow, meanwhile water was measured with an electromagnetic flow meter. The air and water flow rates were selected to cover the working conditions at the commercial facility. Flow patterns correspond to intermittent and dispersed bubble flow, according to Taitel and Dukler (1976). Not all the conditions tested are employed in the commercial unit, nevertheless they were run to generate a wide range of experimental data.

Table 3.4 summarizes the range of conditions tested for the reference configuration. All tests were performed at ambient conditions (20°C and 1 atm), and with the same components pre-mixer, feed pipe, valve, sigh glass and nozzle, for different bubble breakers. Superficial velocities reported are at standard conditions.

Table 3.4: List of the operating conditions tested.

Parameter	Standard Configuration
Liquid Flow	50 – 200 kg/min (25 – 50 usgpm)
Air Flow	1 – 4 kg/min (20 – 70 scfm)
Mixed gas flow	60 – 240 scfm
Pressure in conduit	690 kPa – 2,069 kPa (100 – 300 psig)
Air to liquid ratio, γ	1 – 4 %

Figure 3.5 shows the working conditions used in this work superimposed in a Taitel and Dukler flow pattern map for water-air mixture at 800 kPa and 20°C flowing in a 2.54 cm diameter pipe.

3.1.5 Illumination and detector system

In order to guarantee a complete illumination of the sample, a class 4 double pulsed Nd:YAG laser (λ=532 nm) was used as the source of illumination and to “freeze” the

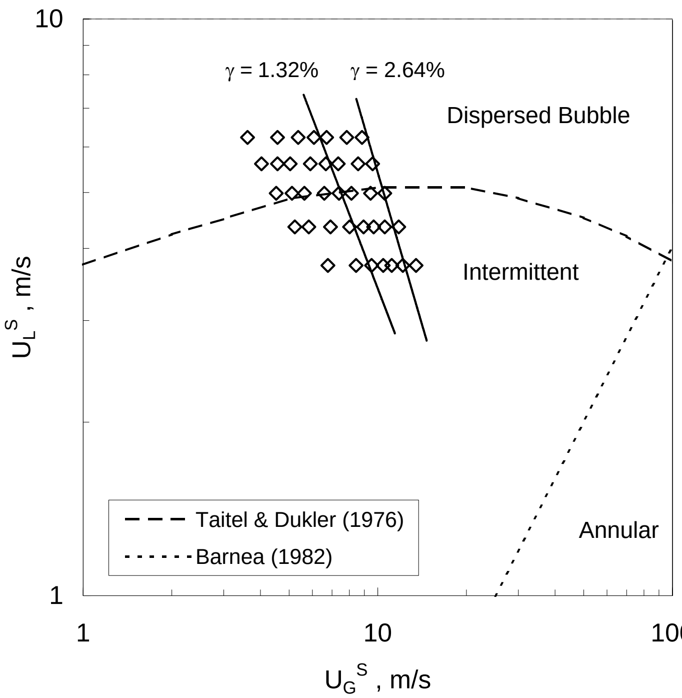

Figure 3.5: Working conditions represented by the markers, $\diamond$, are superimposed on the flow pattern map developed by Taitel and Dukler (1976). The dotted line corresponds to the transition to annular suggested by Barnea et al. (1980). Both models are for water-air, pipe diameter 2.54 cm, 800 kPa and 20°C. Continued lines refer to γ constant.

motion of the bubbles and droplets. The laser beam was dispersed by a lens (Questar M1) and entered a 6 in diameter diffuser tube creating a bright light that illuminated the area of interest with a nearly even intensity. The specifications of the laser and the diffuser are reported in Table 3.5 and Table 3.6, respectively.

The detector was a 12-bit grey scale, 1280x1024 pixels, 2/3" CCD chip digital camera, with a frame rate of 8 Hertz, and a smaller exposure time of 100 ns in double image capturing. In a single shot mode the camera runs at 4 Hertz. The lens has a depth of field from 1.39mm to 0.05mm. For droplet sizing, the camera and the frame rate were found to be sufficient. For instance, the average droplet size encountered in this research was found to be about 250 μm, with a maximum diameter of about 1200 μm, thus an area of interest of 4.9 mm $\times$ 3.9 mm for droplets, was enough to have sufficient droplets per image. The average of the number of droplets detected per run was about 21,200 droplets. For bubbles the area of interest was of 5.2 mm $\times$ 4.2 mm. The camera specifications are presented in Table 3.7.

Table 3.5: Specifications of the Nd:YAG Laser.

Feature	Laser
Model	Solo PIV 120
Wavelength (nm)	532
Repetition Rate (Hz)	15
Energy (mJ) 532nm	120
Pulse Width (ns)	3 – 5
Beam Diameter (mm)	4.5
Beam Diverge (mrad)	< 2

Table 3.6: Specifications of the Diffusor.

Feature	Diffuser
Min. recommended laser power	100 mJ, 527 – 532 nm
Max. light output diameter	120 mm
Light output wavelength	574 – 580 nm
Light output pulse duration (@ 5 ns input)	20 ns

Table 3.7: Technical data of the 12-bit CCD Camera employed.

Feature	CCD-Camera
Resolution	1280(H)$\times$1024(V) pixels
Pixel Size	6.7$\times$6.7 μm^2

3.2 Measurement Set Up

Experiments were performed for several water and air flow rates to try different flow patterns at the different configurations. For every run, the air flow rate was increased at a pre-selected constant value of water flow rate. Once the system reached a steady state for a given condition of air flow and water flow, images were taken and the average and the fluctuating pressure were recorded.

Several alternatives were evaluated to assure a suitable way to perform the image acquisition and obtain representative samples with reproducible results. The bubble size was obtained using inclined front lighting imaging while droplet size distribution was achieved by Shadowgraphy. For both, bubbles in the conduit and droplets in the spray, the same optical equipment, camera and laser, were used. Therefore, given conditions of liquid flow and γ, the experimental conditions were first tested to acquired images in the conduit and later they were repeated for imaging on the spray. A group of runs was tested on different dates to evaluate reproducibility of the test.

3.2.1 Bubble images - acquisition and analysis

Bubble images acquisition

For the conditions tested, Dispersed Bubble and Intermittent flow patterns were run in the feeding conduit and images were acquired to assess bubble size for each flow condition.

For bubble measurement, front lighting was used. Backlighting technique was not suitable because the observance of the multiple scattering phenomena. Light was scattered by the existence of numerous bubbles in the flow, creating no shadows in the images acquired by the camera.

A short duration light pulse was necessary to "freeze" the motion and minimize blurring. A laser light located at an angle of about 45° respect to the feeding pipe, produces shadows that reveal the shape and contour of the bubbles located in the focal depth near the walls of the pipe. Calibration was required to adjust the lens to have the contour of bubbles shown more clearly. Figure 3.6 shows two different image acquired for 151 kg/min and (a) $\gamma = 1$ % and (b) $\gamma = 4$ %. Notice the difference in the contour of the bubbles of the image with inclined light. Since the light is not evenly distributed in the sample, the shadows produced are not at the same intensity.

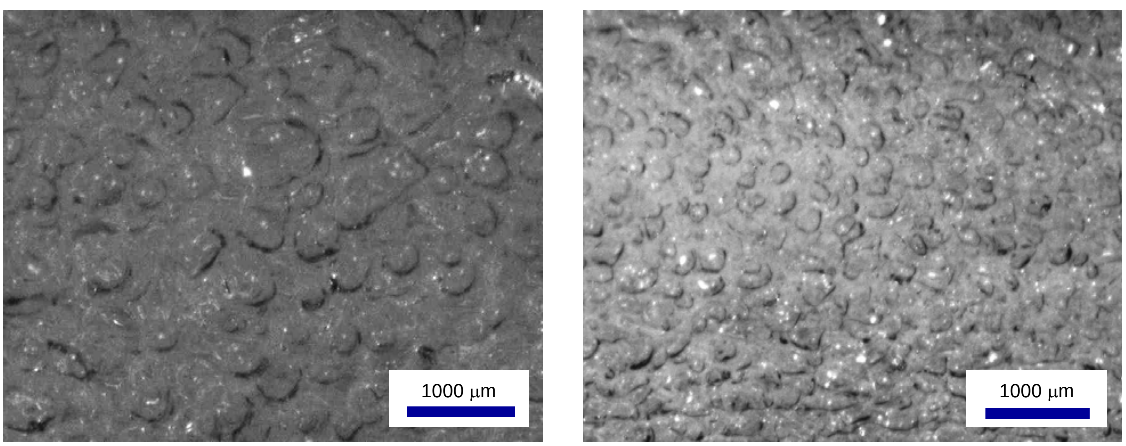

a) b)

Figure 3.6: Bubble images acquired for two different conditions 151 kg/min a) $\gamma = 1\%$ and b) $\gamma = 4\%$.

Location of the sample

In this research, the Taitel and Dukler (1976) pattern flow map was used to categorize the flow patterns of the working conditions, as shown in Figure 3.5. Since the Intermittent flow pattern was obtained for some working conditions, the measured bubble size may vary from location to location. In the Intermittent flow pattern, bubbles are not equally distributed in the radial direction, having more bubbles in the upper part of the pipe, because of buoyancy. Thus, the void fraction varies across the cross-section profile of the pipe. As a consequence, the position of the area of interest has to be selected to represent the total reality in the conduit.

Kocamustafaogullari and Wang (1991) presented a study which evaluates the void fraction radial variation, $\alpha(r)$, for different flow patterns. It was found that as the void fraction and the interfacial area concentration, $C(r)$, have similar trends, the Sauter mean diameter, D_{32}, has small variations along the radial direction. Sauter mean diameter can be considered constant across the cross-section with the exception of the area close to the upper wall where bubble size tends to reduce.

Mathematically, this is explained defining the void fraction and interfacial area concentration with Eq. (3.1) and Eq. (3.2), respectively. The D_{32} is well known as the expression of the average ratio between the volume and the particle surface area and can be calculated from Eq. (3.3).

$$\alpha(r) = \frac{\sum_{i=1}^{N} n_i \widetilde{V_i}}{\widetilde{V_T}} = \frac{\pi}{6} \frac{\sum_{i=1}^{N} n_i D_i^3}{\widetilde{V_T}} \tag{3.1}$$

$$C(r) = \frac{\sum_{i=1}^{N} n_i A_i}{\widetilde{V_T}} = \pi \frac{\sum_{i=1}^{N} n_i D_i^2}{\widetilde{V_T}} \tag{3.2}$$

$$D_{32} = \frac{\text{volume}}{\text{area}} = \frac{\sum_{i=1}^{N} n_i D_i^3}{\sum_{i=1}^{N} n_i D_i^2} \tag{3.3}$$

Where n_i is the number of bubbles of diameter D_i, N is the total bubble size classes, $\widetilde{V_i}$ is the volume of a typical bubble of size D_i in a given class i, A_i is the surface area of a typical bubble in the same class size and $\widetilde{V_T}$ is the total mixture volume.

Combining these three last equations the radial variation of the D_{32}, $D_{32}(r)$, is defined by:

$$D_{32}(r) = \frac{6\pi V_T \alpha(r)}{\pi V_T C(r)} = \frac{6\alpha(r)}{C(r)} \tag{3.4}$$

This expression shows that if the $\alpha(r)$ and $C(r)$ have the same trends $D_{32}(r)$ will behave nearly as a constant.

In summary, a inclined-front illumination that freezes the bubble size was required for the bubble image acquisition. The characteristic diameter selected was the D_{32} and the sample was located at the center line with a sample size of 5262 $\times$ 4209 μm, with a scaling factor of 4.1 μm/pixels. A class 4 double pulsed Nd:YAG laser ($\lambda = 532$ nm) with a 6 in diameter diffuser illuminated the area of interest, and a 12-bit grey scale, 1280 × 1024 pixels, 2/3" CCD chip digital camera was used as detector. Detailed characteristic of the illumination and detection systems are presented in Section 3.1.5.

The DaVis software was used for image acquisition. Its major advantage is that it ensures the synchronicity between the pulse light and the data collection. Adjustments on the intensity of the light were made depending on the amount of bubbles or droplets present at a given condition. For each condition, 50 pictures were taken in the conduit. The number of images was chosen to obtain a representative sample of the condition and no significant changes in the results were observed when a larger sample was analyzed.

Bubble images analysis

The DaVis 7.4 two-phase flow visualization software takes a raw picture of the mixture, enhances it and finally detects, counts and estimates the size of the bubbles.

The package starts the image enhancement with the subtraction of the background, a inherit noise in the image that is constant for all images. For the bubble pictures collected, this first step resulted in a distortioned image because of the uneven illumination intensity of the raw pictures and the similarity between the intensity of the gas the bubbles and the continuous phase. Hence, the bubbles of the sample were identified manually and then "sized" by this software.

This procedure consists of manually indicating the largest and shortest diameter of each bubble. Once all samples are processed, the software performances all the calculation from the 2-D images. Figure 3.7 shows the steps followed; given a bubble image the contrast was changed to expose the boundaries of the particles and select the edges of each particle. One the longest and shortest diameter are indicated by the user, the software estimates the corresponding diameter and draw the equivalent circle Figure 3.7 (c). Finally, the DaVis generates the particle list and the statistical report from the indicated bubbles.

This manual procedure was validated by comparing the results of a group of working conditions with a routine developed in MatLab, and its Images Processing module. This routine processed each image with the objective to enhance the contrast of the intensity image and transform it in a grey scale to intensify the edges of the bubbles captured in the pictures. The processed images were then analyzed in DaVis for the statistical results.

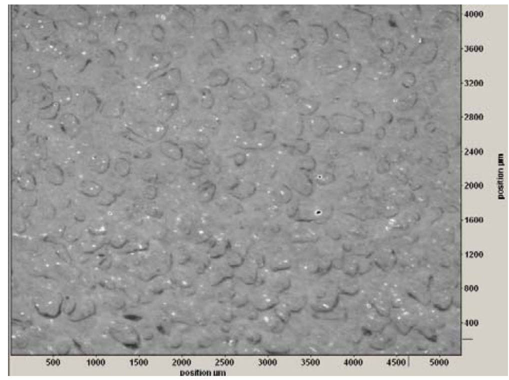

(a) Original

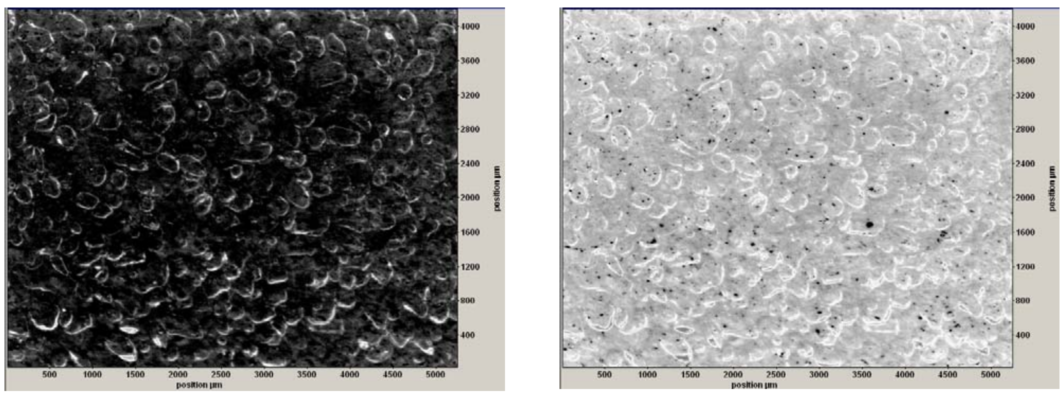

(b) High and low contrast

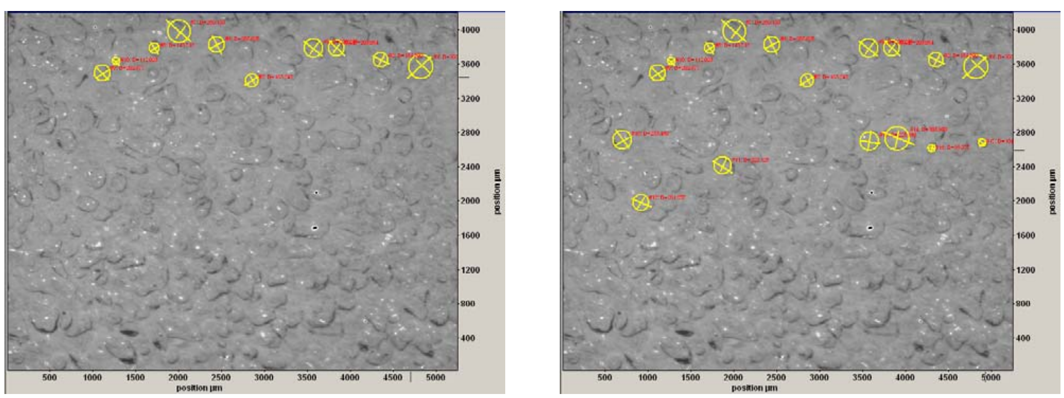

(c) Bubbles identified and measured

Figure 3.7: Bubbles identification and measurement in DaVis, manual option.

3.2.2 Droplet images - acquisition and analysis

Droplet images acquisition

For the acquisition of the spray droplets, the Shadowgraphy technique was selected. This is a non-intrusive imaged based method which uses background illumination. The laser, with a diffuser, illuminates a specific part of the spray with a nearly even intensity light, which is defined as a volume control. The camera, located perpendicular to the center line of the pipe, captured the diffracted light passing through the liquid droplets. Figure 3.8 shows the typical configuration of this technique, light and camera are aligned in one line with the volume control. Location of the volume control was determined experimentally trying different locations along the axial and radial distance.

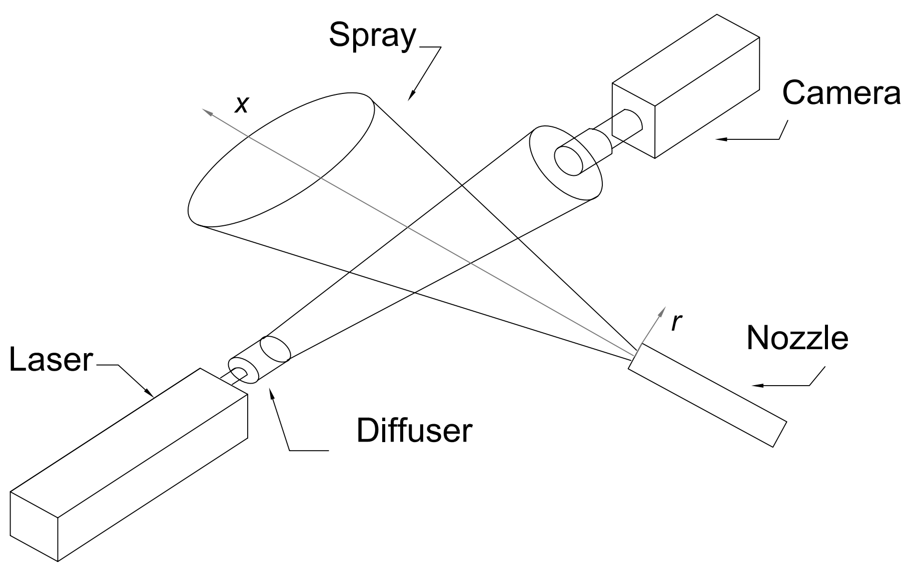

Figure 3.8: Schematic diagram of shadowgraphy for acquiring droplet images on the spray.

As in the bubble measurement, droplet images processing was performed using DaVis software. For each condition, 1000 pictures were taken. The number of pictures was found to generate sufficient data to obtain reliable statistical results, with an average of 21,200 droplets per run. Droplets were measured at different axial ($x/d = 24.5$, 35 and 52.4) and radial locations ($r/d = 0$, 2.1 and 3.4) to study the behavior of the spray. For axial locations lower than $x/d = 24.5$ ligaments were observed. Meanwhile, measurements at $x/d > 54$ were not physically possible in the space provided by the facility. Measurements were restricted to distance between $24 < x/d < 54$ in the axial direction. Radial directions were selected based on the cone created by the spray and its edges.

Shadowgraphy and DaVis, an image processing software

The DaVis software allows the measurements of particle sizes by image analysis of high resolution digital images. The image processing consists of a two-steps algorithm. First is the *globalsegmentation* where it detects the particles and identifies them as individual objects; and second the *particlesizing*, where particles are actually measured.

In the first stage, the *globalsegmentation*, is where particles are recognized. The analysis of each image is based on its intensities. The image is inverted based on intensity, particles are darker than the continuous phase. Now, the image is subtracted from a reference image, which is an image with no particles, to eliminate or reduce the noise and inhomogeneities produced by the background and optics. To finish this stage, the software detects particles based on the changes of the intensity and isolates them to be individually analyzed.

For the *globalsegmentation*, a percentage of the maximum intensity of the inverted image, establishes the presence of a particle. The recommended minimum value is the average intensity of the border of any particle. The software recognizes the particle and creates a rectangle around the area. A pixel is marked as belonging to a particle, when its intensity and its adjacent pixel intensity are larger that the threshold.

Once particles are recognized, the second step, *particlesizing* is performed. Particles are analyzed individually for size, shape and position. High and low level of intensities, introduced by the user, are used to determine the area of the object and calculate the equivalent diameter corresponding to a circle of that area. The software counts the number of pixels with intensities above the high level and below the low level, and uses these values to estimate the area of each threshold and the equivalent diameter assuming the projected area of the particle as a circle.

Figure 3.9 shows a sequence of images to reproduce the steps followed by DaVis to detect and estimate the sizes of the droplets. The image taken, indicated as “Original”, is inverted based on the intensity and subtracted from an reference image to eliminate all non-uniformities caused by the background and the differences of the illumination on the sample from the diffuser. The resulting image is indicated as “Preprocessing”; areas with high intensities represent droplets and low intensity areas indicate the background.

The next step is where the recognition of droplets takes place detecting their boundaries; called as “Global Segmentation” the detected particles for a threshold of 55% the are green-colored in the image, areas with intensities higher than the threshold are marked and a bounding box around the region is estimated. Finally, the particle are sized based on two intensity values than define the droplet region. For Figure 3.9 the high level and low level of intensities were 55% and 45%, respectively. All three percentage are referred to the maximum intensities of the bounding box. The software estimates the diameter of each particle and draw a circle of the equivalent sphere.

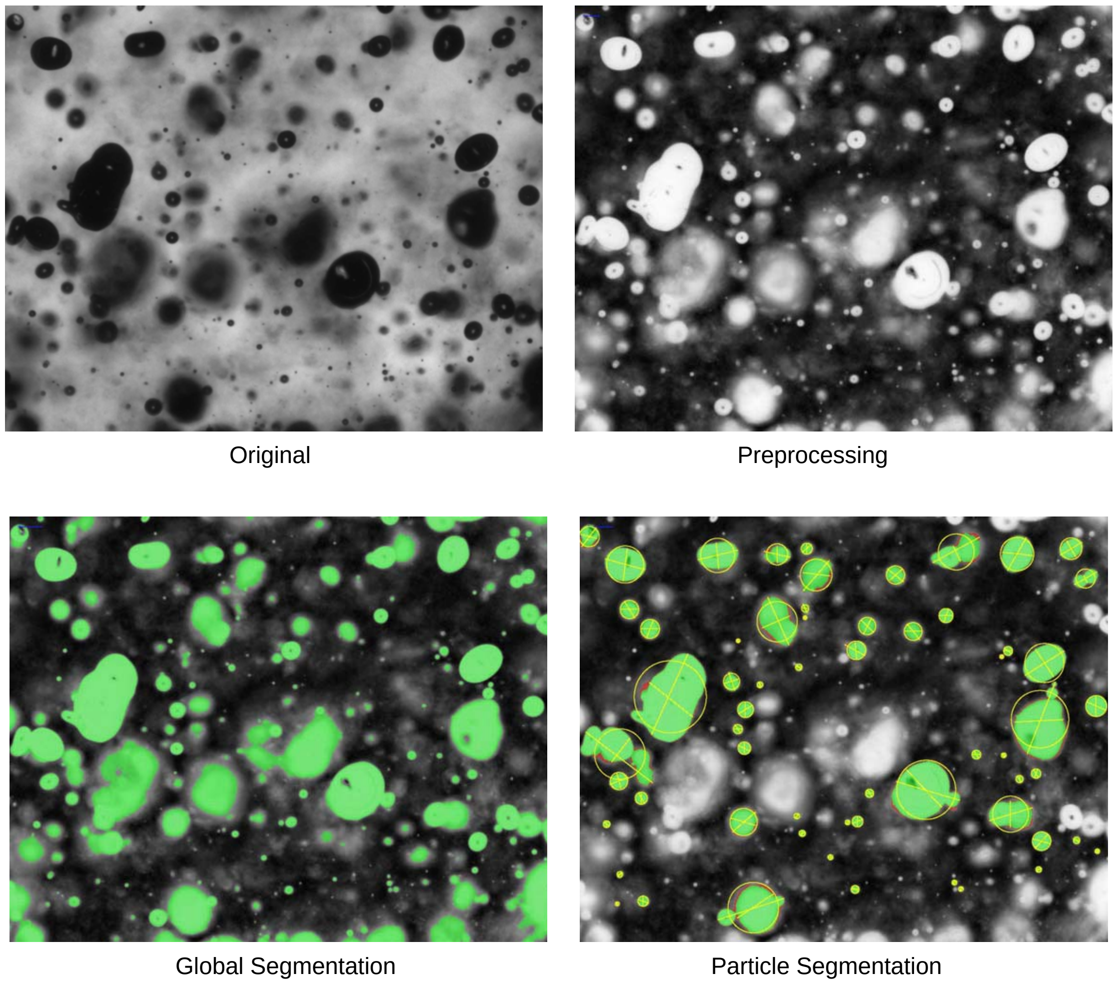

Figure 3.9: The Shadowgraphy process using Davis software from the original images to the image with the detected droplets and their measured area and equivalent diameter. Global segmentation 55% and particle segmentation in high level 55 % and low level 45 %.

As explained in the procedure, it is evident that results depend on the threshold levels introduced by the users. Figure 3.10 depicts the resulting droplets detected and sized for two different Global Segmentation value [Figure 3.10 (a) and Figure 3.10 (c)] and for two set of values in the Particle Segmentation [Figure 3.10 (a) and Figure 3.10 (b)]. The determination of those values is not a standard task and must be made to assure results are not biased. Several algorithms have been used to estimate threshold automatically, manually or a combination; some of them are mentioned by Ranganathan and Kannan. (1994).

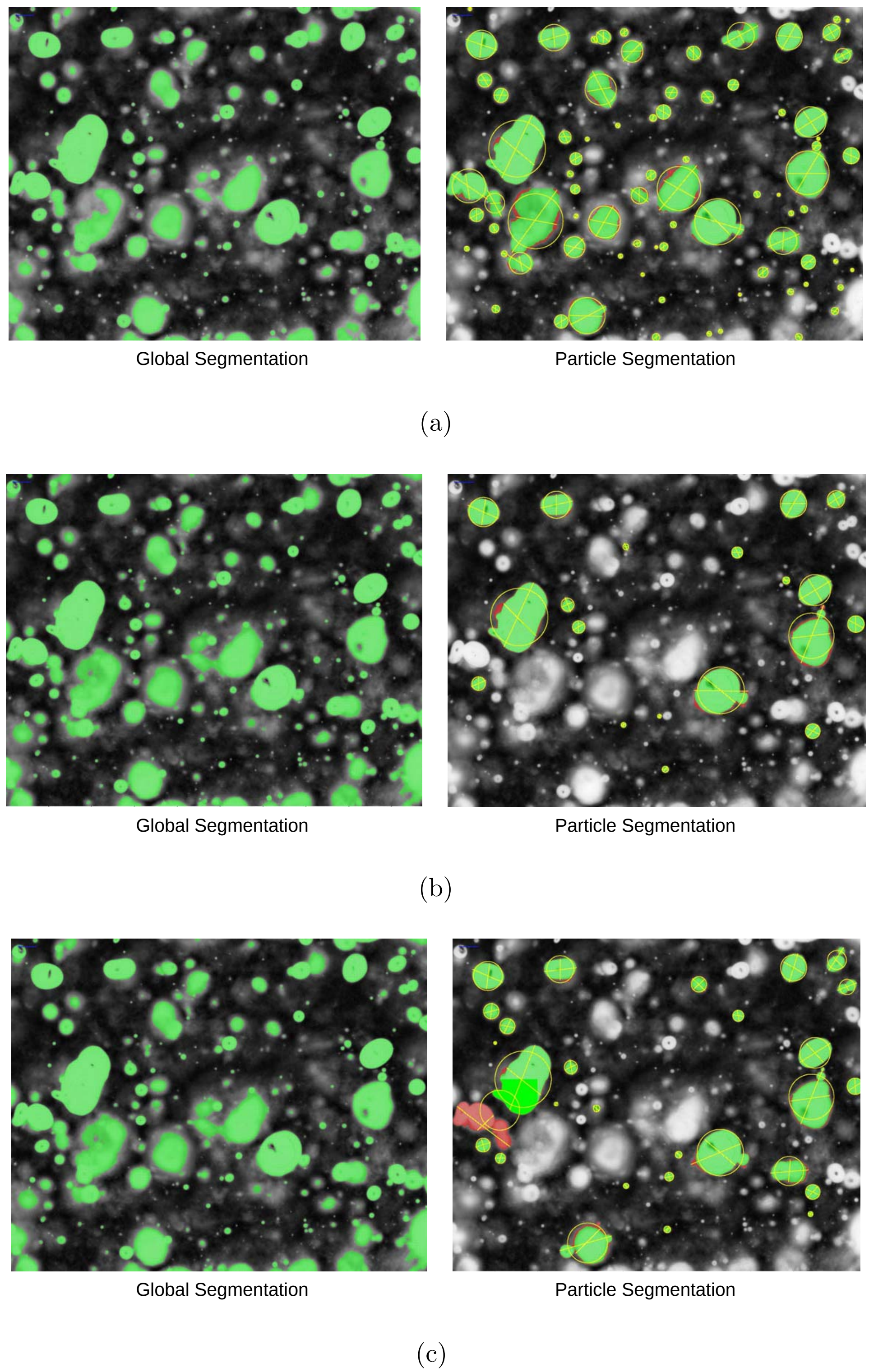

Figure 3.10: Effect of the settings using DaVis software. (a) Global 65 %, highlevel 55 % lowlevel 45 %, (b) Global 55%, highlevel 60% lowlevel 40%; and (c) Global 55 %, highlevel 55 % lowlevel 45 %, area of interest 50 %.

Despite the uncertainties that might arise by the selection of the thresholds, Shadowgraphy has the advantage to allow the visualization of the raw and processed images; thus the user can actually see what the software is doing and measuring. This option is not possible for non-image based techniques as PDA.

A sensitivity test was done trying several threshold ranges to identify the values best suited to the samples and to ensure results are not biased by the selection of these values. It was found that there is a range for each parameter were the results are nearly constant and do not vary significantly.

The software also provides image enhancement options such as changing the contrast to display information available in the image, changing the gray scale, revealing intensity variation. The imaged obtained is improved in visual quality, reducing even the low intensity noise of out of focus particles, since their intensity is not the same that located in the focal depth. Other filters might be applied and have an influence the results reported. Those filters are intended to reduce the inherent noise of the images and prepared them for the sizing particle. A minimum centricity, and removing touching image border are also some options presented in the software. Final setting and options selected are shown in section Appendix C.

3.2.3 Pressure measurements

For the single-phase pressure measurements a program developed in LabView showed and recorded the pressure of the air stream and water stream before the mixing section. This program allows for the control of the flow-rates of the single phase flow through control valves installed in the facility.

For the two-phase pressure measurements, the feeding pipe was equipped with differential and high response pressure transducers to obtain the mean and fluctuating pressures. Figure 3.11 shows an image of the feeding conduit with the transducer installed. The mean pressure measurement were made at three (3) different points of the pipe with pressure transducers, $\overline{P}_j$, located at 26 cm, 49 cm and 67 cm from the nozzle for the standard configuration. High response pressure transducers, $P_1(t)$ and $P_2(t)$, were installed at 26 cm and 49 cm from the nozzle to measure the wall pressure fluctuations and determine spray stability according to Maldonado (2006).

Maldonado in her research reported a pressure parameter based on the area beneath the power spectral density (PSD) for frequencies up to 40 Hz (${P_2}^{40}$) as a factor to characterize the spray stability. Low values of ${P_2}^{40}$ are associated with stable sprays and high values with unstable spray. The limits for the transitions stable-unstable depend on the components and working conditions. Thus, values proposed in her work are not be suited to this study; however the methodology is applicable and was used to determine the working range of the nozzle.

The mean and fluctuating pressures of the two-phase flow were visualized and recorded in a software developed in LabView, which translates the signal from the traducers to the corresponding pressure value. Figure 3.12 shows the signal acquired for two different conditions. An image of this interphase is shown in Appendix D.

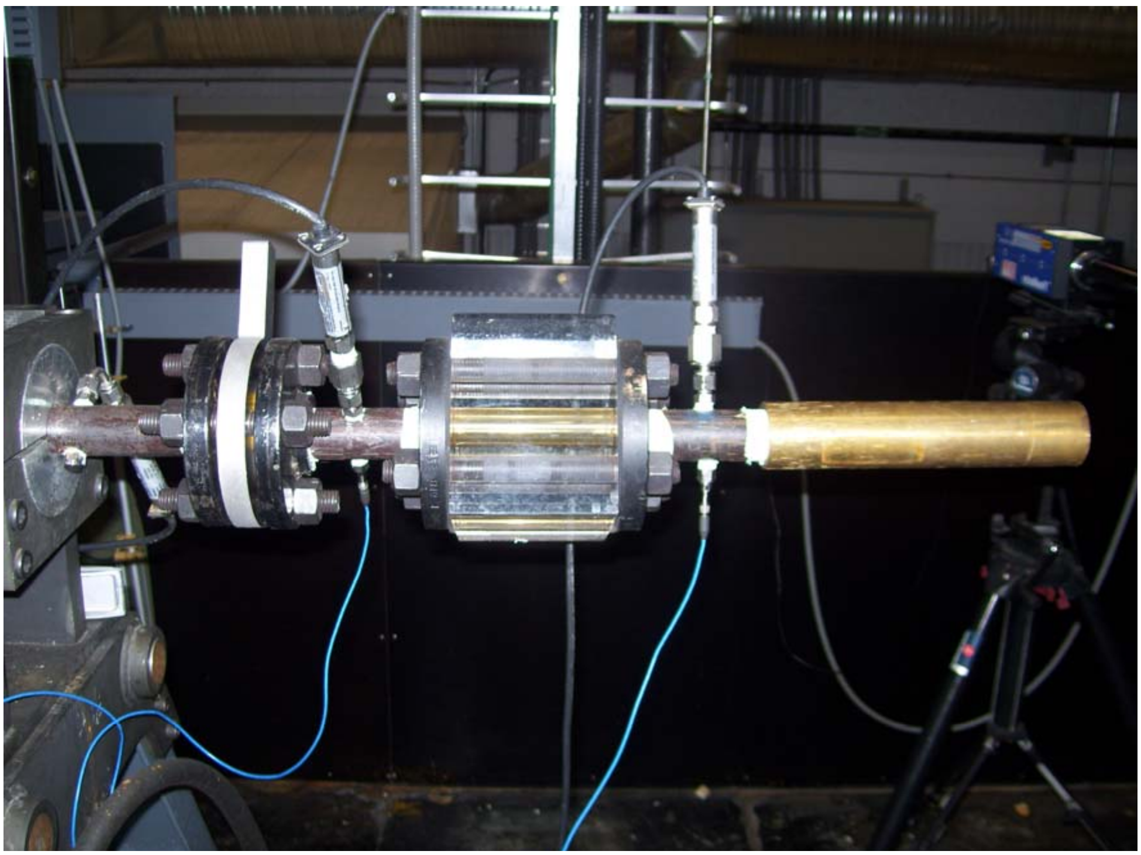

Figure 3.11: Image of the mean and fluctuating pressure transducer installed in the feeding conduit.

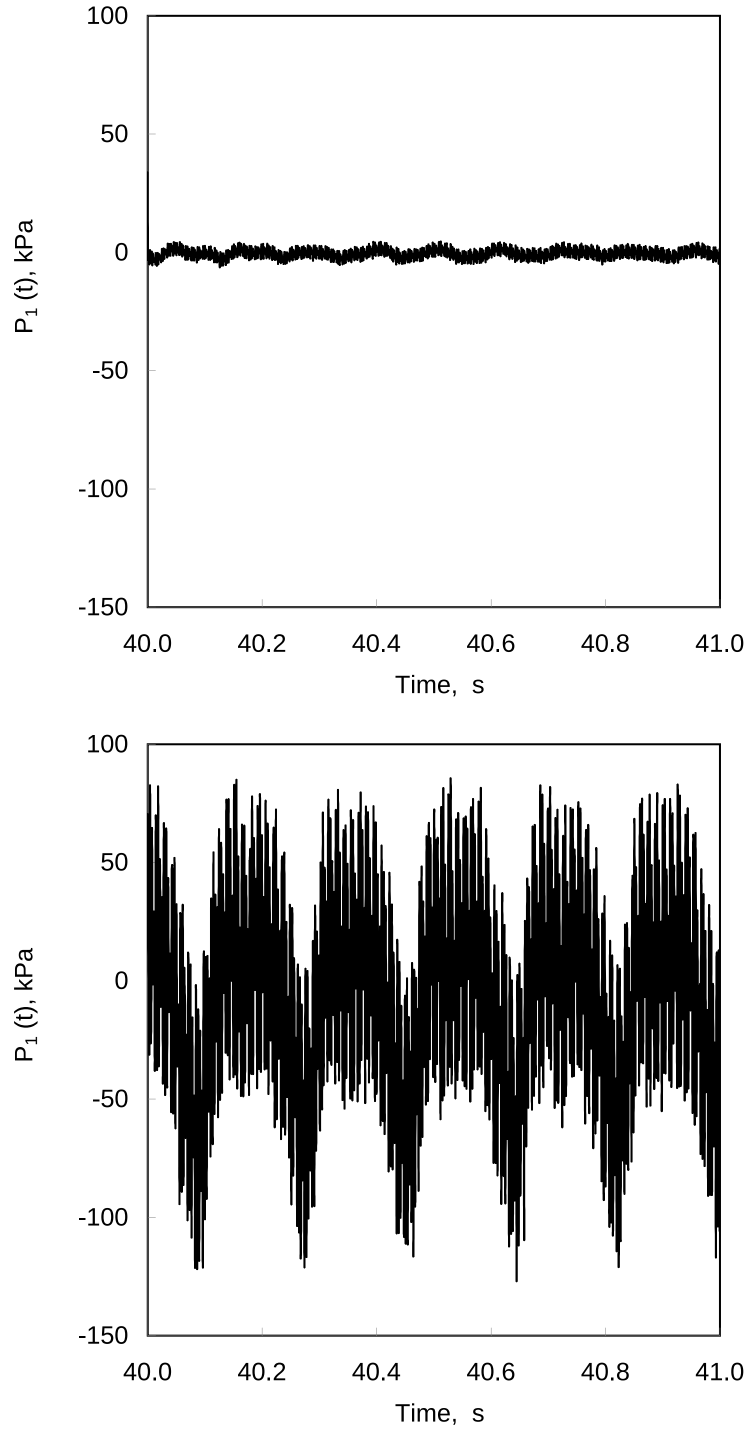

Figure 3.12: Fluctuating Pressure signal for two different conditions (a) stable $Q_{\mathrm{L}} = 151$ kg/min and $\gamma = 2$ % and (b) unstable $Q_{\mathrm{L}} = 76$ kg/min and $\gamma = 2$ %.

References

Barnea, D., Shoham, O., Taitel, Y., and Dukler, A. E. (1980). Flow pattern transition for gas-liquid flow in horizontal and inclined pipes. *International Journal of Multiphase Flow*, 6(3):217–226.

Ejim, C. E., Fleck, B. A., and Amirfazli, A. (2005). A scaling study of the atomization of a two-phase industrial nozzle: Part 1 - effect of surface tension and viscosity on mean drop size profiles. In *Proceedings of the 20^{th} ILASS – Europe*.

Kocamustafaogullari, G. and Wang, Z. (1991). An experimental study on local interfacial parameters in a horizontal bubble twp-phase flow. *International Journal Multiphase Flow*, 17(5).

LaVisionGmbH (2007). Sizing-maser shadow. *Optical Review*, Gottigen, Germany.

Maldonado, S. (2006). Improving the stability of gas-liquid spray. Master's thesis, University of Alberta.

Ranganathan, K. and Kannan., S. (1994). Drop size measurement in two-phases swirling flow using image processing techniques. *International Journal Heat and mass Transfer*, 37(4):559–670.

Taitel, Y. and Dukler, A. (1976). A model for predicting flow regime transitions in horizontal and near horizontal gas-liquid flow. *American Institute of Chemical Engineers Journal*, 22(1):47–55.

Weisman, J., Duncan, D., Gibson, J., and Crawford, T. (1979). Effects of fluid properties and pipe diameter on two-phase flow patterns in horizontal lines. *International Journal of Multiphase Flow*, 5(6):437–462.

Chapter 4

Spray Characterization

4.1 Abstract

This work experimentally studied the evolution of an effervescent spray for different working conditions. Experiments were done to generate information regarding the behavior of the spray at different locations, along the radial and axial location, to determine with confidence the most appropriate location to characterize it. The characterization was done through the Sauter mean diameter, the shape of the droplet, droplet size distribution and velocity distribution. A probe was inserted into the spray at several axial and radial locations to measure the momentum flux rate. Results from this study were partially published on a paper for the 23rd Annual Conference on Liquid Atomization and Spray Systems, Brno, Czech Republic, September 2010. This investigation provides a better understanding of the behavior of this type of atomizer and assist the design and operation of feed nozzles.

4.2 Introduction

Effervescent atomization is a complex two-phase flow problem which is a function of many parameters, such as the physical properties of the fluids involved, working conditions, geometry of the nozzle and measurement technique employed, among others. Several studies have been done to understand the influence of those parameters in the production of a uniform spray with droplets in a specific size range. Some parameters studied are related to the characteristic of the mixture upstream of the nozzle, usually a two-phase flow [**?**], and others to the nozzle geometry [**?**].

Due to the complexity of this two-phase flow problem there is a lack of information in the literature about the prediction of the variation of droplet diameter. Each parameter differently influences the droplet size along each step. **?** mentioned the variables involved and the areas that still remain unknown in this field. For most atomizers, mean droplet size decreases with increasing the gas velocity and increases with increasing liquid flow or liquid viscosity [?].

Many models and correlations have been proposed to predict droplet size with a representative characteristic diameter. Most of them are based on the work of ?. However, usually an analytical model requires the values of one or two characteristic diameters that are assumed or acquired experimentally and the assumption of a break up model [?]. The lack of a completely theoretical model leads to the use of empirical methods as the most common procedure used to analyze particle size and particle size distribution [?; ?; ?]. The limitation of an empirical model is that each model is attached and limited to the conditions of the experiments under which the data were obtained. The extrapolations to other working conditions might lead to different conclusions, for those outside the specific validated range.

4.2.1 Sampling techniques

Many visual techniques have been employed to measure the resulting droplets of a spray [?]. The techniques usually employed are based on diffraction and light scattering. However, they are not suitable for a dense spray produced by effervescent atomization because of the multi-scattering effect, high droplet velocity, high concentration and the presence of non-spherical droplets. The use of these techniques may lead to error in the estimation of the characteristic diameter by not including non-spherical or elongated droplets. An image based method is more suitable to evaluate a spray with droplets that have arbitrary shapes [?; ? and ?]. The principal drawback of these techniques is the consideration of out of focus particles, and over sizing the results. This effect can be reduced by selecting the appropriate group of settings [?; ?].

Two sample techniques are identified: the spatial technique and flux technique. For the former, a large amount of the droplets is measured locally in a small given volume of the whole spray. In *flux* or *temporal* techniques, particles are measured individually when passing through the sampling volume in a given time interval. Data comparison, acquired from different techniques, requires a understanding of the principle to transform the resulting data to the same base line. Identical spatial and flux distributions are obtained only when all particles in the spray travel at the same velocity.

For spatial techniques the location of the volume control, distance from the nozzle and from the center line, have to be chosen properly to have a sample region that represents the entire process. In the literature there is not an established procedure to determine the most representative region to acquire data. ? mentioned several works with the two most common criteria, longest axial distance from the nozzle and closest distance to nozzle. Other suggestion followed is acquired data at different locations and characterize the spray with an average value. In that way, a representative value of the whole process is obtained. This method is mentioned in a Von Karman Institute for Fluid Dynamics report, (2006) and reported by ?.

4.2.2 Mean droplet diameter

The characterization of the spray requires a numeric value or a mathematical model to evaluate its behavior at a given location. As the atomization is a random droplet generating process, the resulting spray contains droplets in a wide size range. The arithmetic mean was commonly used to identify the whole size range. However, spray characterization based on one unique parameter may lead to misleading conclusions. The literature refers to several definitions of diameters to identify and establish the behavior of the spray mainly based on its final application. The detailed definitions are provided by the Von Karman Institute for Fluid Dynamics (2006) report and summarized in Table 4.1. These descriptive diameter quantities are extracted from experimental data and are obtained by Eq. (4.1).

$$D_{pq} = \left(\frac{\sum D_i^p N_i}{\sum D_i^q N_i} \right) \tag{4.1}$$

where N_i is the number of particles with diameter D_i and p, q are parameters used to define a specific characteristic diameter according to Table 4.1.

Table 4.1: Definition of typical characteristic diameters.

Characteristic diameter	Best suited application	p	q
Arithmetic mean Diameter	Calculating evaporating rate and comparison	1	0
Sauter mean diameter	Efficiency and mass transfer	3	2
Surface mean diameter	Surface controlling applications (absorption)	2	0
Volume mean diameter	Volume controlling applications (hydrology)	3	0
Mean evaporating diameter	Evaporation and molecular diffusion	3	1
Herdan diameter	Combustion	4	3

Sauter mean diameter

The Sauter mean diameter (D_{32}) is defined as the ratio between the particle cumulative volume and particle overall surface area. Usually it is used to characterize break up processes with rapid surface generation. D_{32}, also denominated as SMD, is defined by

$$D_{32} = \left(\frac{\sum D_i^3 N_i}{\sum D_i^2 N_i} \right) \tag{4.2}$$

From its definition D_{32} places emphasis on large diameters with a major contribution to the volume and less to the area.

4.2.3 Mathematical distributions

In the analysis of droplet size distributions (DSD) usually experimental data are treated with the purpose of relating them to a known mathematical model. These models consolidate a large amount of data in one expression, allowing an easier calculation of the characteristic diameters and the extrapolation of the data outside the experimental ranges [**?**]. For atomization, the models most commonly used in the analysis of droplet size are: normal, log-normal, Nukiyama-Tanasawa and Rosin-Rammler.

Studies of DSD generally require the use of probability density function for the characterization of the droplet size population. Usually, the distributions are presented with histograms or curves. For this study, DSD are represented by plotting the percentage (%) of the particles with the same diameter respect to the total particles detected versus the droplet diameter, D.

Normal distribution

In the normal distribution, a number distribution function $f(D)$ is used to determine the number of droplets of diameter D, by Eq. (4.3)

$$f(D) = \left(\frac{1}{\sqrt{2\pi} S_n} \exp\left[-\frac{1}{2S_n^2} (D - \overline{D})^2 \right] \right) \tag{4.3}$$

where S_n is the standard deviation, $\overline{D}$ is mean value and S_n^2 is the variance. Usually the data are characterized using the mean value and the standard deviation by the expression $\overline{D} \pm S_n$. This distribution usually does not fit properly the experimental droplet size data acquired from effervescent atomizers.

Log-normal distribution

The log-normal distribution is derived from the normal distribution when the logarithm of the particle diameters is used as variable. Thus, the log-normal distribution is defined by Eq. (4.4)

$$f(D) = \left(\frac{1}{\sqrt{2\pi} S_g} \exp\left[-\frac{1}{2S_g^2} (\ln(D) - \ln(\overline{D_g}))^2 \right] \right) \tag{4.4}$$

where D_g is the geometric mean droplet diameter and S_g is the geometric standard deviation. The geometric mean and geometric standard deviation are defined by Eq. (4.5) and Eq. (4.6), respectively.

$$D_g = \sqrt[n]{\prod D_i} \tag{4.5}$$

$$S_g = \exp\left(\sqrt{\frac{\sum(\ln D_i - \ln \overline{D_g})}{n}}\right) \tag{4.6}$$

The rest of the mentioned distributions, Nukiyama-Tanasawa, Rosin-Rammler, and modified Rosin-Rammler, are empirical distributions in which some values have to be assumed or calculated from the data. A summary is represented in Table 4.2.

Table 4.2: Empirical distribution functions commonly used in atomization.

Distribution	Expression	Independent variables	q
Nukiyama-Tanasawa	$\frac{dN}{dD} = aD^p\exp(-(bD)^q)$	a,b,p and q	0
Rosin-Rammler	$1 - Q = \exp - \left(\frac{D}{X}\right)^q$	X and q	2
Modified Rosin-Rammler	$1 - Q = \exp - \left(\frac{\ln D}{\ln X}\right)^q$	X and q	0

Due to the randomness of the effervescent atomization a characteristic diameter, a shape parameter and velocity distributions are used to analyze the spray. D_{32} and DSD are considered to be standard parameters to characterize the spray effectiveness. However, as the final droplet size is obtained after radical changes of the two-phase flow through and after the nozzle, with the influence of many parameters including the sampling technique, the measurement of droplet size is not a simple procedure.

4.3 The Experiments

Experiments were performed in a horizontal commercial scale nozzle facility, with air and water as the testing fluids. The fluids were mixed at a mixing device to enter as a two-phase flow in a feeding pipe with diameter of 2.54 cm. Water and air mass flow rates were controlled and measured as single phases with a magnetic flow meter and Coriolis meter, respectively. Experiments were performed at room conditions, temperature 20° C and pressure of 1 atm. Operating conditions are listed in Table 4.3.

Pressure was measured at three different points of the feeding conduit 26 cm, 49 cm and 67 cm from the nozzle tip. The former measured the inlet pressure and other two transducers measured the pressure drop along the pipe. Wall pressure fluctuations were monitored with two high speed pressure transducers located at 26 cm and 49 cm from the nozzle tip. For a diagram of the assembly with the pressure transducers and their technical specifications refer to Figure 3.2, Table 3.1 and Table 3.2, respectively.

Measurement of droplet size and velocity were done with shadowgraphy. This technique allows for the visualization of the shape of the particles not fully atomized without any sphericity rejection criteria. Estimation of the diameter is done by the

Table 4.3: Working conditions used in this study for the spray characterization.

Water flow (kg/min)	Air flow (kg/min)	γ (%)
113.42	3.0	2.64
113.42	4.0	3.53
113.42	5.0	4.41
151.23	2.0	1.32
151.23	3.0	1.98
151.23	4.0	2.64
189.04	2.0	1.06
189.04	2.5	1.32
189.04	3.0	1.59
189.04	4.0	2.12

equivalent diameter of a sphere with the same projected area as the projected area of each particle.

The image acquisition was performed with a class 4 double pulsed Nd:YAG laser ($\lambda = 532$ nm) as the source of illumination and a 12-bit grey scale, 1280 x 1024 pixels, 2/3" CCD chip digital camera as the detector. To create a volume control with a near even intensity a lens (Questar M1) and a 142.5 mm diameter diffuser were used. The size of the volume was an area of 4.9 x 3.9 mm (3.80 μm/pixel). Typical droplet sizes for this system were on the order of 0.1 mm so the area of interest was large enough to provide enough droplets per image.

As variation of the droplet size and size distributions is found depending on the location, several locations were selected along the radial r and axial x axes, measured from the nozzle tip ($x/d = 24.5$, 35 and 52.4) and from the centre line ($r/d = 0$, 2.1 and 3.4), respectively as shown in Figure 4.1. To identify each position of the measurement, the designation (x/d; r/d) was used. For each location, 1000 images were recorded to generate enough data to obtain reliable statistical results. Considering all runs, on average 21,200 droplets were detected per run.

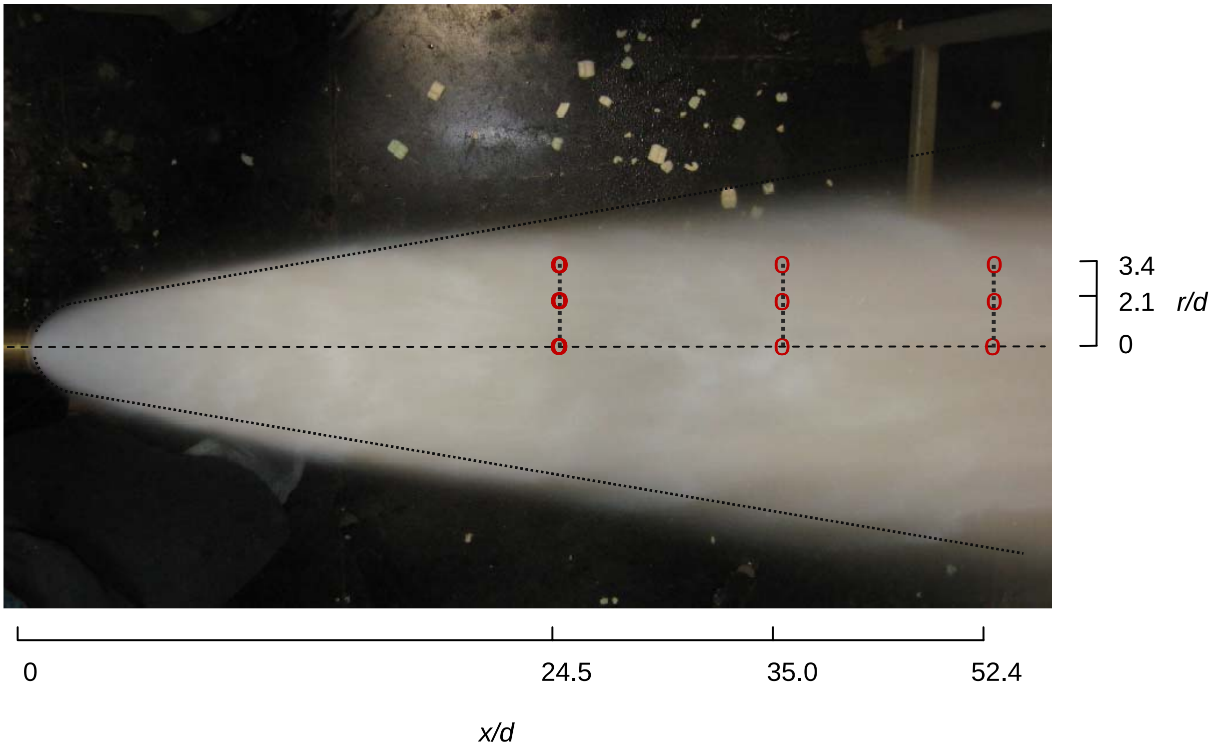

Figure 4.1: Different locations tested superimposed on a spray image at $Q_{\mathrm{L}} = 151$ kg/min and $\gamma = 2$ %.

4.4 Spray Characterization

A typical image acquired with shadowgraphy for this type of nozzle is presented in Figure 4.2. The DSD, D_{32}, shape and velocity vary with location for the same water and air flow rates. The spray was characterized at three locations along the centerline (x/d = 24.5, 35 and 52.4). For distances closer to x/d = 24.5 the spray was too dense, resulting in images excessively obscured, the majority of liquid was presented as ligaments or sheets and droplets were barely observed.

The evolution of the D_{32} along the centreline for different air–to–liquid mass ratio, γ, is presented in Figure 4.3. As the results are influenced by many parameters, the trends of the size evolution are not parallel; however D_{32} seems to have a tendency to decrease as the spray evolves downstream. The results suggest that for the centreline the secondary break up, where droplets achieve their final size, occurs beyond $x/d = 52.4$. The radial variation in droplet size was tested at three locations (r/d = 0, 2.1 and 3.4) positioned at x/d = 24.5 and 32.0. Figure 4.4 shows the variation of the droplet size along the radial axis for $x/d = 24.5$. The D_{32} decreases with increasing r, for the conditions tested. This is due to the presence of larger droplets and ligaments close

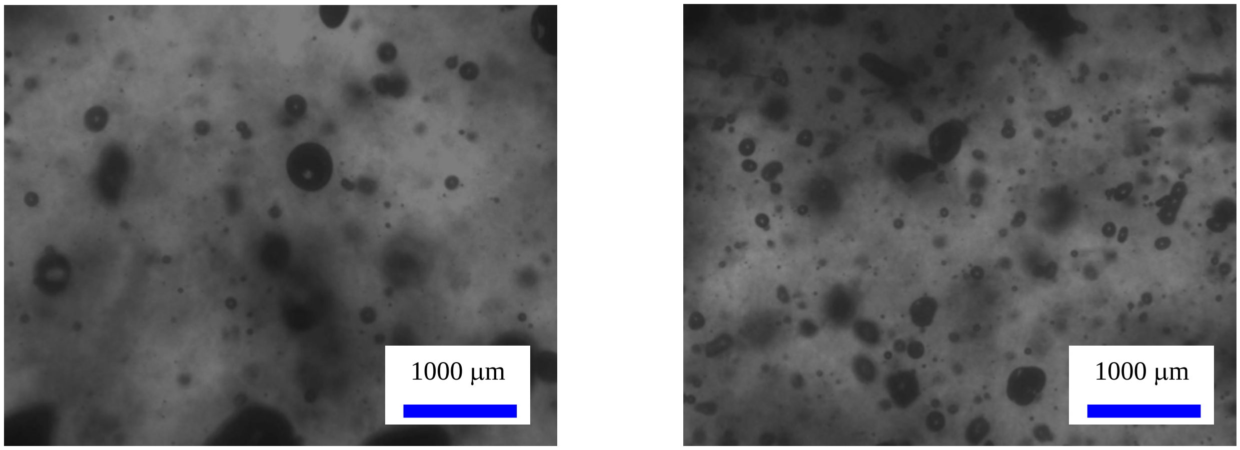

Figure 4.2: Images acquired with shadowgraphy for $Q_\mathrm{L} = 151\ kg/min$ and $\gamma = 2$ % at location (24.5 ; 2.1)

to the centreline, increasing the average droplet diameter.

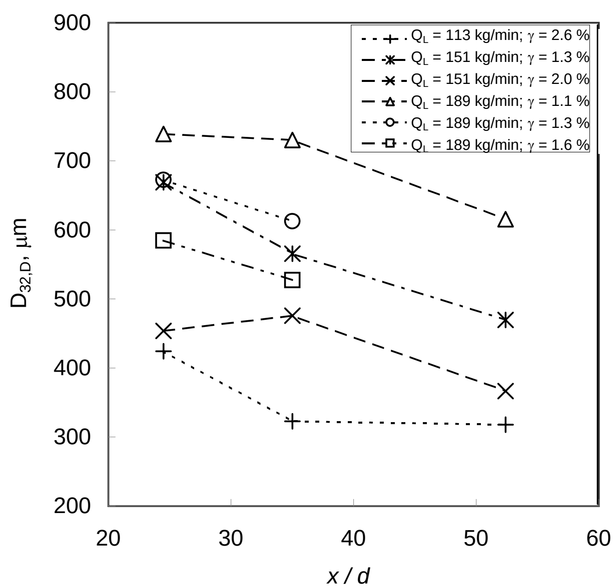

Figure 4.3: Droplet Sauter mean diameter axial variation along the centre line.

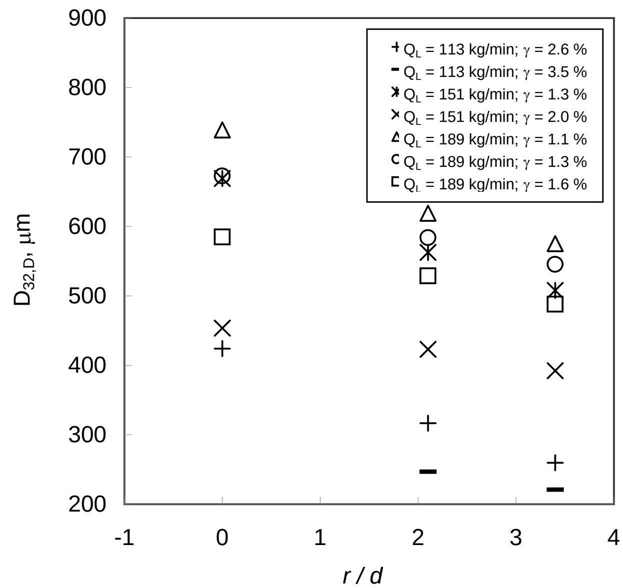

Figure 4.4: Droplet Sauter mean diameter radial profile at $x/d = 24.5$.

As expected for effervescent atomization, increasing the air flow rate, meaning increasing γ, produced a decrease in the D_{32} [**?**; **?**]. Figure 4.6 shows the experimental results for different liquid flow rates at a specific location (24.5 ; 3.4). The more air available, the higher the forces shredding the liquid sheets into ligaments and the ligaments into droplets. Note also, the relative insensitivity to the feed rate.

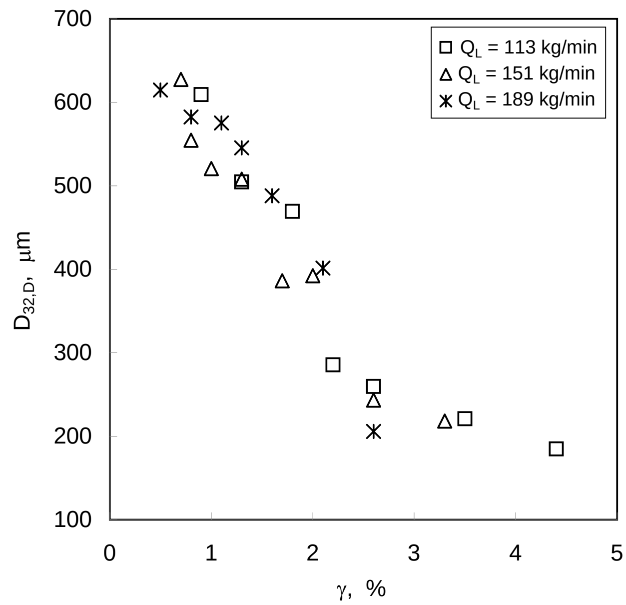

Figure 4.5: Droplet Sauter mean diameter as function of γ at location (24.5 ; 3.4) for different liquid flow rates, $Q_{\mathrm{L}} = 113$, 151 and 189 kg/min.

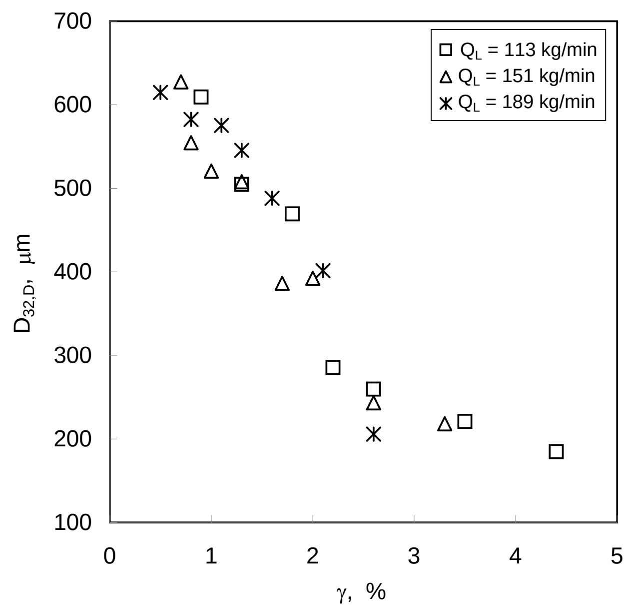

Figure 4.6: Droplet Sauter mean diameter as function of γ at location (24.5 ; 3.4) for different liquid flow rates, $Q_{\mathrm{L}} = 113$, 151 and 189 kg/min.

4.4.1 Droplet size distribution

In some spray applications, such as combustion, the efficiency of the process is a function of the resulting droplets from the atomization. Some studies have shown that not only the mean droplet diameter but also the droplet size distribution, (DSD), influences the downstream process, as it was shown experimentally by **?**. They found that a narrower DSD enhances the combustion efficiency compared to a wider distribution. **?** also investigated DSD in order to reach optimal operating conditions. They obtained samples with different DSD and with the same D_{32}, changing γ.

Several investigations have been done to determine a representative mean droplet diameter, but a relatively few publications refers to droplet size distribution. Some models to predict droplet size distributions are: normal, log-normal, root-normal, and log-hyperbolic, Rosin-Rammler, Nukiyama-Tanasawa, etc. Analytical methods are also been developed based on the maximum entropy principle and the discrete probability function [**?**].

A typical droplet size distribution obtained from the experimental results is presented in Figure 4.7. Three DSD, corresponding to three different radial positions for the same axial location, were plotted respect to a normalized frequency as functions of the diameter classes selected to discretize the distributions.

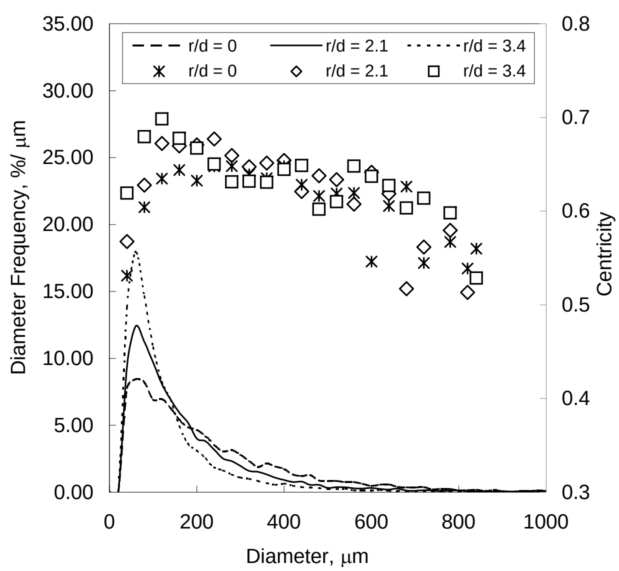

Figure 4.7: Droplet size distribution for normal diameter classes. Radial profile at $x/d = 24.5$ for $Q_{\mathrm{L}} = 151$ kg/min and $\gamma = 1$ %. Lines correspond to the diameter frequency by the left edge, whereas markers depict centricity by the right edge.

In the DSD plots the diameter frequency (% / μ) is the percentage of number of droplets in a bin diameter, respect to the number total of the sample, divided by the size of the bin. The DSD plots also depict the average centricity of the droplets by the right axis; centricity and its distribution are defined and discussed in Section 4.4.2.

The distributions are unimodal, with a larger presence of smaller droplets at locations furthest from the centreline. Long tails are presented at $r/d = 0$ and 2.1, indicating the detection of larger droplets ($D > 400$ μm) for both cases, which is usually an undesired condition for combustion processes, since large fuel droplets often result in soot or incomplete combustion. The $r/d = 3.4$ shows the formation of a larger amount of smaller droplets for this type of nozzle.

When the same DSD data are plotted as a the diameter frquency normalized by the logarithm of the size bin as a function of classes based on the logarithm of the diameter a normal-like distribution is obtained, as it is shown in Figure 4.8. This suggests data can be fitted to a log-normal distribution. Thus, distributions are characterized by the geometric mean D_g and the geometric standard deviation S_g.

No theory is presented to explain why size distributions fit to specific mathematical model. It is merely an empirical trail and error process to evaluate how a model predicts the experimental data. There is no accurate measure of the "goodness of fit" of those models; instead several statistical expressions have been proposed to be used as selection criteria, such as: sum of square residuals (SSR), the Anderson-Darling test, the Chi-square test and Kolmogorov-Smirvov test. For this study the Anderson-Darling (A-D) test was selected to evaluate the agreement of the model to the experimental values.

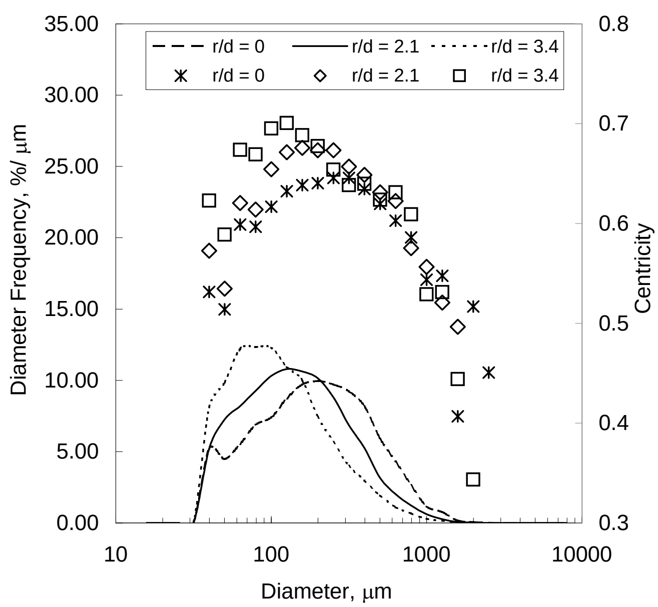

Figure 4.8: Droplet size distribution for log - binned diameter classes. Radial profile at $x/d = 24.5$ for $Q_{\mathrm{L}} = 151$ kg/min and $\gamma = 1$ %.

The agreement with the log-normal distribution for the data plotted in Figure 4.8 is represented in Figure 4.9; each plot corresponds to one of the three radial locations tested. The mathematical models and the experimental results were plotted as function of the log-bin diameter classes. For most all the conditions tested, the model fitted the data and it was found to be a better "goodness of fit" for locations further from the centreline, according to the A-D test. For those locations, more droplets were detected, thus more data were available for the model.

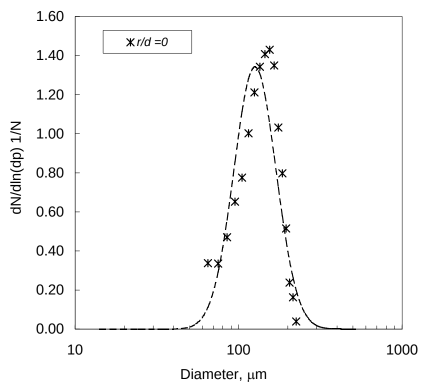

(a)

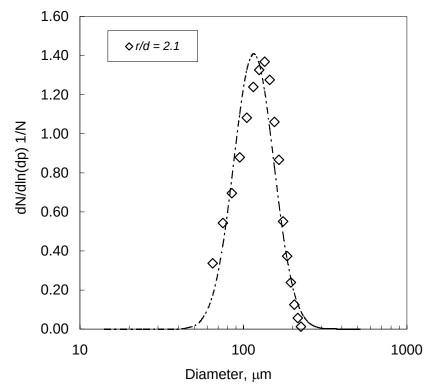

(b)

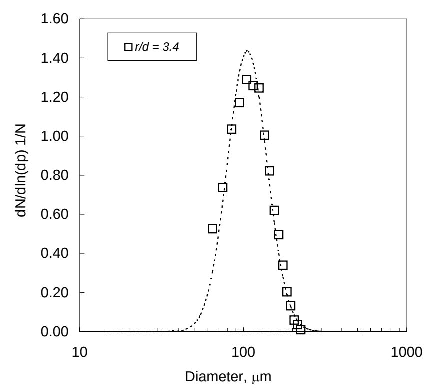

(c)

Figure 4.9: Log-normal model fitted to different droplet size distributions for $Q_{\mathrm{L}} = 151$ kg/min and $\gamma = 1$ %, at $x/d = 24.5$. The dotted lines represent the mathematical models.

The DSD presented in Figure 4.8 corresponds to the radial profile at $x/d = 24.5$ for a liquid rate of 151 kg/min and γ of 1 %. A larger amount of small droplets are found for locations further from the centreline ($r/d = 3.4$). This shows that liquid located at the edges of the spray is already transformed into droplets. The size range also decreases with the increase of r/d. Larger droplets ($D > 1000$ μm) are only observed at the centerline.

This is also observed in Figure 4.9 where the distributions of three different locations and corresponding mathematical model are depicted, that the models are symmetric or even distributed on both sides of the mean. Symmetry of a distribution is usually measured with its skewness. As the mathematical models are symmetric their skewness is equal to zero. However, the distributions at the centerline are negative skew [Figure 4.9 (a)], indicating an asymmetry caused by the presence of larger droplets and a long tail at that specific location. Meanwhile at the edge of the spray, [Figure 4.9 (c)], distributions reveal values for skewness were closer to zero; thus, they are in a "better" agreement with the mathematical models.

Moreover Figure 4.8 shows left-shifted distributions indicate an increment in the amount of small droplets detected. It is also produced, as expected, with the increase of the gas flow rate. Since the gas phase shears the liquid sheets into ligaments and droplets, the more air added, the more and smaller droplets are formed, as it is shown in Figure 4.10. An increase of the air flow rate enhances the atomization quality and the DSD is shifted to a range of smaller diameter values. The effect of increasing γ is more evident for higher liquid flow rates and for axial positions further from the nozzle tip, as shown in Figure 4.10 and Figure 4.11.

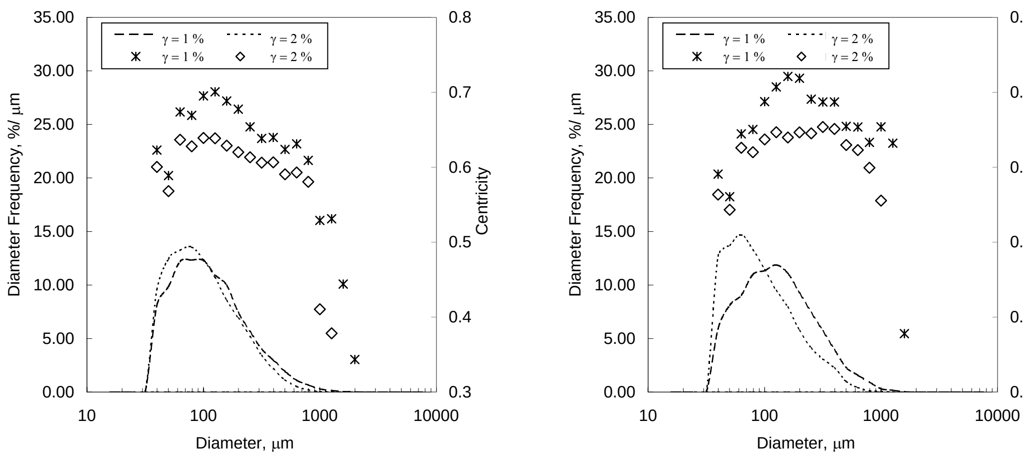

(a) (b)

Figure 4.10: Droplet size distribution for $Q_{\mathrm{L}} = 151$ kg/min for different air to liquid ratio γ at: (a) (24.5 ; 3.4) and (b) (32.0 ; 3.4).

The radial profile for $Q_{\mathrm{L}} = 151$ kg/min and $\gamma = 1\%$ at a different axial location ($x/d = 35$) is shown in Figure 4.12. As was discussed for ($x/d = 24.5$), larger droplets are found in the centreline and smaller droplets were detected close to the edge of the spray. An analysis of two radial distributions at two different axial locations is possible by comparing Figure 4.8 with Figure 4.12. DSD have the same trends with similar shape compared to those acquired at $x/d = 24.5$; the larger values of r/d result in larger amounts of smaller droplets and in a narrower distribution. Meanwhile, a wider distribution is found for locations further the nozzle tip.

It is observed for locations further from the nozzle tip (Figure 4.12) the distributions

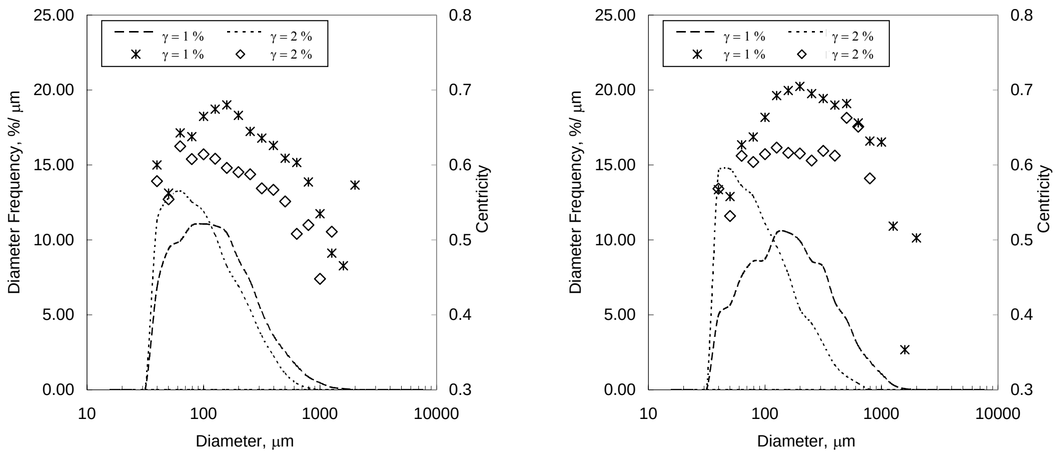

(a) (b)

Figure 4.11: Droplet size distribution for $Q_{\mathrm{L}} = 189$ kg/min for different air to liquid ratio γ at location: (a) (24.5 ; 3.4) and (b) (32 ; 3.4).

are similar and the geometric mean does not show a significantly variation along the radial profile. Thus the DSD evolves downstream to become less dependent on radius. The diameter values with the highest frequency are larger compared to $x/d = 24.5$ with higher average diameter. An important amount of droplets larger D > 500 μm is detected at all distributions, specially for $r/d = 2.1$ and 3.4.

At $r/d = 3.4$ more droplets were observed for locations closer to the nozzle tip, $x/d = 24.5$ compared to $x/d = 35$. This is caused by the shape of the spray envelope making some locations close to the bubble explosion zone of the spray where droplets are not completely formed.

Similar results were found for a higher flow rates. Figure 4.13 shows the droplet size distribution for $Q_{\mathrm{L}} = 189$ kg/min and $\gamma = 2$ % at three radial position at two different axial locations $x/d = 24.5$ and $x/d = 32$.

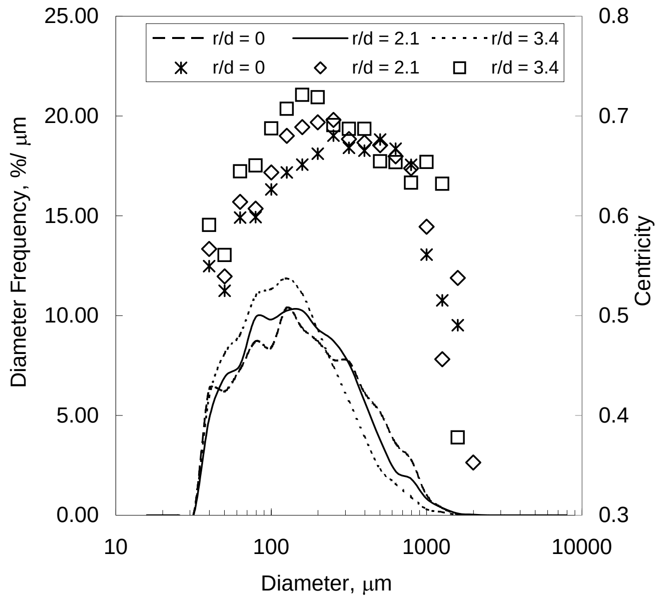

Figure 4.12: Droplet size distribution radial profile at $x/d = 35.0$ for $Q_{\mathrm{L}} = 151$ kg/min and $\gamma = 1$ %.

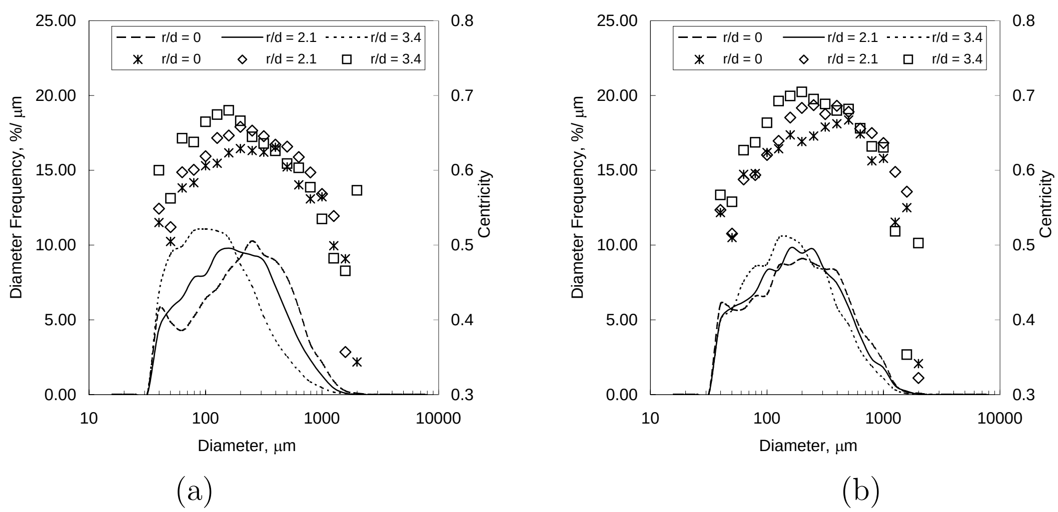

Figure 4.13: Droplet size distributions for $Q_{\mathrm{L}} = 189$ kg/min and $\gamma = 2$ % for (a) $x/d = 24.5$; and (b) $x/d = 35$.

For most of the conditions tested, the radial profile of the DSD at $x/d = 24.5$ and 35 has similar to the ones already represented. The data followed a log-normal distribution, a better "goodness of fit" was reported for $r/d = 3.4$, according to A-D test, with a lower geometric mean and a narrower distribution. Figure 4.14 shows the radial profile of the DSD for $Q_{\mathrm{L}} = 113$ kg/min – $\gamma = 3$ %; the comparison between the mathematical model and the experimental data is depicted in Figure 4.15. For a higher liquid flow rate, $Q_{\mathrm{L}} = 189$ kg/min – $\gamma = 2$ %, the data for the DSD and the comparions with the mathematical model are shown in Figure 4.16 and Figure 4.17, respectively.

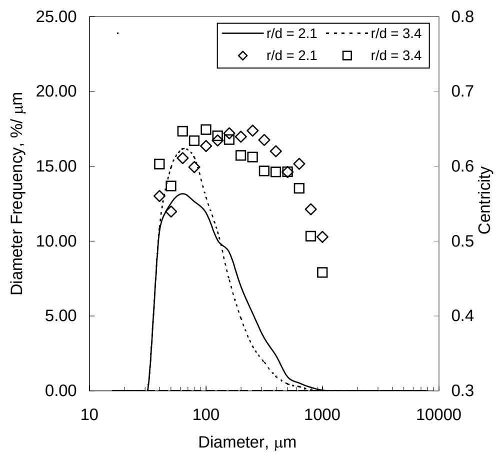

Figure 4.14: Radial profile of the droplet size distribution at $x/d = 24.5$ for $Q_{\mathrm{L}} = 113$ kg/min and $\gamma = 3$ %.Log-normal model fitted to droplet size distributions.

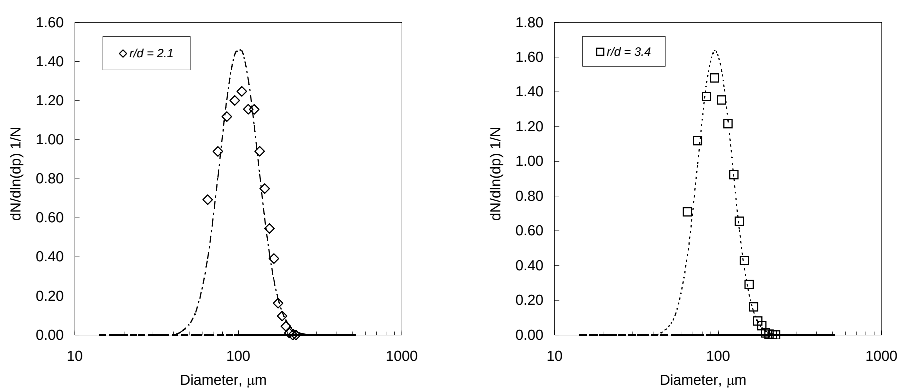

(a) (b)

Figure 4.15: Log-normal model fitted to different droplet size distributions for $Q_{\mathrm{L}} = 113$ kg/min and $\gamma = 3$ %, at $x/d = 24.5$ and three different radial locations. The dotted lines represent the mathematical models.

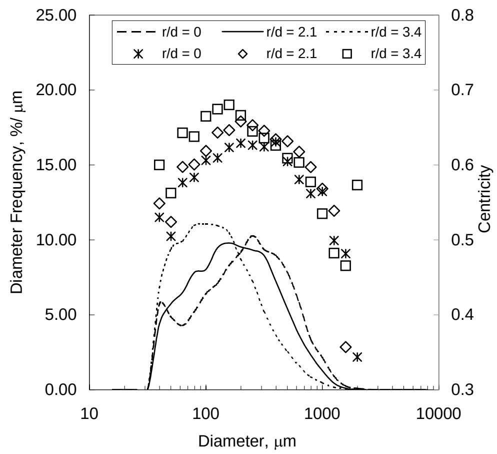

Figure 4.16: Droplet size distribution radial profile at $x/d = 24.5$ for $Q_{\mathrm{L}} = 189$ kg/min and $\gamma = 2$ %

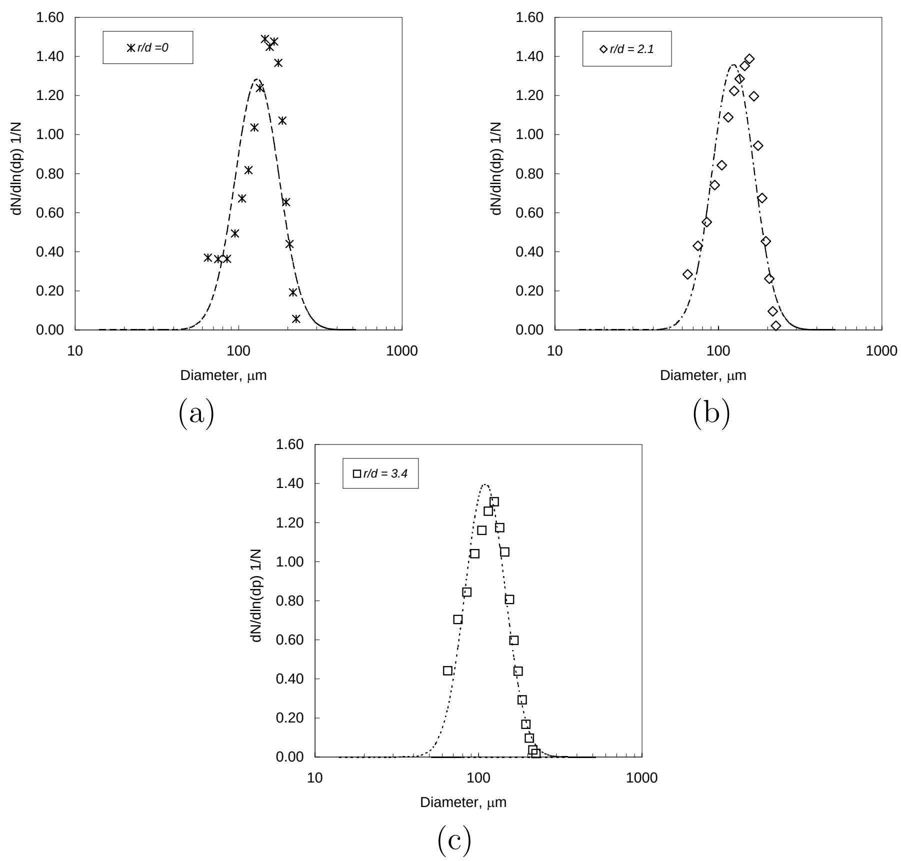

Figure 4.17: Log-normal model fitted to different droplet size distributions for $Q_{\mathrm{L}} = 189$ kg/min and $\gamma = 2$ %, at $x/d = 24.5$ and three different radial locations. The dotted lines represent the mathematical models.

One effect observed at the high liquid flow rate tested ($Q_{\mathrm{L}} = 189$ kg/min) at the centerline was a bimodal distribution shown in Figure 4.16 (a). There was not obvious explanation to attribute this bimodal nature, other than the droplet formation process is not completed in that zone for those conditions, reducing the size of the sample in comparison with other locations. As previously discussed, at the centerline, less droplets are completely formed.

The evolution of the spray along the centreline is presented in Figure 4.18. The lowest values of the "goodness of fit" were found at the centerline; however, the log-normal model still doest fit the experimental data, as shown in Figure 4.18 and Figure **??**.

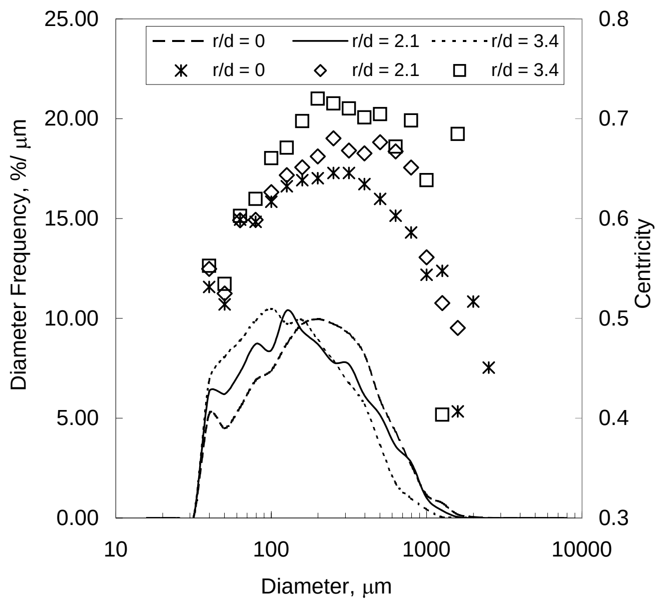

Figure 4.18: DSD Axial evolution along the centreline for $Q_{\mathrm{L}} = 151$ kg/min and $\gamma = 2$ %.

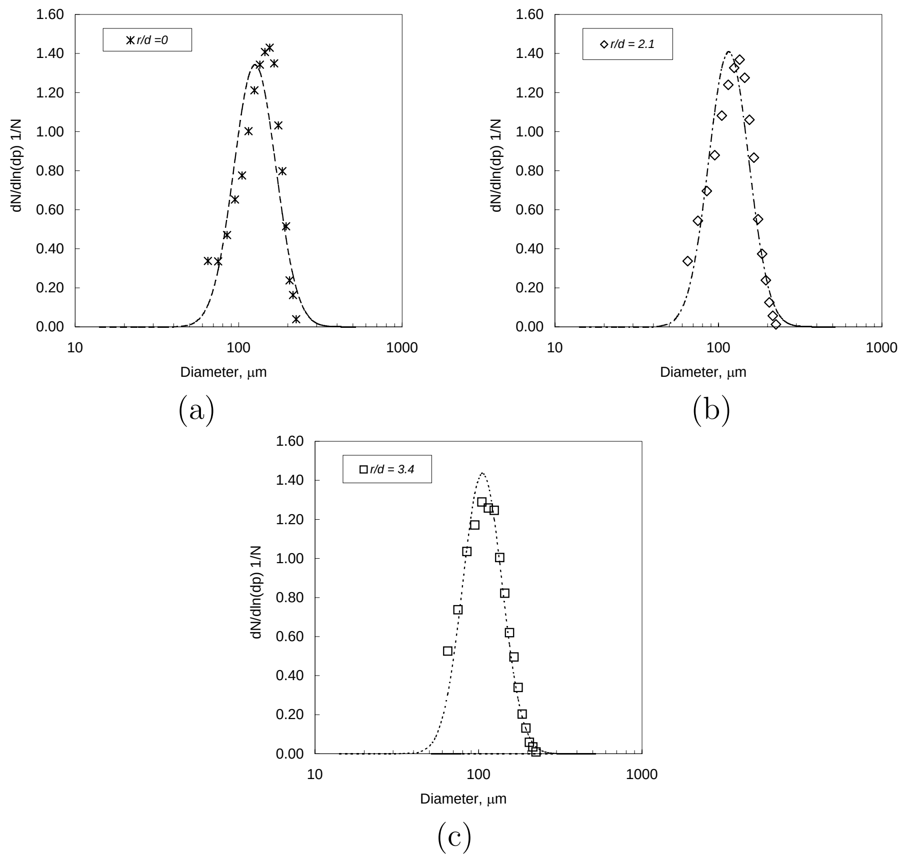

Figure 4.19: Log-normal model fitted to different droplet size distributions for $Q_{\mathrm{L}} = 151$ kg/min and $\gamma = 2$ %, at $x/d = 24.5$ and three different radial location. The dotted lines represent the mathematical models.

4.4.2 Droplet shape distribution

The shape of the droplets, represented by centricity, is also reported in all the DSD plots. Since droplets are three– dimensional objects usually characterize them by only one parameter, such as one diameter, does not reveal information regarding the geometric or morphologic features. Based on that reason, centricity was selected to analyze the shape of the resulting droplets. Centricity is defined as the ratio from the shortest to longest axis as shown by Eq. 4.7.

$$\text{Centricity} = \frac{a}{b} \tag{4.7}$$

where “a” is the shortest axis and “b” the longest axis of the particle. From this definition, the centricity values are from 0 to 1; a perfect sphere has a centricity equals to one, meanwhile an elongated particle has centricity closer to zero. Figure 4.20 depicts examples of droplets and their centricity with indications of the shortest and longest diameters.

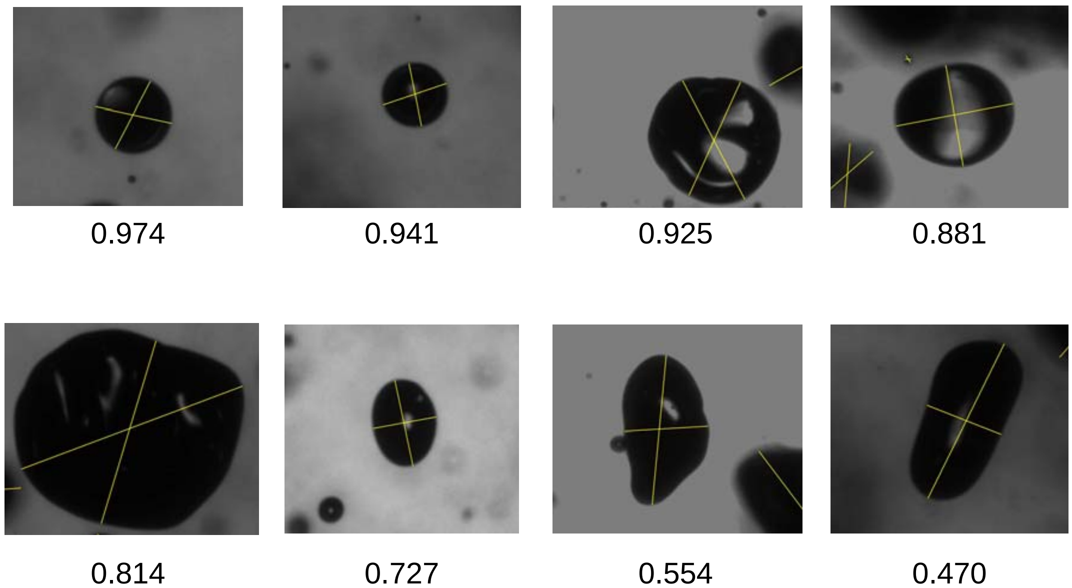

Figure 4.20: Examples of droplets with their centricity values. The shortest and longest diameters are superimposed on each particle

The peak droplet diameter has the higher centricity for most of the conditions tested. Smaller, spherical droplets (circularity near to 1.0) are found for $r/d = 3.4$; while droplets located at the centreline have a lower centricity. The presence of not fully atomized particles or ligaments at the centreline, where external stress plays a dominant role over the surface tension, indicates that elongated droplets are formed. The results also indicate that for larger droplets ($D > 200$ μm) centricity is less correlated to diameter. Large droplets ($D > 1000$ μm) tend to present values of centricity lower than 0.5, as expected since large droplet are not spherical and tend to be elongated.

Smaller droplets are expected to be more spherical, because the surface tension is larger than the external forces. However, for all locations, low centricity values are observed for the smallest droplets ($D < 40$ μm). The standard deviation of the shape parameter is higher for the smaller diameter droplets than for the larger diameter droplets. One possible cause could be the magnification, which may not be appropriate for imaging analysis of such smaller droplets. This effect was also observed in other studies [**?**; **?**], and investigated by **?** and **?**, leading to the same suggestion that a more sensitive technique has to be employed for smaller particle diameters.

For pharmaceutical applications **?**, suggested a minimum magnification of 20 μ m/pixel. However, their results may not be suitable for the industrial application related to this study. A high magnification significantly reduces the depth of field and the field of view, which may produce a lower edge definition and increase of the number of images required to be taken.

4.4.3 Velocity distributions and velocity vs. droplet size

In order to establish the relation between droplet size and the droplet velocity, velocity measurements were performed with shadowgraphy. Two images were taken at the same volume control separated by a known time interval, Δt. Each droplet was identified in the two images; the displacement was estimated as the variation of position in the second image with respect to the first one. Knowing the displacement and the value of Δt, the software estimates the velocity. Velocity was measured at the same locations for size measurements shown in Figure 4.1.

Velocity measurements have unimodal distributions as expected for effervescent sprays, as shown in Figure 4.21(a). For the same location, an increment in the amount of air produces a higher average velocity indicating that droplets move with the air velocity, and a wider distribution is obtained. This effect is also observed for higher liquid flow rates Figure 4.21 (b), however velocity distributions become narrower for this case.

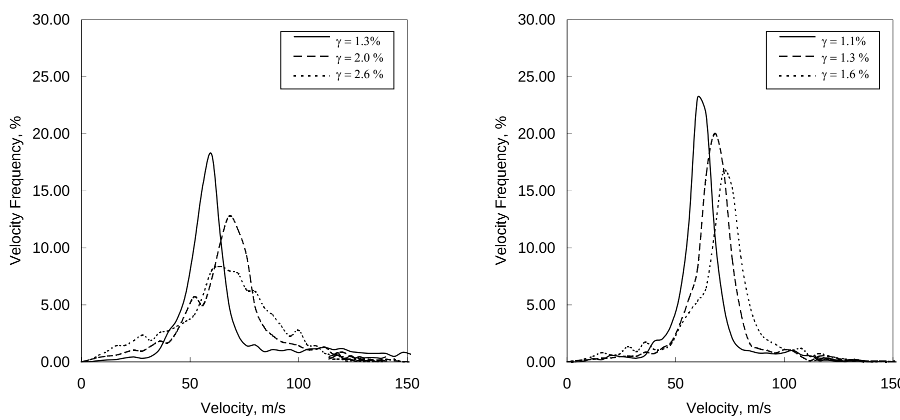

(a) (b)

Figure 4.21: Velocity distribution for different air to liquid ratio, γ, at (24.5 ; 3.4) for (a) $Q_{\mathrm{L}} = 151\ kg/min$ and (b) $Q_{\mathrm{L}} = 189 kg/min$.

Evaluating the radial profile at two different axial positions ($x/d = 24.5$ and 35), Figure 4.22, the bell shaped curves shift to the left for positions further along the centreline; meaning that at the edge of the spray droplets travels at lower velocities compared to centerline. For instance, the velocity distribution for a liquid flow rate of 151 kg/min and $\gamma = 2$ %, the peak of the distribution at $r/d = 3.4$ is for 9 % of the droplets at 56 m/s, meanwhile at the centreline 10 % of the droplets travel at 72 m/s. Similar results were obtained for a higher liquid flow rate, as show in Figure 4.23.

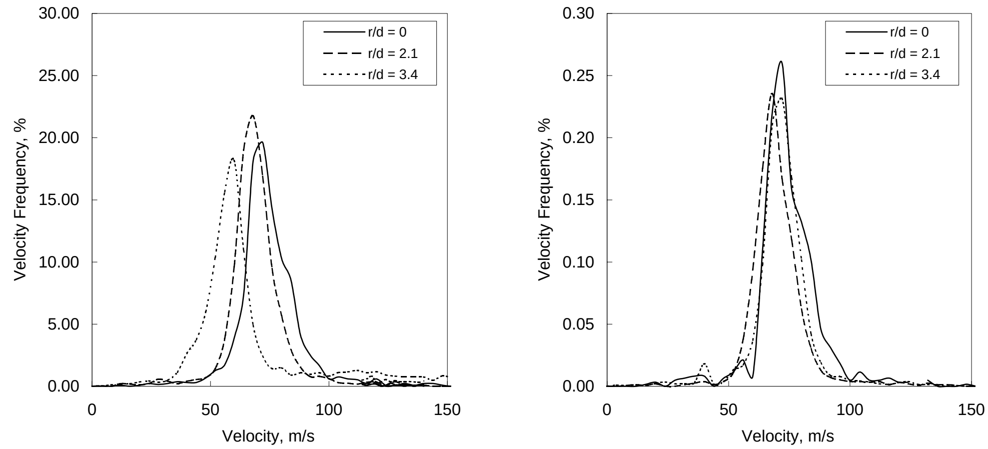

(a) (b)

Figure 4.22: Velocity distribution radial profile at for (a) $Q_{\mathrm{L}} = 151\ kg/min\ \gamma = 2\ \%$ for (a) $x/d = 24.5$ and (b) $x/d = 32$.

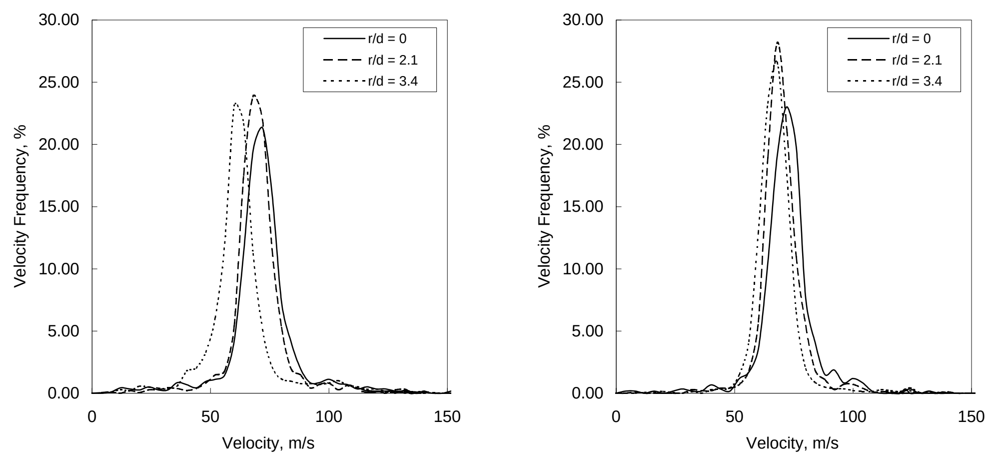

(a) (b)

Figure 4.23: Velocity distribution radial profile at for a) $Q_{\mathrm{L}} = 189\ kg/min - \gamma = 2\%$ for (a) $x/d = \mathit{24.5}$ and (b) $x/d = \mathit{35}$.

The axial evolution was analyzed taking the velocity at three positions along the centreline (x/d = 24.5, 35 and 52.4). No significant changes were observed in the distributions, with the exception of the reduction of the average velocity for locations further from the nozzle tip.

An analysis of the effect of the diameter on the velocities was done plotting the droplet diameter in the abscissa and in the axis the average corresponding to all droplets included in that size bin on diameter. Velocity tends to increase with the decrease of diameter for positions at the edge of the spray, for most of the conditions tested.

Droplets with smaller diameters have lower velocities, as shown in Figure 4.24, because of the entrainment effect; meanwhile at the centerline, velocity is poorly correlated to diameter. This is caused by aerodynamic forces of the turbulent air flow at the edge of the spray and the presence of non fully atomized particles, as observed by **?**.

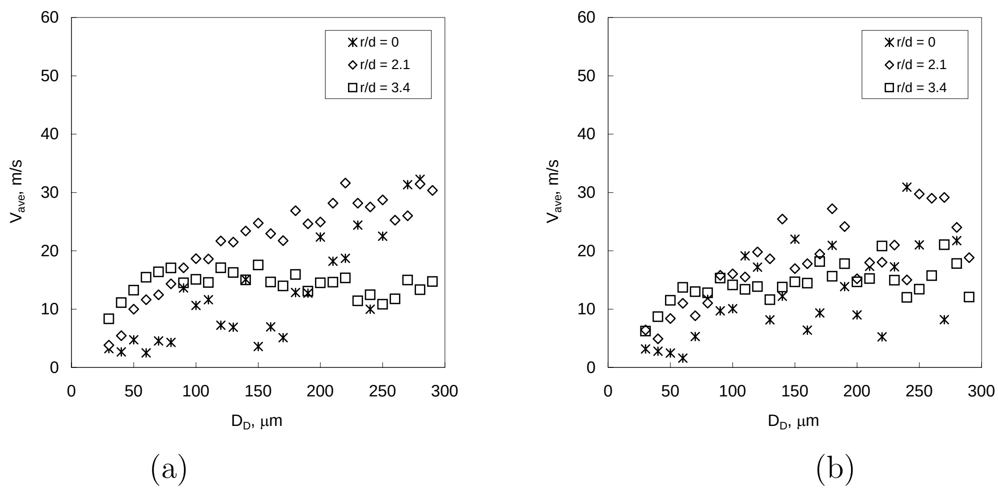

Figure 4.24: Average velocity versus the diameter of the droplet at $x/d = 24.5$ for (a) $Q_\mathrm{L} = 151\ kg/min - \gamma = 2$ % and (b) $Q_\mathrm{L} = 189\ kg/min - \gamma = 2$ %.

4.4.4 Impact probe

The droplet size depends on the location where it is measured. A representative control volume will have the maximum momentum rate. For a two-phase flow, an analytical calculation of the momentum rate is quite complex because it requires the determination of the velocities of both phases calculated through the solutions of the constitutive equations.

Due to the complexity of the analytical calculations, many instruments have been proposed for measuring the momentum experimentally. Particulary, for effervescent atomization, a probe has been developed [**?**]. The momentum rate is proportional to the force acting on the probe.

For this investigation, an impact probe was installed inside the spray to observe its behavior and establish the spot of maximum momentum among the locations tested. The distribution and behavior of the spray is represented by the distribution and behavior of the droplets of the sample.

The momentum was measured by inserting the probe into the spray at the same locations tested for size measurement and shown in Figure 4.1. The objective was to measure the force acting on the probe and thus the momentum rate. The output of the probe, linearly proportional to the force in Newtons, was obtained in volts, observed and recorded on an oscilloscope. Results from the measurements with the impact probe are shown in Figure 4.25. A large impact or force was found for values of r furthest the centreline and increased with increasing γ. The larger the value of γ the larger amount of gas is available to break up the liquid ligaments.

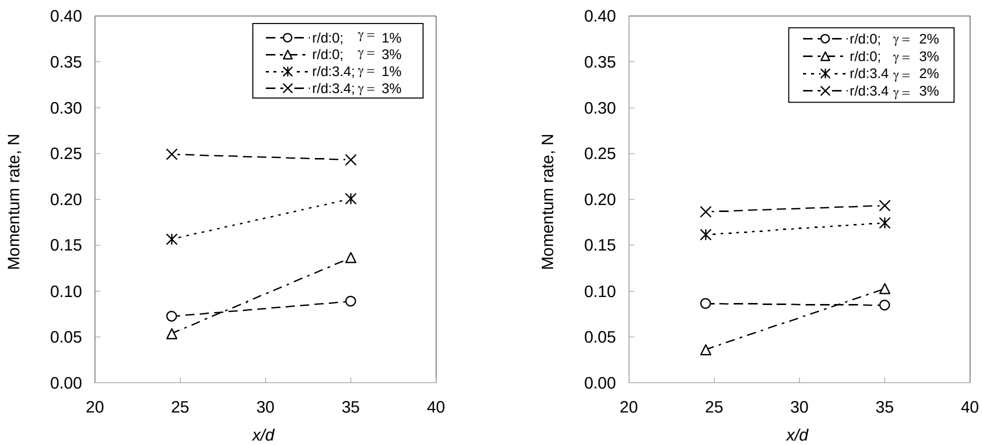

Figure 4.25: Results of the impact probe at different axial and radial locations for (a) $Q_{\mathrm{L}} = 151\ kg/min$ and (b) $Q_{\mathrm{L}} = 189\ kg/min$.

4.4.5 Bubble breaker

A plate with holes perforated in it, referred to as a bubble breaker, was installed in the feeding conduit upstream of the nozzle to study its influence in the atomization particularly in the resulting droplets. Experiments were performed with the same working conditions and at the same locations. Pressure after the bubble breaker was also measured to ensure that the inlet pressure was kept almost constant, compared to the corresponding run without the bubble breaker.

The incorporation of the bubble breaker produced DSD with the same trends compared to those obtained without it. A log-normal distribution also fitted to the data. An important effect observed in the DSD was the major presence of smaller droplets as it is shown in Figure 4.26 with a higher frequency of droplets with a diameter lower than 200 μ. This effect was detected for most of the conditions tested also observed at high liquid flow rate $Q_{\mathrm{L}} = 189\ kg/min$, as shown in Figure 4.27.

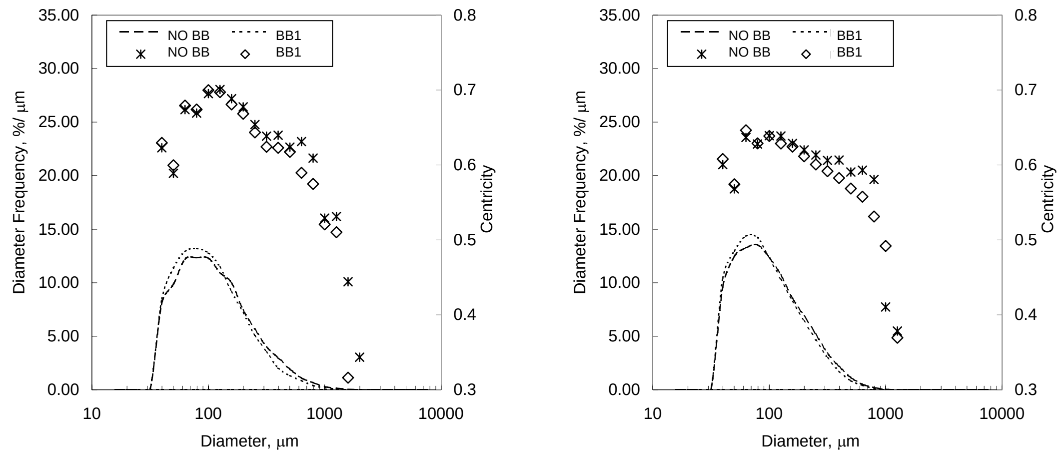

Figure 4.26: Droplet size distributions for two configurations, without bubble breaker and with a bubble breaker, at (24.5 ; 3.4) for $Q_{\rm L} = 151\ kg/min$ and (a) $\gamma = 1$ %; (b) $\gamma = 2$ %.

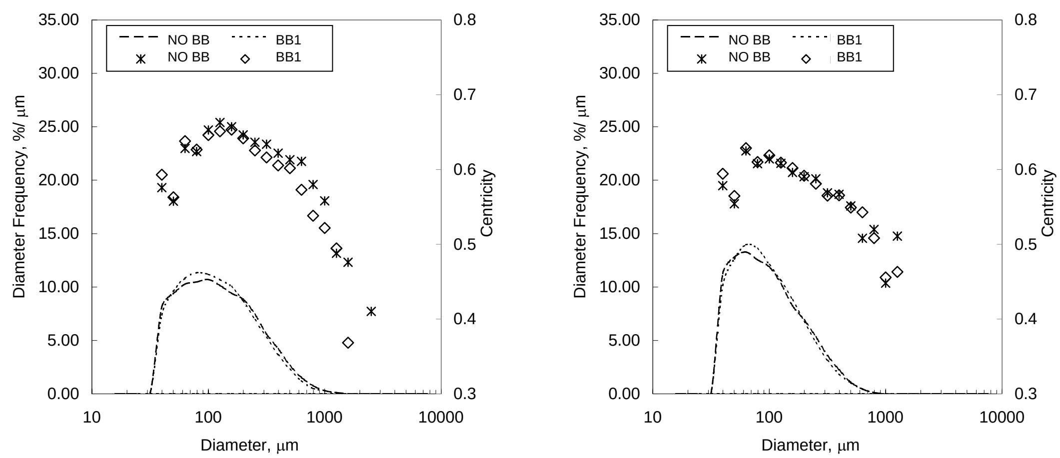

Figure 4.27: Droplet size distributions for two configurations, without bubble breaker and with a bubble breaker, at (24.5 ; 3.4) for $Q_{\rm L} = 189\ kg/min$ (a) $\gamma = 1$ %; (b) $\gamma = 2$ %.

4.5 Proposed procedure for droplet size measurement

The literature does not show an unique procedure to measure droplet size in a spray. Nevertheless, most of them follow these proposed steps:

- Identify the range size of droplets to be measured.
- Select the type of measurement technique.
- Define the instrumentation required.
- Select the locations where measurement will be done.
- Select the characteristics diameters and averaging approaches.
- Select the working conditions.
- Based on the technique, select settings to be evaluated or used.
- Take measurements and analyze the results.
- Repeat experiment to verify repeatability.

4.6 Conclusions

A characterization of the performance of an effervescent atomizer was investigated in terms of DSD, sphericity and velocity, all with respect to variations in working conditions, liquid mass flow and air to liquid ratio. Droplet size has a strong dependency of the technique and locations selected. The characterization of an effervescent spray is not a standard procedure. Raw data have to be analyzed to find the mathematical model more appropriated to interpret, extrapolate or analyze the results.

The shadowgraphy measurement technique produces images that not only estimate the size and velocity of the resulting droplets, but also reveals their shape. This technique provides information on the conditions required to create droplets of a desired size and shape.

Non-spherical droplets are observed at each location, mainly at locations near the nozzle tip and along the centreline. Studies of the shape of small droplets should include an analysis of the principles of the technique employed, in terms of the discretization error and the pixel per particles required to avoid erroneous conclusions. The D_{32} is highly sensitive to changes in the working conditions and the measurement locations.

An appropriate location for spray characterization was determined with an impact probe. Droplet size distribution data fitted a log-normal distribution, with a closer agreement for locations further from the centreline. Velocity distributions were unimodal as expected for effervescent atomization. A correlation was found between velocity and droplet size, smaller droplets travel at lower velocity.

Findings reported in this study may be applicable for other atomizer designs for the same working conditions and configurations. However the geometry of the atomizer influences the droplet size, shape and velocity. To extend the conclusions of this study an analysis of new working conditions, settings and configurations should be conducted to avoid yield to erroneous conclusions.

References

Chapter 5

Bubble Size Influence on an Effervescent Spray

5.1 Abstract

An experimental study is presented of a spray atomizer used in heavy oil upgrading. Bubble size in the feed flow was observed to determine its influence on the atomization of an effervescent nozzle. Experiments were conducted with water and air in a two-phase flow commercial-scale facility at room conditions (horizontal air/water bubbly feed in a 25.4 mm tube to a single contraction throat diameter of 12.7 mm). Different mixtures were tested with water flow rates from 113 to 200 kg/min and 1 to 4 kg/min for air flow rate, achieving an air liquid mass ratio, γ, from 1 % to 4 %. The range of feed parameters result in flow regimes that are either bubbly or intermittent in equilibrium horizontal flow. Two bubble breakers (perforated plates) were used to modify the size of the bubbles in the conduit feeding the nozzle. Bubble and droplet sizes were measured with visualization techniques using front lighting for bubbles and shadowgraphy for droplets. A single location in the spray cone was chosen as the characteristic location in the flow where droplet size and distribution are most representative of the mass flow of the spray liquid. Acquired images were used to estimate the size and calculate the Sauter mean diameter. The experiments indicate the influence of the scale of bubbles in the feed on the reduction of the size of the resulting droplets in the atomization and support the need for attention in designing the feed delivery premixing and transport to the nozzle.

5.2 Introduction

The need of the production of a spray with appropriate quality for combustion purposes has increased the investigation in effervescent atomization. This technique, developed by Lefebvre (1989), generates good atomization at a lower injection pressure that the one required for other types of atomizers. It is characterized by a two-phase flow entering the nozzle as twin-fluid atomization; however, in this case the gas phase is not intended to transmit its energy to the liquid, instead the droplets are created by the explosion of the gas bubbles to the atmospheric pressure when exiting the nozzle tip. Gas bubbles explode shearing the liquid into ligaments and finally into fine droplets.

Many studies have been done regarding the parameters that determine the quality of the atomization and the experimental conditions required to create droplets in a specific size range. It has been established that the characteristics of the two-phase flow upstream of the nozzle affects the atomization [Lefebvre, 1989; Ballester and Dopazo, 1996; Sovani et al., 2001].

With respect to the influence of the flow pattern it has been demonstrated that Intermittent flow generates an unsteady spray [Maldonado, 2006]. On the other hand, smaller droplets are achieved for higher values of γ [Lefebvre, 1989; Jedelsky et al., 2009; Sovani et al., 2001] suggesting annular flow as the most desirable flow pattern to obtain smaller droplets in the spray, though this requires high gas rates. It seems that Dispersed Bubble (DB) flow pattern is the most achievable and advantageous condition to generate an appropriate spray.

Several flow pattern maps have been proposed in the literature to theoretically predict the flow pattern given a set of conditions. One of the most cited works for horizontal pipe was developed by Taitel and Dukler (1976). According to their map, two flow patterns are encountered in this investigation: intermittent and dispersed bubble.

In the dispersed bubble flow pattern the gas is roughly uniformly distributed in the form of bubbles in the continuous liquid phase. Although, in effervescent atomization the production of the droplets is generated by the explosion of bubbles, no literature has been found regarding the influence of the bubble size, bubble distribution and bubble concentration on the spray.

This study utilized a plate with perforated holes to generate fine and uniformly distributed bubbles as an option to achieve this necessary condition in two phase flow feeding the nozzle. Understanding the operation of a two-phase flow system, to optimize the performance and increase its efficiency, is only possible through the comprehension of the flow patterns and its mechanism for transitions.

Image techniques were employed to measure bubble size, represented by the Sauter mean diameter, $D_{32,\mathrm{B}}$, (a detailed definition is presented in Section 4.2.2). Due to the possible uneven radial distribution of the bubbles in the pipe for some conditions, D_{32} was selected because its independency from any radial bubble distribution and concentration in the cross section of the pipe [Kocamustafaogullari and Wang, 1991]. Then, bubble sizes were compared to the droplet sizes of the resulting spray. This investigation was performed in an effort to provide measurements of the bubbles and their influence on spray performance, and with it, assist in the analysis of the proper working conditions to achieve a quality spray for effervescent nozzles.

5.3 The Experiments

Experiments were performed in a liquid-gas horizontal flow in a nozzle assembly to investigate bubble size. A detailed description of the components and the followed procedure is provided in Chapter 3.

5.4 Bubble Size

To enhance the dispersion and distribution of gas bubbles in the two-phase flow entering the nozzle, a bubble breaker was proposed. The objective was to produce a larger amount of smaller bubbles, uniformly distributed, along the feeding conduit. The Bubble Breaker consists of a plate perforated with multiple orifices in a concentric position relative to a central axis of the conduit.

Ideally, larger bubbles will decrease their sizes into a larger amount of smaller bubbles. In addition they will be uniformly distributed because of the position of the orifices in the plate. As the size of the bubble decreases, smaller and finer bubbles are dispersed and this causes an increase in the average void fraction. However, the gain in the void fraction is made at the price of a pressure drop over the obstruction.

Figure 5.1 shows the evolution of bubble size as function of the air to liquid mass ratio, γ, with and without the bubble breaker for three water flow rates. For each run, increasing γ creates smaller bubbles as expected. The more air available in the mixture, the higher the turbulent forces shredding elongated gas bubbles into smaller bubbles. Increasing γ also determines the transition of the intermittent flow to dispersed bubble flow, characterized by the presence of small and distributed gas bubbles.

The data plotted in Figure 5.1 clearly demonstrate the capacity of a bubble breaker to reduce the bubble size. For instance, for $Q_{\mathrm{L}} = 113$ kg/min the bubble diameter $D_{32,\mathrm{B}}$ is in the range of 225 – 420 μm without bubble breaker; meanwhile for BB_1 is 101-251 μm. The plate with smaller diameter holes, identified as BB_1, creates smaller bubbles compared to BB_2; however a higher pressure drop through the plate was measured. Similar trends were observed for higher liquid flow rate $\mathrm{Q_L} = 189$ kg/min, as it is shown in Figure 5.1 (c).

The shape of the bubbles in the two-phase flow was also characterized by their centricity (the ratio from the shortest to longest axis). Bubbles breakers also affect the shape of the bubbles by making them more spherical (centricity near to 1.0). On average over all flow rates, the bubbles without any accessory have centricity value of 0.67; meanwhile the BB_2 produces bubbles of centricity equals to 0.79.

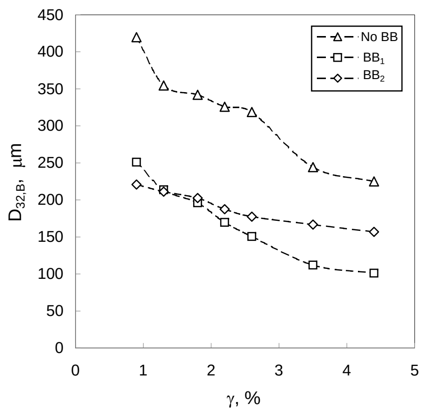

(a)

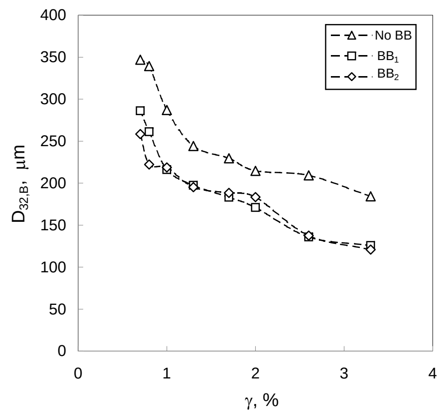

(b)

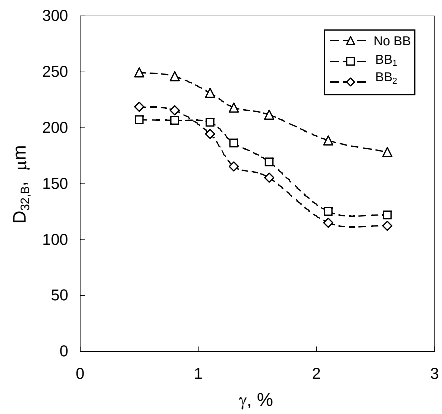

(c)

Figure 5.1: Influence of the bubble breaker on the bubble size for (a) $Q_{\mathrm{L}} = 113$ kg/min, (b) $Q_{\mathrm{L}} = 151$ kg/min and (c) $Q_{\mathrm{L}} = 189$ kg/min.

5.4.1 Bubble breaker and pressure

The investigation of the influence of one parameter (bubble size) on the spray must be done keeping other potentially confounding parameters invariant. For this reason, pressure was measured for each run, since it is the individual parameter with the greatest impact on atomization [Lefebvre et al., 1988]. Figure 5.2 shows the injection pressure for the standard configuration (No BB) and two modified configurations, with BB_1 and BB_2. The pumping pressure was adjusted so that the inlet pressure did not change significantly with the presence of the bubble breaker in the feeding pipe, compared with the standard configuration. Variations of the injection pressure of both modified configurations was of 3.2 % average compared to the standard configuration for all the conditions tested.

For all cases, it is observed that the injection pressure has the same trend for all the

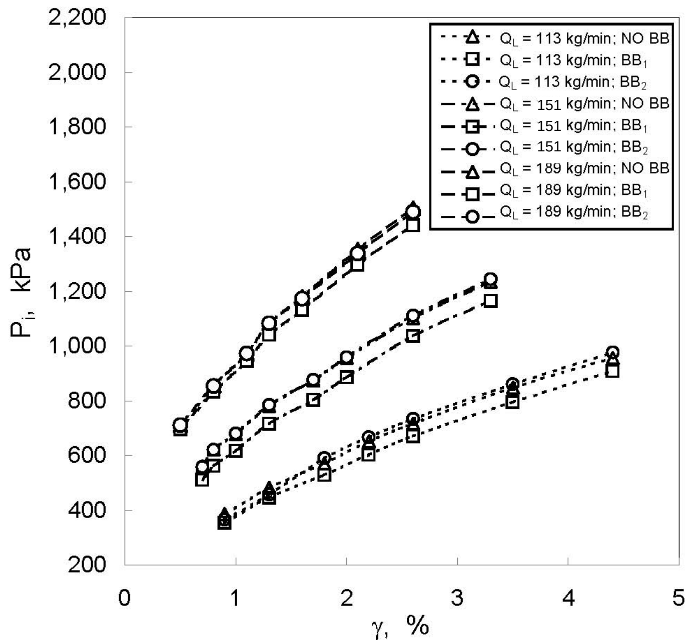

Figure 5.2: Delivery pressure versus γ for different configurations, with and without bubble breaker, at different liquid flow rates.

configurations. BB_2 produces an inlet pressure nearer to the values of the standard configuration compared to BB_1, particularly for high liquid flow rate, $Q_L = 189$ kg/min. For instance, without bubble breaker for $Q_L = 151$ kg/min and $\gamma = 1.3$ %, the inlet pressure is 784 kPa, meanwhile for BB_1 is 716 kPa which corresponds to 8.66% variation and for BB_2 is 781 kPa with 0.5 % variation from the standard configuration. For all cases the inlet pressure of the proposed configurations does not change larger than 9.2 %.

Since the injection pressure was kept constant, a pressure drop is presented through the bubble breakers, caused by back pressure created by the air and water flow as single phase flows. Without bubble breaker the pressure does not change significantly along the pipe but once the bubble breaker is installed a significant pressure drop was measured. Experimental results are presented in Figure 5.3. These values depend on the flow rates and number, size and distribution of the holes of the accessory.

Despite the abundant literature available about pressure drop through pipe accessories such as orifice plate, nozzles, venture and diffuser, most of the information is for single orifice plates and one phase flow. Limited information is available for two-phase flow through a multiple-orifice plate, with results applicable for certain conditions. For a single orifice plate, the pressure drop depends mainly on the vena contracta; meanwhile in a multiple orifices plate depends on many parameters as the operating pressure, orifice configuration, thickness of the plate, etc. In addition, in a two-phase

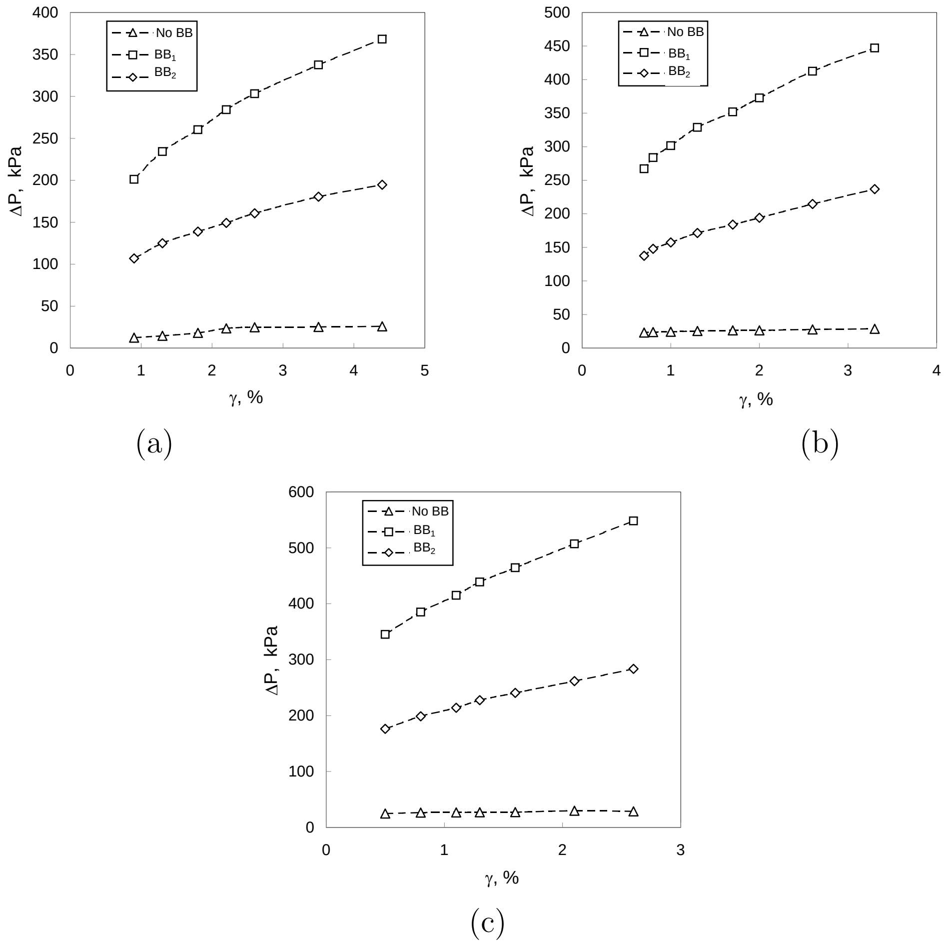

Figure 5.3: Pressure drop along the feeding pipe, with and without bubble breaker (a) $Q_{\mathrm{L}} = 113$ kg/min, (b) $Q_{\mathrm{L}} = 151$ kg/min and (c) $Q_{\mathrm{L}} = 189$ kg/min.

flow, the pressure drop is affected by the compressible phase.

With the insertion of the bubble breaker, larger bubbles will decrease their sizes into larger amount of smaller bubbles, uniformly distributed. As the size of the bubbles decreases, smaller and finer bubbles are dispersed, and as a consequence there is a higher average void fraction. However, the gain in the void fraction is made at the price of a pressure drop over the obstruction. At the same time, a higher void fraction reduces the average fluid density and a lower pressure drop is caused. This might balance the pressure drop over the plate.

In this study, it was observed that decreasing γ, decreases the pressure drop measured, as shown in Figure 5.3. At low γ, less air is fed into the mixture, having a low superficial velocity. Similar to single phase flow case, the pressure drop is lower due to the low gas velocity.

5.4.2 Bubble size versus droplet size

Assuming that in the spray the sample distribution represents the total distribution of the resulting spray, droplets were sized at a specific location from the nozzle tip in the axial axis, x, and from the centre line in radial direction, r. The location was selected as the spot where droplets have their maximum momentum among the locations tested. An impact probe was inserted in the spray to measure the force of the droplets and with it the maximum momentum (a detailed procedure is explained in Section 4.4.4). The sample was selected to be at $x/d = 24.5$ and $r/d = 3.4$. Figure 5.4 presents the change in droplet size caused by the presence of the bubble breakers.

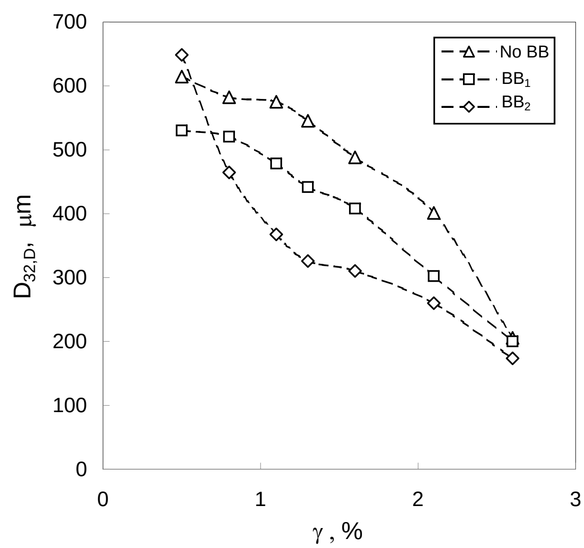

Figure 5.4: Influence of the bubble breakers in the droplet size for $Q_{\mathrm{L}} = 189$ kg/min.

Once bubbles are characterized, a relationship between the bubbles in the conduit and the resulting droplets in the spray was found. The presence of a bubble breaker clearly resulted in a reduction of the bubble size, and with it, a size reduction of droplets generated on the spray, as shown in Figure 5.5. For a effervescent nozzle it is believed that atomization is produced by the explosion of the air bubbles that shear the liquid into ligaments and finally into droplets [Lefebvre, 1989]. Thus, these results confirm that as smaller and finer bubbles are dispersed in the two-phase flow for the same water and air flow rates. Therefore with more gas bubbles available to shear the liquid phase, droplets with smaller diameter are formed.

Figure 5.6 indicates the relationship found between the bubbles and the droplets for $Q_{\mathrm{L}} = 189$ kg/min, markers indicate γ constant. Thus, the experimental runs with the same marker correspond to the same condition: same water and air flow rates.

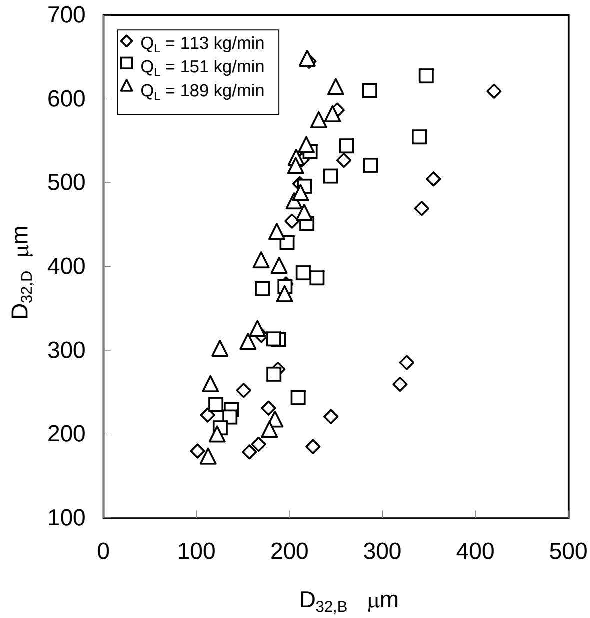

Figure 5.5: Bubble size versus droplet size for different flow rates and different configurations, without bubble breaker, BB_1 and BB_2.

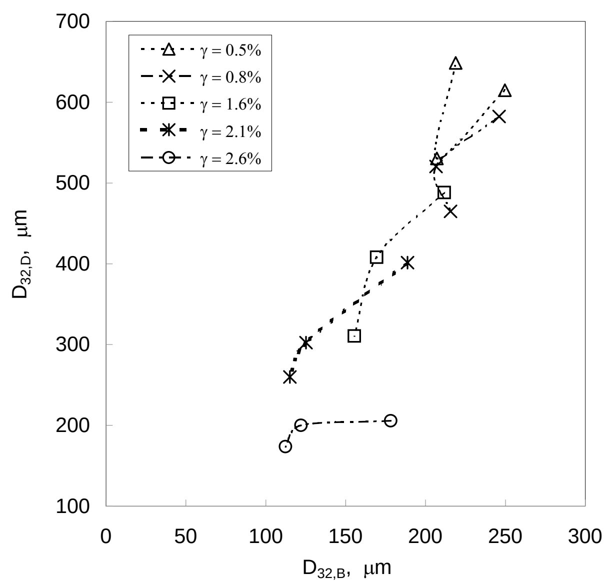

Figure 5.6: Bubble size versus droplet size for $Q_{\mathrm{L}} = 189$ kg/min. Each group is for the same γ, meaning the same water and air flow rate at the same delivery pressure.

The reduction in size is not linear, bubbles presented a higher relative reduction than droplets did. Similar results were found for lower water flow rates $\mathrm{Q_L} = 113$ kg/min as it is shown in Figure 5.5. Increasing liquid flow rate a higher reduction in droplet size was observed. At low liquid flow rate (Q_L = 113 kg/min), bubbles experience less reduction in size than for higher liquid flow rate (Q_L = 189 kg/min).

The relationship between bubble size and droplet size is characterized defining a new parameter the Bubble Size Sensitivity, Φ, as the slope of the $D_{32,\mathrm{B}}$ vs. $D_{32,\mathrm{D}}$ curve (see Eq. 5.1). Figure 5.7 shows how for lower values of γ, the bubbles have a major influence on the droplet size. For higher γ there is a larger amount of air available, that creates smaller bubbles that cannot be broken up into bubbles of smaller size. Clearly the peak sensitivity to bubble size occurs at γ of 1 – 2 % for these flows.

$$\Phi = \frac{dD_{32,\mathrm{D}}}{dD_{32,\mathrm{B}}} \tag{5.1}$$

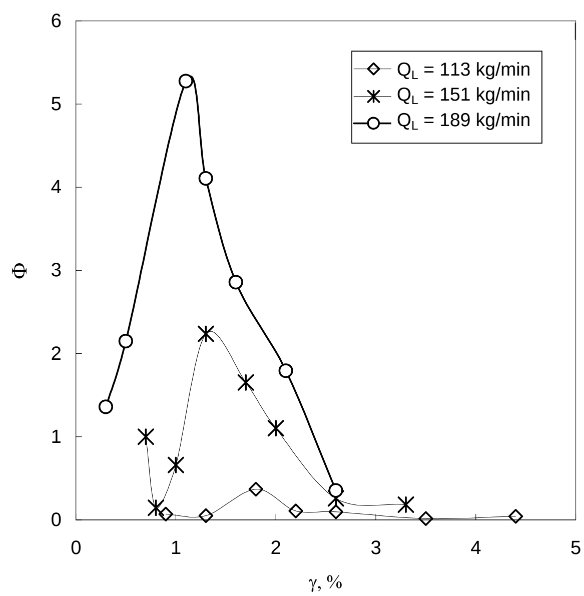

Figure 5.7: Bubble size sensitivity as a function of the air to liquid mass ratio, γ, performed for different liquid flow rates, Q_L.

Considering only the highest liquid flow rate tested (Q_L = 189 kg/min), as the flow pattern according to Taitel and Dukler (1976) is dispersed bubble, the flow can be described by the homogeneous model. In the homogeneous case, where zero slip is assumed, the void fraction is defined by Eq. 2.3.

The Figure 5.8 depicts the Bubble Size Sensitivity, Φ, as a function of the γ and α_{HOM} for Q_L = 189 kg/min. As α_{HOM} is proportional to γ, the Figure 5.7 and Figure 5.8 present the same trends. The latter figure shows that in a range of $\alpha_{HOM} = 45 – 55$ % is where feed bubble size has the greatest impact on the resulting droplets.

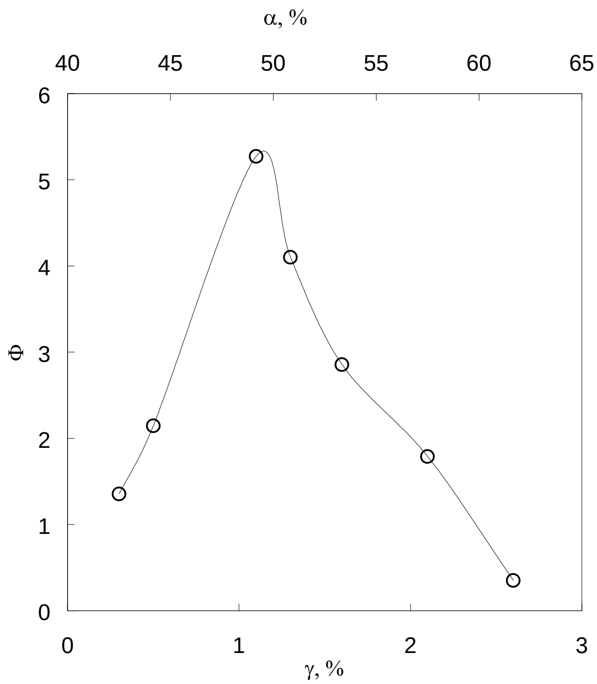

Figure 5.8: Bubble size sensitivity as a function of the air to liquid mass ratio and void fraction for $Q_{\mathrm{L}} = 189$ kg/min

5.4.3 Regression analysis

To study the influence of the bubble size on the droplet size a regression analysis was done. This statistical tool consists on building an expression that predicts the dependent variable as a function of one or more independent variables. This indicates the relationship between the variables and also shows which among the independent variables are actually related to the dependent variable and the strength of the relationship.

The regression analysis basically builds an expression that predicts the dependent variable as a function of one or more independent variables. Thus it perhaps erroneously assumes uncorrelated input parameter. The regression can be linear, or non-linear. For the former the expression has the form:

$$Y = \zeta + \alpha_1 X_1 + \alpha_2 X_2 + \ldots.\alpha_n X_n \tag{5.2}$$

where ζ is a constant and α_i are the regression coefficients or multipliers which show the size and sign of the influence that the corresponding independent variable, X_i, has on the dependent variable Y.

The analysis is focused on determining appropriate values for the coefficients assuming a linear or non-linear relationship. The value of α_i indicates how the dependent variable is expected to increase (positive sign) or decrease (negative sign) when the independent variable increase by a unit, keeping the rest of the independent variables constant.

Generally, the null hypothesis is adopted to find the coefficients. In the null hypothesis is assumed that the variable has no effect on Y ($\alpha_i = 0$), or that the two variables in study are not linearly related, and the opposite is demonstrated. Once the coefficients are found and the expression is built, other statistical tools such as standard deviation, t-Statistic, R-squared and significance are used to evaluate the "goodness" of expression. This is how well the calculated values from the model predict the experimental values.

The difference between the actual and predicted is the sum of at least three sources, error in measuring the independent variable, error measuring the dependent variables and inherent randomness in the dependent variables.

A non-linear regression of the model is a combination of a non-linear expression between the independent and dependent variables. A non-linear regression can take any form: power, exponential, logarithmic, reciprocal, etc. However, some of them can be expressed in a linear domain by a suitable transformation of the model. The most common non-linear expressions and theirs transformation are shown in Table 5.1

Table 5.1: Non-linear regression expressions and the corresponding linear transformations.

Type	Non-Linear Expression	Linear Transformation
Power	$Y = \alpha X^{\beta}$	$\lg(Y) = \lg(\alpha) + \beta \lg(X)$
Exponential	$Y = \alpha \beta^{X}$	$\lg(Y) = \lg(\alpha) + X \lg(\beta)$
Exponential	$Y = \alpha \exp(\beta X)$	$\ln(Y) = \ln(\alpha) + \beta X$
Logarithmic	$Y = \ln(\alpha X)^{\beta}$	$Y = \ln(\alpha) + \beta \ln(X)$
Reciprocal	$Y = \frac{1}{\alpha+\beta X}$	$\frac{1}{Y} = \alpha + \beta X$
Reciprocal	$Y = \frac{1}{(\alpha+\beta X)^2}$	$\frac{1}{\sqrt{Y}} = \alpha + \beta X$
Square-Root	$Y = \alpha + \beta\sqrt{X}$	$Y = \alpha + \beta X$

For this case the dependent variable was defined as the droplet size($D_{32,\mathrm{D}}$) and as the independent variables the the bubble size ($D_{32,\mathrm{B}}$), water flow rate (Q_{L}), air to liquid ratio (γ) and inlet pressure (P_i). Before the regression analysis, a correlation analysis was done to determine if there is a relationship between two variables in study, $D_{32,\mathrm{B}}$ and $D_{32,\mathrm{D}}$. For three cases study, No BB, BB_1 and BB_2, there was a positive agreement between those two variables. Values must be from -1 to +1, suggesting a strong negative relationship for -1 and a positive relation for +1. Values for each configuration were NO BB: 0.4339; BB_1: 0.9401 ;BB_2: 0.8143.

To create the expression, a correlation coefficient matrix was used to estimate whether a linear or non-linear regression had to be fitted. Many combinations are possible, from a linear regression to any combination of non-linear expression (power, exponential, logarithmic, reciprocal, etc.) for each variable. However, the best fit for the experimental results is linear for Q_L, and power for the $D_{32,\mathrm{B}}$, P_i and γ. Polymath 6.10, a software for numerical analysis, was used to obtain the corresponding coefficients. The model follows the expression:

$$D_{32,\mathrm{D}} = A + B{D_{32,\mathrm{B}}}^C + DQ_\mathrm{L} + E\gamma^F + GP_i^H \tag{5.3}$$

Using Polymath the values of each coefficient were found. The expression takes the form:

$$D_{32,\mathrm{D}} = -893.8 + 5.21{D_{32,\mathrm{B}}}^{0.62} + 1.21Q_\mathrm{L} + 609.1\gamma^{-0.25} + 5051.0P_i^{-0.38} \tag{5.4}$$

The coefficients of the model are found by the method of successive approximations done with the objective of minimizing the sum of squares of the errors. The error was defined as the difference between the actual values and values given by the model.

P_i and γ are clearly the parameters that most affect the droplet size, as it was established by Lefebvre [Lefebvre, 1989]. However, when keeping these parameters constant the bubble size also influences the resulting droplets.

5.5 Conclusions

The influence of the feed flow bubble size on the droplet formation for an effervescent nozzle was investigated with respect to variations in working conditions, liquid flow rate and γ. Imaged-based techniques were used to determine the size of the bubbles and droplets. Particles measurement is not a standard procedure; experimental configurations, location, technique employed and characteristic diameters selected influence the final particle size measured. Sauter mean diameter was selected for comparison reasons.

Bubbles were measured in a control volume located in the center of the pipe and the optimal location of the sample for droplets was determined with an impact probe. Bubble breakers inserted in the feeding pipe reduced the bubble size and the droplet size in the spray.

A non-linear relationship was found between the bubbles present in the two-phase flow feeding the nozzle and the droplets generated in the spray. This indicates an influence of the bubble size on the efficiency of the spray. An analysis of the experimental results indicates the two major parameter that determined droplet size are P_i and γ as expected for an effervescent atomizer. The third parameter is bubble size, with a positive correlation factor. To determine its influence the other two parameters,P_i and γ, were kept constant.

References

Ballester, J. and Dopazo, C. (1996). Drop size measurements in heavy oil sprays from pressure-swirl nozzles. *Atomization Sprays*, 6:377–408.

Jedelsky, J., Jicha, M., Slama, J., and Otahal, J. (2009). Development of an effervescent atomizer for industrial burners. *Energy Fuels*, 23(12):6121–6130.

Kocamustafaogullari, G. and Wang, Z. (1991). An experimental study on local interfacial parameters in a horizontal bubble twp-phase flow. *International Journal Multiphase Flow*, 17(5).

Lefebvre, A. H. (1989). *Atomization and Sprays*. Hemisphere.

Lefebvre, A. H., Wang, X. F., and Martin, C. A. (1988). Spray characteristics of aerated-liquid pressure atomizers. *AIAA Journal of Propulsion and Power*, 4(4):293–298.

Maldonado, S. (2006). Improving the stability of gas-liquid spray. Master's thesis, University of Alberta.

Sovani, S. D., Sojka, P. E., and Lefebvre, A. H. (2001). Effervescent atomization. *Progress in Energy and Combustion Science*, 27:483–521.

Taitel, Y. and Dukler, A. (1976). A model for predicting flow regime transitions in horizontal and near horizontal gas-liquid flow. *American Institute of Chemical Engineers Journal*, 22(1):47–55.

Chapter 6

Summary and Conclusions

This work experimentally studied the influence of bubble sizes in an effervescent atomization in a commercial scale facility with a feeding pipe diameter of 2.54 cm. The effects of the bubble size for different conditions were investigated. Different locations of the spray were tested to characterize the resulting droplets. Particles measurements was performed taking images and using the particle projected areas to estimate their sizes. A characterization of the performance of an effervescent atomizer was investigated in terms of DSD, sphericity and velocity. This chapter summarized the conclusion of each chapter.

1. Shadowgraphy technique allows the characterization of droplets through their size, size distribution, shape and velocity, without any sphericity rejection criteria. For combustion purposes in an appropriate size range and morphology.
2. There is not a standard procedure to measure droplets in a effervescent spray. Estimated droplet size has a strong dependency on the working conditions, technique and locations.
3. A representative control volume for the spray was determined by measuring the momentum rate with an impact probe
4. Bubble size and droplet size reduction is not linear.
5. Bubble size has an effect on droplet size in a specific range of air to liquid mass ratio.

A characterization an effervescent atomizer was investigated in terms of droplet size distribution, shape (sphericity) and velocity, for a set of working conditions. The spray characterization is not a standard procedure; the final droplet size has a strong dependency on the technique and locations selected. The experimental data was analyzed and fitted the log-normal mathematical model, this allows the comparisons between different runs and with other experiments, as well as the extrapolation of the results to other working conditions.

Shadowgraphy is an imaged based measurement technique that produces images in order to estimate the size, velocity and shape of the resulting droplets. All these three variables depend on the location and working conditions. Smaller droplets were measured at locations further from the nozzle tip and from the center line. Non-spherical droplets were observed at all the locations, with a major presence in the "spray formation" zone, where droplets are not fully atomized and liquid is presented as ligaments or sheets. The measurement of the shape for smaller droplets must include an analysis of the principles of the technique employed, in terms of the discretization error and the pixel per particles required to obtain reliable results to avoid erroneous conclusions. A representative location of the spray was selected based on the momentum rate, measured with a impact probe.

The insertion of the bubble breaker results in a reduction on the bubble size and with it a reduction of the droplet size. A non-linear relationship between the size of bubbles present in the two-phase flow feeding the nozzle and the droplets generated in the spray was found. A parameter, Bubble Size Sensitive (Φ), was defined to express that relationship. It was found that Φ has a dependency with the air to liquid mass ratio, γ.

References

Almeida-Prieto, S., Blanco-Mendez, J., and Otero-Espinar, F. (2006). Microscopic image analysis techniques for the morphological characterization of pharmaceutical particles: influence of process variables. *Journal of Pharmaceutical Sciences*, 95:348357.

Almeida-Prieto, S., Blanco-Mendez, J., and Otero-Espinar, F. (2007). Microscopic image analysis techniques for the morphological characterization of pharmaceutical particles: influence of the software, and the factor al-gorithms used in the shape factor estimation. *European Journal of Pharmaceutics and Biopharmaceutics*, 67(3):766–776.

Andreussi, P., Paglianti, A., and Sanchez, F. (1999). Dispersed bubble flow in horizontal pipes. *Chemical Engineering Science*, 54:1101–1107.

Ariyapadi, S., Berruti, F., Briens, C., Knapper, B., Skwarok, R., and Chan, E. (2005). Stability of horizontal gas-liquid sprays in open-air and in a gas-solid fluidized bed. *Powder Technology*, 155(3):161–174.

Babisnky, E. and Sojka, P. (2002). Modeling drop size distribution. *Progress in Energy and Combustion Science*, 28:303–329.

Baker, O. (1954). Simultaneous flow of oil and gas. *Oil and Gas Journal*, 53(12):185–190.

Ballester, J. and Dopazo, C. (1996). Drop size measurements in heavy oil sprays from pressure-swirl nozzles. *Atomization Sprays*, 6:377–408.

Barnea, D., Shoham, O., Taitel, Y., and Dukler, A. E. (1980). Flow pattern transition for gas-liquid flow in horizontal and inclined pipes. *International Journal of Multiphase Flow*, 6(3):217–226.

Baukal, C. (2001). *The John Zink Combustion Handbook*. CRC Press.

Blaisot, J. and Yon, J. (2005). Droplet size and morphology characterization for dense sprays by image processing: application to the diesel spray. *Experiments in Fluids*, 39(6):977–994.

Bossard, J. and Pecks, R. (1996). Droplet size distribution effects in spray combustion. *Twenty-Sixth Symposium (International) on Combustion The Combustion Institute*, 26(1):1671–1677.

Bush, S. G.; Sojka, P. E. (1993). Entrainment by effervescent sprays at low mass flowrates. *Fluid Mechanics and Heat Mass Transfer in Sprays*, pages 117–121.

Bush, S., Bennett, J., Sojka, P., Panchagnula, M., and Plesniak, M. (1996). Momentum rate probe for use with two-phase flow. *Review of Scientific Instruments*, 67(5):1878–1885.

Carvahlo, M., Costa, M., Lockwood, F., and Semiao, V. (1989). *International Conference on Mechanics of Two-Phase Flows. Taipei, Taiwan.*

Ejim, C. E., Fleck, B. A., and Amirfazli, A. (2005). A scaling study of the atomization of a two-phase industrial nozzle: Part 1 - effect of surface tension and viscosity on mean drop size profiles. In *Proceedings of the 20^{th} ILASS – Europe.*

Ghaemi, S., Rahimi, P., and Nobes, D. (2008). Measurement of droplet centricity and velocity in the spray field of an effervescent atomizer. *14th International Symposium on Applications of Laser Techniques to Fluid Mechanics, Lisbon Portugal*, July 7-10.

Gregory, G., Nicholson, M., and Aziz., K. (1974). Correlation of the liquid volume fraction in the slug for horizontal gas-liquid slug flow. *International Journal of Multiphase Flow*, 4:33–39.

Hesketh, R., Fraser, T., and Etchell, A. (1987). Bubble size in horizontal pipe. *American Institute of Chemical Engineers Journal*, 33(4).

Hinze, O. (1955). Fundamentals of the hydrodynamic mechanism of splitting dispersion processes. *American Institute of Chemical Engineers Journal*, 1:289.

Jedelsky, J., Jicha, M., Slama, J., and Otahal, J. (2009). Development of an effervescent atomizer for industrial burners. *Energy Fuels*, 23(12):6121–6130.

Kashdan, J., Shrimpton, J., and Whybrew, A. (2003). Two-phase flow characterization by automated digital image analysis. part 1: Fundamental principles and calibration of the technique. *Particle and Particle Systems Characterization*, 20:387–397.

Kocamustafaogullari, G. and Wang, Z. (1991). An experimental study on local interfacial parameters in a horizontal bubble twp-phase flow. *International Journal Multiphase Flow*, 17(5).

Kolmogorof, A. (1949). Sizing of spray particles using image processing techniques. *Dokl. Akad. Nauk. SSSR*, 66:825.

Lasheras, J. and Hopfinger, E. (2000). Liquid jet instability and atomization in coaxial gas streams. *Annual Review of Fluids Mechanics*, 32:275–308.

LaVisionGmbH (2007). Sizing-maser shadow. *Optical Review*, Gottigen, Germany.

Lee, S. and Kim, Y. (2004). Sizing of spray particles using image processing techniques. *KSME International Journal*, 18:879–894.

Lefebvre, A. H. (1989). *Atomization and Sprays*. Hemisphere.

Lefebvre, A. H., Wang, X. F., and Martin, C. A. (1988). Spray characteristics of aerated-liquid pressure atomizers. *AIAA Journal of Propulsion and Power*, 4(4):293–298.

Levich, V. (1962). *Physiochemical Hydrodynamics*. Prentice Hall, Englewood Cliffs, NJ, 464.

Liu, S. and Li, D. (1999). Drop coalescence in turbulent dispersions. *Chemical Engineering Science*, 32:195–202.

Maldonado, S. (2006). Improving the stability of gas-liquid spray. Master's thesis, University of Alberta.

Malot, H. and Blaisot, J. (2000). Droplet size distribution and sphericity measurements of low-density sprays through image analysis. *Part. Part. System Characteristic*, 17:146–158.

Mandhane, J. M., Gregory, G. A., and Aziz, K. (1974). A flow pattern map for gas-liquid flow in horizontal pipes. *International Journal of Multiphase Flow*, 1:537–553.

Podczeck, F., Rahman, S., and Newton, J. (1999). Evaluation of a standardised procedure to assess the shape of pellets using image analysis. *International Journal of Pharmaceutics*, 192:123–138.

Ranganathan, K. and Kannan., S. (1994). Drop size measurement in two-phases swirling flow using image processing techniques. *International Journal Heat and mass Transfer*, 37(4):559–670.

Razzaque, M., Afacan, A., Liu, S., Nandakumar, K., Masliyah, J., and Sean, S. (2003). Bubble size in coalescence dominant regime of turbulent air-water flow through horizontal pipes. *International Journal of Multiphase Flow*, 29:1451–1471.

Reitz, R. and Bracco, F. (1982). Mechanism of atomization of a liquid jet. *Physics of Fluids*, 25(10):1730–1742.

Schick, R. (2006). Spray technology reference guide: Understanding drop size. *Spraying System Co.*

Sovani, S. D. (2001). High pressure gas-liquid flow inside an effervescent diesel injector ans its effect on spray characteristics. Master's thesis, Purdue University.

Sovani, S. D., Sojka, P. E., and Lefebvre, A. H. (2001). Effervescent atomization. *Progress in Energy and Combustion Science*, 27:483–521.

Sutherland, J., Sojka, P., and Plesniak, M. (1997). Ligament controlled effervescent atomization. *Atomization Sprays*, 7(4):383–406.

Tafreshi, Z. M., Kirpalani, D., Bennett, A., and McCracken, T. W. (2002). Improving the efficiency of fluid cokers by altering two-phase feed characteristics. *Powder Technology*, 125(2-3):234–241.

Taitel, Y. and Dukler, A. (1976). A model for predicting flow regime transitions in horizontal and near horizontal gas-liquid flow. *American Institute of Chemical Engineers Journal*, 22(1):47–55.

Weisman, J., Duncan, D., Gibson, J., and Crawford, T. (1979). Effects of fluid properties and pipe diameter on two-phase flow patterns in horizontal lines. *International Journal of Multiphase Flow*, 5(6):437–462.

Whitlow, J. D. and Lefebvre, A. H. (1993). Effervescent atomizer operation and spray characteristics. *Atomization and Sprays*, 3:137–155.

Zama, Y., Kawahash, M., and Hirahara, H. (2004). Simultaneous measurement of droplet size and three-components of velocity in spray. *Optical Review*, 11(6):358–364.

Appendix A

Experimental conditions and results for different configurations

A.1 Experimental Conditions for the Taitel and Dukler Flow Pattern Map

Table A.1: Experimental conditions and corresponding superficial velocities for the Taitel and Dukler flow pattern map.

Water flow (kg/min)	Air flow (kg/min)	γ (%)	Mixture pressure (kPa)	U_L^S (m/s)	U_G^S (m/s)
113.4	1.0	0.88	406.56	3.74	6.92
113.4	1.5	1.32	497.39	3.74	8.48
113.4	2.0	1.76	587.58	3.74	9.57
113.4	2.5	2.20	672.03	3.74	10.46
113.4	3.0	2.64	753.16	3.74	11.20
113.4	4.0	3.53	917.56	3.74	12.26
113.4	5.0	4.41	1031.56	3.74	13.63
132.3	1.0	0.76	528.85	4.36	5.32
132.3	1.3	0.94	560.68	4.36	6.27
132.3	1.5	1.13	604.39	4.36	6.98
132.3	2.0	1.51	688.42	4.36	8.17
132.3	2.5	1.89	778.35	4.36	9.03
132.3	3.0	2.27	860.30	4.36	9.80
132.3	4.0	3.02	1055.16	4.36	10.66
132.3	5.0	3.78	1186.08	4.36	11.85
151.2	1.0	0.66	690.68	4.98	4.07
151.2	1.3	0.83	679.96	4.98	5.17
151.2	1.5	0.99	737.13	4.98	5.72
151.2	2.0	1.32	945.52	4.98	5.95
151.2	2.5	1.65	848.66	4.98	8.28
151.2	3.0	1.98	1030.77	4.98	8.18
151.2	4.0	2.64	1183.77	4.98	9.50
151.2	5.0	3.31	1322.97	4.98	10.63
170.1	1.0	0.59	613.31	5.61	4.58
170.1	1.3	0.73	762.57	5.61	4.61
170.1	1.5	0.88	945.02	5.61	4.46
170.1	2.0	1.18	965.26	5.61	5.83
170.1	2.5	1.47	1048.19	5.61	6.71
170.1	3.0	1.76	1143.66	5.61	7.37
170.1	4.0	2.35	1305.44	5.61	8.61
170.1	5.0	2.94	1451.26	5.61	9.69

Water flow (kg/min)	Air flow (kg/min)	γ (%)	Mixture pressure (kPa)	U_L^S (m/s)	U_G^S (m/s)
189.0	1.0	0.53	770.46	6.23	3.65
189.0	1.5	0.79	913.26	6.23	4.62
189.0	2.0	1.06	1036.60	6.23	5.42
189.0	2.5	1.32	1148.57	6.23	6.12
189.0	3.0	1.59	1245.00	6.23	6.77
189.0	4.0	2.12	1423.32	6.23	7.90
189.0	5.0	2.64	1579.59	6.23	8.90

A.2 Pressure Measurement

Table A.2: Mean and fluctuating pressure measurements without bubble breaker for the experimental conditions tested.

Water flow (kg/min)	Air flow (kg/min)	γ (%)	Mean pressure, $\overline{P_3}$ (kPa)	Mean pressure, $\overline{P_2}$ (kPa)	P_{40}^2 Ch 1	P_{40}^2 Ch 2	Inlet pressure, $\overline{P_1}$(kPa)	Pressure Drop (kPa)
113.42	1.0	0.9	378.83	366.82	102.29	87.15	366.02	12.00
113.42	1.5	1.3	473.74	467.32	106.15	88.87	457.72	6.41
113.42	2.0	1.8	610.33	598.04	75.45	62.83	589.7	12.29
113.42	2.5	2.2	695.13	685.81	7.02	4.85	665.84	9.32
113.42	3.0	2.6	766.8	755.72	5.42	3.46	733.71	11.08
113.42	4.0	3.5	894.95	886.00	5.14	3.34	860.19	8.96
113.42	5.0	4.4	1013.38	1005.08	5.26	3.57	975.81	8.30
151.23	1.0	0.7	596.39	576.70	1.70	1.28	557.9	19.69
151.23	1.3	0.8	658.92	638.64	1.63	1.23	620.04	20.28
151.23	1.5	1.0	719.02	699.87	2.04	1.50	679.49	19.15
151.23	2.0	1.3	827.84	807.92	1.79	1.27	784.39	19.93
151.23	2.5	1.7	922.71	902.25	2.77	2.02	875.98	20.46
151.23	3.0	2.0	1009.5	987.44	2.43	1.73	958.68	22.06
151.23	4.0	2.6	1162.57	1143.48	2.54	1.74	1110.17	19.10
151.23	5.0	3.3	1299.71	1280.8	2.73	1.88	1243.49	18.92
189.04	1.0	0.5	750.87	731.46	0.50	0.41	710.15	19.41
189.04	1.5	0.8	895.43	880.59	0.78	0.59	854.94	14.84
189.04	2.0	1.1	1019.93	1001.32	0.77	0.58	972.15	18.61
189.04	2.5	1.3	1130.94	1114.94	0.71	0.51	1082.47	16.00
189.04	3.0	1.6	1225.9	1214.36	1.00	0.87	1178.99	11.53
189.04	4.0	2.1	1405.39	1391.9	0.85	0.63	1351.36	13.48
189.04	5.0	2.6	1558.46	1548.14	1.04	0.73	1503.04	10.33

Table A.3: Mean and fluctuating pressure measurements with bubble breaker 1 for the experimental conditions tested.

Water flow (kg/min)	Air flow (kg/min)	γ (%)	Mean pressure, $\overline{P_3}$ (kPa)	Mean pressure, $\overline{P_2}$ (kPa)	P_{40}^2 Ch 1	P_{40}^2 Ch 2	Inlet pressure, $\overline{P_1}$(kPa)	Pressure Drop (kPa)
113.42	1.0	0.9	601.47	400.31	6.12	12.53	354.54	201.16
113.42	1.5	1.3	721.52	487.35	13.69	21.54	446.34	234.17
113.42	2.0	1.8	825.84	565.57	17.78	26.49	529.05	260.27
113.42	2.5	2.2	926.31	642.25	15.97	24.28	602.66	284.06
113.42	3.0	2.6	1016.90	713.84	15.14	22.95	670.13	303.06
113.42	4.0	3.5	1174.33	836.85	16.67	25.04	794.89	337.48
113.42	5.0	4.4	1323.63	955.45	14.80	21.47	907.86	368.18
151.23	1.0	0.7	826.94	559.89	3.56	3.47	510.96	267.05
151.23	1.3	0.8	906.25	622.45	3.48	3.79	562.18	283.81
151.23	1.5	1.0	980.29	678.76	4.11	4.47	617.26	301.53
151.23	2.0	1.3	1107.57	778.80	5.74	6.61	716.44	328.77
151.23	2.5	1.7	1222.70	870.91	6.61	7.96	803.28	351.79
151.23	3.0	2.0	1327.93	955.29	6.40	7.56	885.72	372.64
151.23	4.0	2.6	1512.77	1100.37	7.02	8.07	1036.40	412.39
151.23	5.0	3.3	1683.05	1236.02	7.34	8.63	1165.02	447.03
189.04	1.0	0.5	1051.39	706.09	1.11	0.85	696.36	345.30
189.04	1.5	0.8	1231.59	846.35	1.80	1.39	832.65	385.24
189.04	2.0	1.1	1377.34	962.29	2.79	2.20	944.57	415.04
189.04	2.5	1.3	1506.96	1068.15	3.62	3.13	1041.10	438.81
189.04	3.0	1.6	1629.45	1165.04	3.66	3.22	1130.73	464.40
189.04	4.0	2.1	1840.69	1333.64	4.16	4.27	1296.20	507.05
189.04	5.0	2.6	2035.91	1487.69	3.82	3.97	1440.99	548.22

Table A.4: Mean and fluctuating pressure measurements with bubble breaker 2 for the experimental conditions tested.

Water flow (kg/min)	Air flow (kg/min)	γ (%)	Mean pressure, $\overline{P_3}$ (kPa)	Mean pressure, $\overline{P_2}$ (kPa)	P_{40}^2 Ch 1	P_{40}^2 Ch 2	Inlet pressure, $\overline{P_1}$(kPa)	Pressure Drop (kPa)
113.42	1.0	0.9	506.28	399.52	4.13	6.31	386.08	106.76
113.42	1.5	1.3	610.73	485.71	9.32	10.26	480.79	125.03
113.42	2.0	1.8	708.12	569.23	10.04	11.49	571.31	138.89
113.42	2.5	2.2	803.02	653.8	6.49	8.07	650.57	149.22
113.42	3.0	2.6	878.53	717.91	10.22	12.13	716.02	160.62
113.42	4.0	3.5	1024.5	844.09	11.53	13.61	847.31	180.41
113.42	5.0	4.4	1155.44	960.78	9.43	11.51	956.02	194.67
151.23	1.0	0.7	693.1	555.53	1.92	2.70	559.69	137.57
151.23	1.3	0.8	767.9	620.10	1.88	2.70	622.15	147.80
151.23	1.5	1.0	835.55	678.13	2.44	3.27	678.51	157.42
151.23	2.0	1.3	950.23	778.81	2.77	3.70	781.22	171.42
151.23	2.5	1.7	1060.53	876.65	3.12	4.06	874.07	183.88
151.23	3.0	2.0	1148.01	954.00	3.00	3.79	956.04	194.01
151.23	4.0	2.6	1315.87	1101.24	3.81	4.85	1101.80	214.63
151.23	5.0	3.3	1472.96	1236.19	4.12	5.05	1233.80	236.77
189.04	1.0	0.5	880.93	704.64	0.56	0.62	710.15	176.29
189.04	1.5	0.8	1042.40	843.61	1.01	1.05	852.99	198.79
189.04	2.0	1.1	1179.29	965.37	1.46	1.54	972.15	213.92
189.04	2.5	1.3	1295.58	1068.04	1.53	1.63	1082.47	227.54
189.04	3.0	1.6	1404.02	1163.41	1.65	1.94	1172.10	240.61
189.04	4.0	2.1	1593.36	1331.63	2.10	2.40	1337.57	261.73
189.04	5.0	2.6	1766.98	1483.27	1.97	2.25	1489.26	283.70

A.3 Experimental Conditions for Bubble Size

Table A.5: Experimental conditions and results for bubble size ($D_{32,\mathrm{B}}$) without bubble breaker.

Water flow (kg/min)	Air flow (kg/min)	γ (%)	Water pressure (kPa)	Air pressure (kPa)	Bubble $D_{32,\mathrm{B}}$ (μm)
113.42	1.0	0.88	508	447	420
113.42	1.5	1.32	606	556	355
113.42	2.0	1.76	699	659	342
113.42	2.5	2.20	791	760	326
113.42	3.0	2.64	876	857	319
113.42	4.0	3.53	1051	1054	244
113.42	5.0	4.41	1176	1201	225
132.33	1.0	0.76	660	572	369
132.33	1.3	0.94	723	640	368
132.33	1.5	1.13	740	662	373
132.33	2.0	1.51	839	769	366
132.33	2.5	1.89	930	874	347
132.33	3.0	2.27	1022	974	308
132.33	4.0	3.02	1215	1189	208
132.33	5.0	3.78	1353	1351	220
151.23	1.0	0.66	82	661	347
151.23	1.3	0.83	839	730	339
151.23	1.5	0.99	906	797	287
151.23	2.0	1.32	1020	919	244
151.23	2.5	1.65	1122	1032	230
151.23	3.0	1.98	1214	1133	215
151.23	4.0	2.64	1380	1320	209
151.23	5.0	3.31	1524	1488	184
170.13	1.0	0.59	883	740	285
170.13	1.3	0.73	957	817	280
170.13	1.5	0.88	1027	891	277
170.13	2.0	1.18	1151	1022	239
170.13	2.5	1.47	1266	1140	250
170.13	3.0	1.76	1361	1245	221
170.13	4.0	2.35	1542	1441	200
170.13	5.0	2.94	1689	1625	200

Water flow (kg/min)	Air flow (kg/min)	γ (%)	Water pressure (kPa)	Air pressure (kPa)	Bubble $D_{32,\mathrm{B}}$ (μm)
189.04	1.0	0.53	1000	822	250
189.04	1.5	0.79	1156	987	246
189.04	2.0	1.06	1288	1122	231
189.04	2.5	1.32	1404	1247	218
189.04	3.0	1.59	1513	1361	212
189.04	4.0	2.12	1700	1570	189
189.04	5.0	2.64	1860	1762	178

Table A.6: Experimental conditions and results for bubble size ($D_{32,\mathrm{B}}$) with bubble breaker 1.

Water flow (kg/min)	Air flow (kg/min)	γ (%)	Water pressure (kPa)	Air pressure (kPa)	Bubble $D_{32,\mathrm{B}}$ (μm)
113.42	1.0	0.88	733	665	251
113.42	1.5	1.32	870	809	214
113.42	2.0	1.76	989	937	196
113.42	2.5	2.20	1088	1049	170
113.42	3.0	2.64	1191	1153	151
113.42	4.0	3.53	1355	1338	112
113.42	5.0	4.41	1510	1520	101
132.33	1.0	0.76	876	785	270
132.33	1.3	0.94	955	869	210
132.33	1.5	1.13	1029	942	179
132.33	2.0	1.51	1158	1085	203
132.33	2.5	1.89	1276	1202	181
132.33	3.0	2.27	1382	1316	149
132.33	4.0	3.02	1558	1522	135
132.33	5.0	3.78	1740	1713	138
151.23	1.0	0.66	1015	900	286
151.23	1.3	0.83	1105	991	261
151.23	1.5	0.99	1183	1071	216
151.23	2.0	1.32	1327	1222	197
151.23	2.5	1.65	1458	1360	183
151.23	3.0	1.98	1567	1477	171
151.23	4.0	2.64	1767	1700	136
151.23	5.0	3.31	1951	1894	126
170.13	1.0	0.59	1165	1019	245
170.13	1.3	0.73	1256	1109	223
170.13	1.5	0.88	1348	1201	215
170.13	2.0	1.18	1503	1360	195
170.13	2.5	1.47	1630	1503	181
170.13	3.0	1.76	1752	1634	155
170.13	4.0	2.35	1975	1862	135
170.13	5.0	2.94	2167	2077	123

Water flow (kg/min)	Air flow (kg/min)	γ (%)	Water pressure (kPa)	Air pressure (kPa)	Bubble $D_{32,\mathrm{B}}$ (μm)
189.04	1.0	0.53	1318	1137	207
189.04	1.5	0.79	1509	1334	207
189.04	2.0	1.06	1667	1497	205
189.04	2.5	1.32	1813	1648	186
189.04	3.0	1.59	1940	1779	169
189.04	4.0	2.12	2167	2031	125
189.04	5.0	2.64	2375	2250	122

Table A.7: Experimental conditions and results for bubble size ($D_{32,\mathrm{B}}$) with bubble breaker 2.

Water flow (kg/min)	Air flow (kg/min)	γ (%)	Water pressure (kPa)	Air pressure (kPa)	Bubble $D_{32,\mathrm{B}}$ (μm)
113.42	1.0	0.88	628	562	221
113.42	1.5	1.32	724	660	211
113.42	2.0	1.76	865	811	203
113.42	2.5	2.20	957	920	187
113.42	3.0	2.64	1046	1008	177
113.42	4.0	3.53	1209	1201	157
113.42	5.0	4.41	1346	1359	157
132.33	1.0	0.76	760	669	284
132.33	1.3	0.94	836	745	276
132.33	1.5	1.13	901	815	243
132.33	2.0	1.51	1022	940	206
132.33	2.5	1.89	1122	1056	193
132.33	3.0	2.27	1220	1160	205
132.33	4.0	3.02	1396	1352	168
132.33	5.0	3.78	1545	1528	180
151.23	1.0	0.66	888	771	258
151.23	1.3	0.83	971	854	222
151.23	1.5	0.99	1043	929	219
151.23	2.0	1.32	1175	1063	195
151.23	2.5	1.65	1289	1191	188
151.23	3.0	1.98	1392	1302	183
151.23	4.0	2.64	1578	1505	138
151.23	5.0	3.31	1744	1689	120
170.13	1.0	0.59	1022	872	234
170.13	1.3	0.73	1105	960	214
170.13	1.5	0.88	1187	1043	225
170.13	2.0	1.18	1324	1186	207
170.13	2.5	1.47	1448	1319	192
170.13	3.0	1.76	1558	1437	187
170.13	4.0	2.35	1753	1651	159
170.13	5.0	2.94	1935	1846	155

Water flow (kg/min)	Air flow (kg/min)	γ (%)	Water pressure (kPa)	Air pressure (kPa)	Bubble $D_{32,\mathrm{B}}$ (μm)
189.04	1.0	0.53	1159	973	219
189.04	1.5	0.79	1332	1155	216
189.04	2.0	1.06	1480	1307	195
189.04	2.5	1.32	1612	1443	165
189.04	3.0	1.59	1732	1568	155
189.04	4.0	2.12	1934	1793	115
189.04	5.0	2.64	2126	1999	112

A.4 Experimental conditions for droplet size at location (24.5; 3.4)

Table A.8: Experimental conditions and results for droplet size ($D_{32,\mathrm{D}}$) without bubble breaker.

Water flow (kg/min)	Air flow (kg/min)	γ (%)	Water pressure (kPa)	Air pressure (kPa)	Droplet $D_{32,\mathrm{D}}$ (μm)
113.42	1.0	0.88	508	447	609.18
113.42	1.5	1.32	606	556	504.60
113.42	2.0	1.76	699	659	469.23
113.42	2.5	2.20	791	760	285.41
113.42	3.0	2.64	876	857	259.53
113.42	4.0	3.53	1051	1054	220.78
113.42	5.0	4.41	1176	1201	184.84
151.23	1.0	0.66	82	661	627.38
151.23	1.3	0.83	839	730	554.57
151.23	1.5	0.99	906	797	520.73
151.23	2.0	1.32	1020	919	507.92
151.23	2.5	1.65	1122	1032	386.13
151.23	3.0	1.98	1214	1133	392.18
151.23	4.0	2.64	1380	1320	243.26
151.23	5.0	3.31	1524	1488	218.05
189.04	1.0	0.53	1000	822	614.77
189.04	1.5	0.79	1156	987	582.29
189.04	2.0	1.06	1288	1122	575.14
189.04	2.5	1.32	1404	1247	545.45
189.04	3.0	1.59	1513	1361	488.13
189.04	4.0	2.12	1700	1570	401.38
189.04	5.0	2.64	1860	1762	205.65

Table A.9: Experimental conditions and results for droplet size ($D_{32,\mathrm{D}}$) with bubble breaker 1.

Water flow (kg/min)	Air flow (kg/min)	γ (%)	Water pressure (kPa)	Air pressure (kPa)	Droplet $D_{32,\mathrm{D}}$ (μm)
113.42	1.0	0.88	733	665	586.84
113.42	1.5	1.32	870	809	527.59
113.42	2.0	1.76	989	937	379.17
113.42	2.5	2.20	1088	1049	317.86
113.42	3.0	2.64	1191	1153	252.07
113.42	4.0	3.53	1355	1338	222.53
113.42	5.0	4.41	1510	1520	179.75
151.23	1.0	0.66	1015	900	609.92
151.23	1.3	0.83	1105	991	543.79
151.23	1.5	0.99	1183	1071	495.65
151.23	2.0	1.32	1327	1222	428.63
151.23	2.5	1.65	1458	1360	313.27
151.23	3.0	1.98	1567	1477	373.22
151.23	4.0	2.64	1767	1700	220.14
151.23	5.0	3.31	1951	1894	207.23
189.04	1.0	0.53	1318	1137	530.38
189.04	1.5	0.79	1509	1334	520.49
189.04	2.0	1.06	1667	1497	478.50
189.04	2.5	1.32	1813	1648	441.75
189.04	3.0	1.59	1940	1779	408.07
189.04	4.0	2.12	2167	2031	302.27
189.04	5.0	2.64	2375	2250	200.05

Table A.10: Experimental conditions and results for droplet size ($D_{32,\mathrm{D}}$) with bubble breaker 2.

Water flow (kg/min)	Air flow (kg/min)	γ (%)	Water pressure (kPa)	Air pressure (kPa)	Droplet $D_{32,\mathrm{D}}$ (μm)
113.42	1.0	0.88	628	562	644.87
113.42	1.5	1.32	724	660	498.79
113.42	2.0	1.76	865	811	454.05
113.42	2.5	2.20	957	920	277.49
113.42	3.0	2.64	1046	1008	231.02
113.42	4.0	3.53	1209	1201	187.81
113.42	5.0	4.41	1346	1359	178.55
151.23	1.0	0.66	888	771	526.67
151.23	1.3	0.83	971	854	537.30
151.23	1.5	0.99	1043	929	451.24
151.23	2.0	1.32	1175	1063	375.96
151.23	2.5	1.65	1289	1191	312.55
151.23	3.0	1.98	1392	1302	271.28
151.23	4.0	2.64	1578	1505	229.29
151.23	5.0	3.31	1744	1689	235.27
189.04	1.0	0.53	1159	973	648.69
189.04	1.5	0.79	1332	1155	464.74
189.04	2.0	1.06	1480	1307	367.66
189.04	2.5	1.32	1612	1443	325.91
189.04	3.0	1.59	1732	1568	310.50
189.04	4.0	2.12	1934	1793	259.90
189.04	5.0	2.64	2126	1999	173.66

Appendix B

Drawings

In this appendix the drawings of the sight glass and the two different bubbler breakers used for this study are presented. Sight glass was installed in the feeding conduit to visualize the gas bubbles in the two-phase flow entering the nozzle; meanwhile a bubble breaker was installed for the modified configuration before the sight glass to influence the gas bubbles.

B.1 Sight glass

BILL OF MATERIAL						
PIPE						
MK	QTY	SIZE	SCHEDULE	DESCRIPTION	MATERIAL	STANDAR MATERIAL
1	1	25.4mm	80	PIPE	SA-312 TP316/316H	B31.1, B31.3, B36 19M, ASTM A-312
FLANGES						
MK	QTY	SIZE	RATING	DESCRIPTION	MATERIAL	STANDAR MATERIAL
2	2	25.4mm	300#	FLANGE THRO., RF	SA-182 F316/F316L	ANSI B16.5 B31.3, ASTM A-182
GASKETS						
MK	QTY	SIZE	RATING	DESCRIPTION	MATERIAL	STANDAR MATERIAL
3	2	25.4mm	300#	GASKET 1/8" SPIRAL WOUND	SA-167 316	B46.1, ASTM A-167
BOLTS						
MK	QTY	SIZE		DESCRIPTION	MATERIAL	STANDAR MATERIAL
4	1 SET	5/8"X7 ½"		STUD BOLTS C/2 NUTS-4/SET	SA-312 Gr. 138/SA-194 GrBB	B16.5, ASTM A-320, ASTM A-194
MISCELLANEOUS						
MK	QTY	SIZE		DESCRIPTION	MATERIAL	STANDAR MATERIAL
5	1	100mmx124mmx124mm		POLYCARBONATE SIGHT GLASS	POLYCARBONATE	ASTM 0-3935, ASTM 0-2513, B31.3

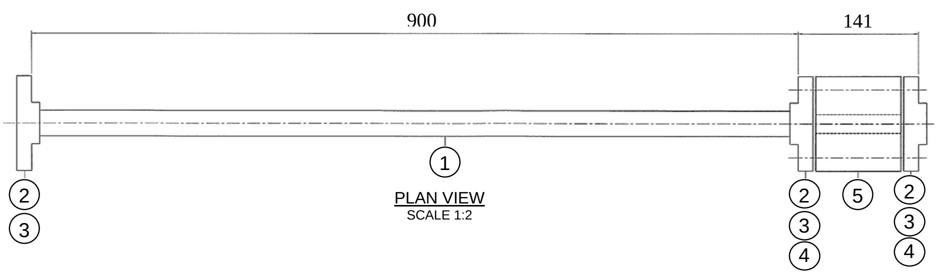

PLAN VIEW
SCALE 1:2

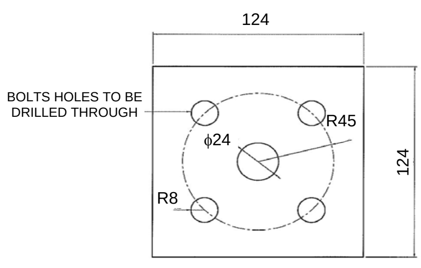

SIGHT GLASS
SCALE 1:2

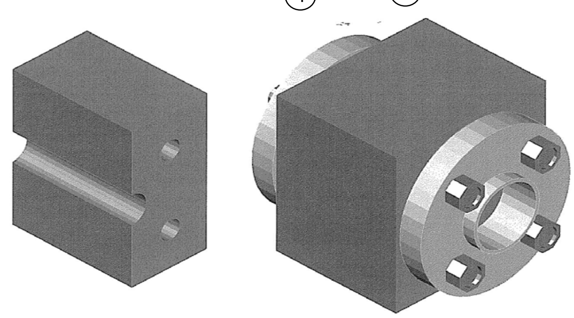

ISOMETRIC VIEW

B.2 Bubble breaker 1

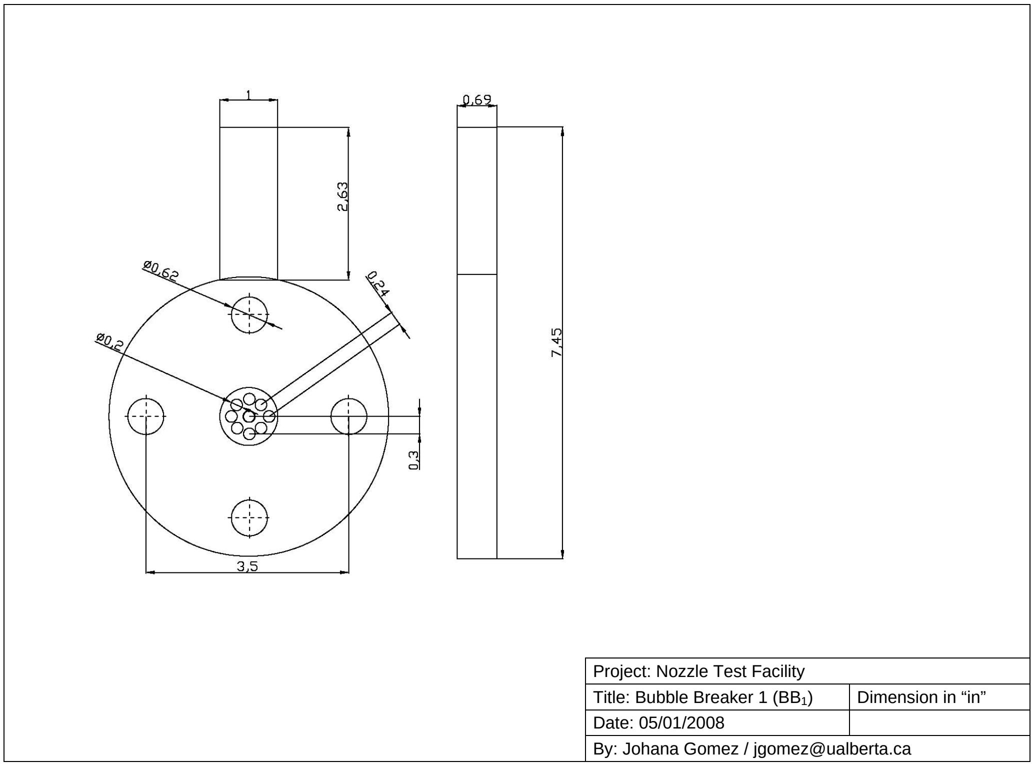

B.3 Bubble breaker 2

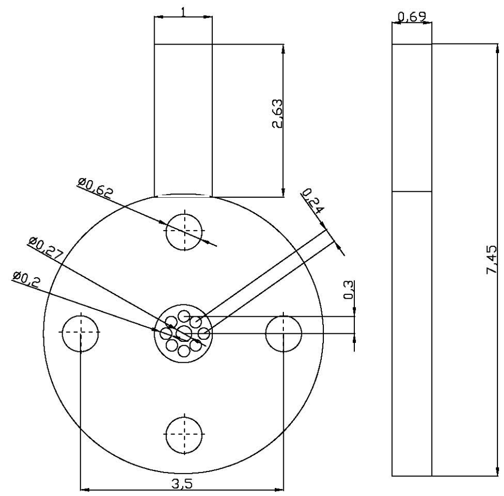

Project: Nozzle Test Facility	
Title: Bubble Breaker 2 (BB_2)	Dimension in “in”
Date: 05/01/2008	
By: Johana Gomez / jgomez@ualberta.ca	

Appendix C

Shadowgraphy-DaVis settings

This appendix contains the parameters used for the Shadowgraphy images processing in DaVis software. This technique allows the estimation of the size and velocity of the particles captured in each image.

C.0.1 Shadowgraphy-DaVis Settings

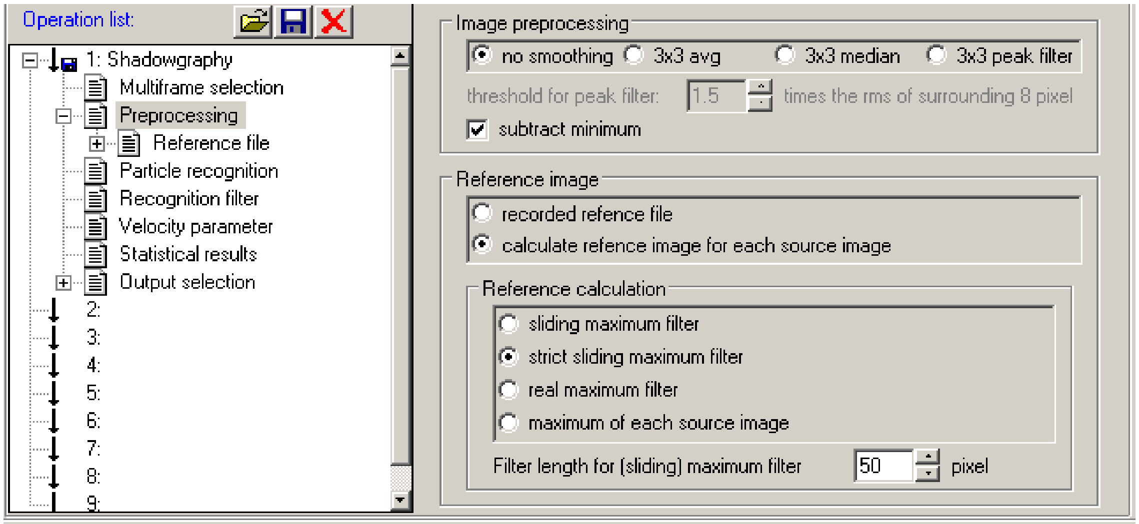

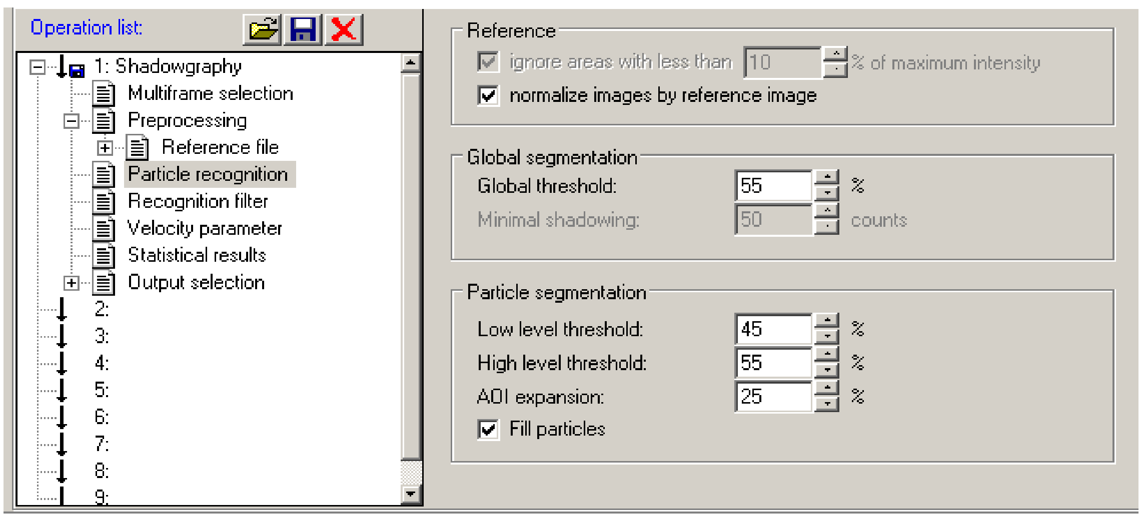

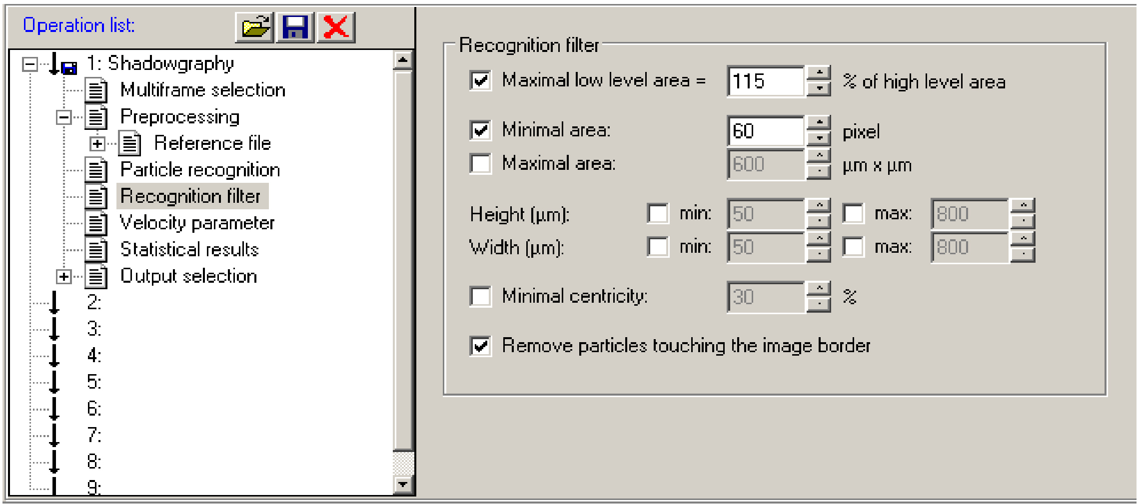
Operation list:
1: Shadowgraphy
Multiframe selection
Preprocessing
Reference file
Particle recognition
Recognition filter
Velocity parameter
Statistical results
Output selection
2:
3:
4:
5:
6:
7:
8:
9:
Recognition filter
Maximal low level area = 115 % of high level area
Minimal area: 60 pixel
Maximal area: 600 µm x µm
Height (µm): min: 50 max: 800
Width (µm): min: 50 max: 800
Minimal centricity: 30 %
Remove particles touching the image border

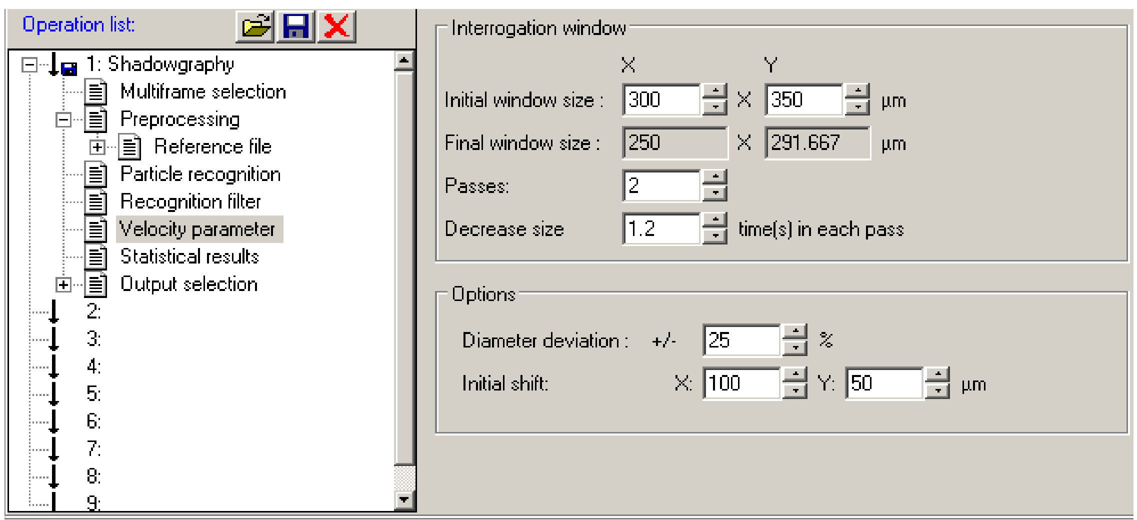
Operation list:
1: Shadowgraphy
Multiframe selection
Preprocessing
Reference file
Particle recognition
Recognition filter
Velocity parameter
Statistical results
Output selection
2:
3:
4:
5:
6:
7:
8:
9:
Interrogation window
X Y
Initial window size : 300 X 350 µm
Final window size : 250 X 291.667 µm
Passes: 2
Decrease size 1.2 time(s) in each pass
Options
Diameter deviation : +/- 25 %
Initial shift: X: 100 Y: 50 µm

Appendix D

Pressure measurement interphase

This appendix contains images of the interphases for the control of water and air flow rates, as well as for the pressure measurements. Both interphases were developed in LabView.

D.0.2 Images of the interphase for pressure measurements

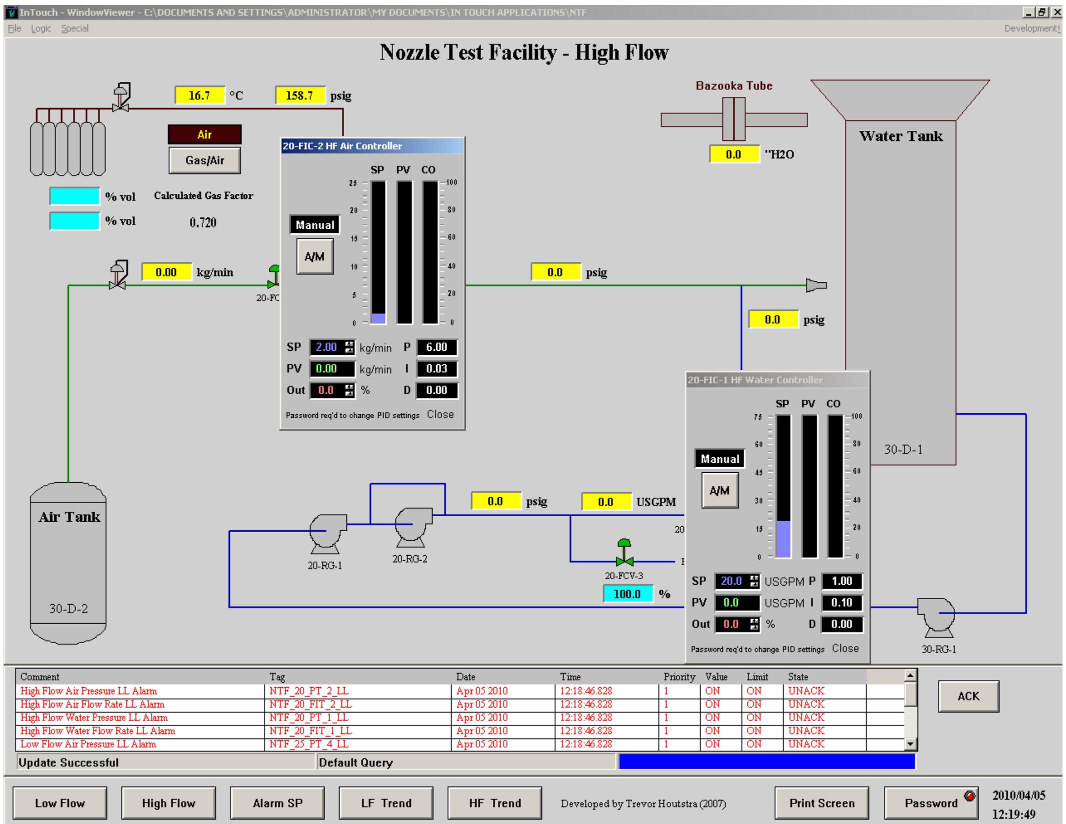

Figure D.1: Image of the interphase used to visualize and record the single-phase pressures.

Figure D.2: Image of the interphase used to visualize and record the two-phase mean and fluctuating pressures.

Appendix E

Estimation of the maximum bubble diameter for different models

Different models have been proposed to predict the maximum diameter of bubbles in a two-phase flow. This appendix shows results obtained in terms of bubble size estimation.

Hinze [Hinze, 1955] indicated that breaking up of bubbles was according to the following expression:

$$D_{\max} = k\left(\frac{\sigma}{\rho_{\mathrm{L}}}\right)^{0.6}\epsilon^{-0.4} \tag{E.1}$$

Where ε is the energy dissipation rate defined as:

$$\varepsilon = \left(\frac{dP}{dx}\right)\frac{U_{\mathrm{m}}}{\rho_{\mathrm{m}}} \tag{E.2}$$

Assuming that the energy is dissipated in five (5) pipe diameters, the Figure E.1 shows the estimation $D_{\max}$ for this model. The value of the constant k is equal to 0.725 and the water surface tension, σ, of 72 mN/m.

In addition, among other theories that have been proposed to predict bubble size it is found the work done by Kolmogoroff et al. [Kolmogorof, 1949] and Levich et al. [Levich, 1962]. The model assumes that the break up occurs when the Weber number,We, is larger than a critical value according to:

$$\mathrm{We}_{\mathrm{crit}} = \frac{\tau_c}{\sigma/D_{\max}} \tag{E.3}$$

$$\mathrm{We}^*_{\mathrm{crit}} = \frac{\tau_c}{\sigma/D_{max}}\left(\frac{\rho_d}{\rho_c}\right)^{1/3} \tag{E.4}$$

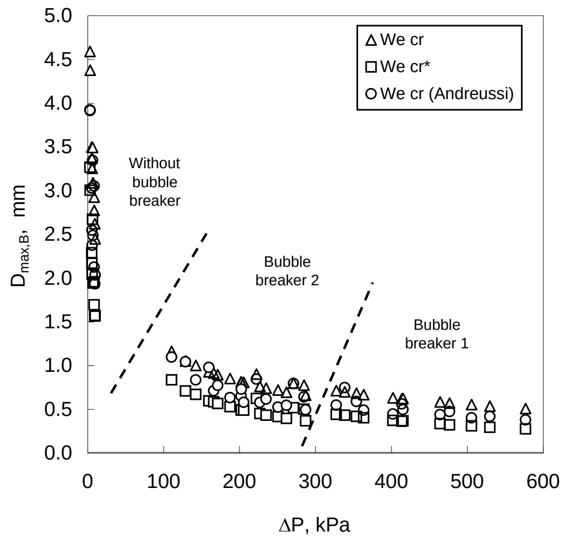

Figure E.1: Maximum bubble diameter according to Hinze model.

Hesketh et al. [Hesketh et al., 1987] used those equations to suggest that the maximum diameter is given by the following equation

$$D_{\max} = \left(\frac{\mathrm{We}_{\mathrm{crit}}}{2}\right)^{0.6} \left(\frac{\sigma}{\rho_c}\right)^{0.6} \epsilon^{-0.4} \tag{E.5}$$

$$D_{\max} = \left(\frac{\mathrm{We}^*_{\mathrm{crit}}}{2}\right)^{0.6} \left(\frac{\sigma^{0.6}}{(\rho_c^2 \rho_d)^{0.2}}\right)^{0.6} \epsilon^{-0.4} \tag{E.6}$$

Most recently, Andreussi et al. [Andreussi et al., 1999] studied the $\mathrm{We}_{\mathrm{crit}}$ as function of the void fraction. The following equation was proposed:

$$\mathrm{We}_{\mathrm{crit}} = 0.11(1 + 8.3\alpha^{-0.8}) \tag{E.7}$$

For this study, the void fraction was estimated based on the non-homogeneous Chisholm model and reported by Kojasoy et al. (1997), where the slip is considered and void fraction is

$$\alpha = \frac{1}{1 + \left(\frac{1-x}{x}\right)\frac{\rho_{\mathrm{G}}}{\rho_{\mathrm{L}}} S} \tag{E.8}$$

where

$$S = \left(1 + x\frac{\rho_{\mathrm{G}}}{\rho_{\mathrm{L}}} - 1\right)^{1/2} \qquad \text{for } X_{TT} > 1.0 \tag{E.9}$$

$$S = \frac{\rho_{\mathrm{G}}}{\rho_{\mathrm{G}}}^{1/4} \qquad \text{for } X_{TT} < 1.0 \tag{E.10}$$

and

$$X_{TT} = \left(\frac{1-x}{x}\right)^{0.9} \left(\frac{\rho_{\mathrm{G}}}{\rho_{\mathrm{L}}}\right)^{0.5} \left(\frac{\mu_{\mathbf{L}}}{\mu_{\mathrm{G}}}\right)^{0.1} \tag{E.11}$$

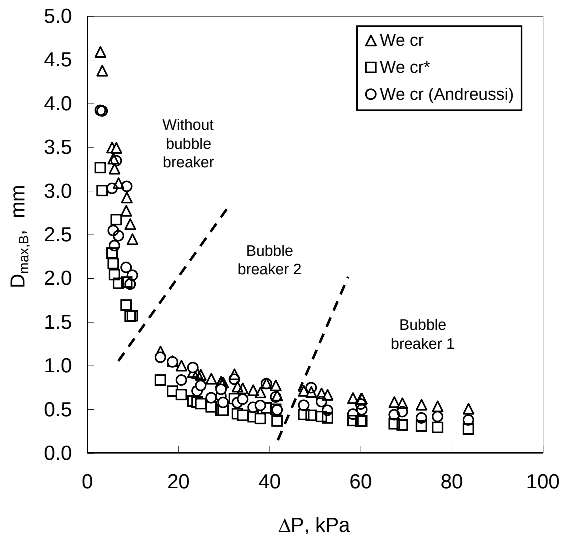

Figure E.2: Maximum bubble diameter for different models.

The different models to estimate $D_{\max}$ as a function of the pressure drop are shown in Figure E.2. It is observed that the bubble size is a function of the pressure drop. However, once the pressure drop reaches a value of 200 kPa the diameter of the bubble size does not change significantly. It is also notice that clearly the bubble breaker reduce the bubble size. Nevertheless, this reduction in $D_{\max}$ is at the cost of a higher pressure drop.

Appendix F

Pressure drop of the two-phase flow through the bubble breakers

The reduction of droplet size in a two-phase flow can be produced by a plate with perforated holes. This plate is called bubble breaker in this investigation. As any other accessory installed in a pipe such as orifice plates, venturi, valves, etc, these bubble breakers produce a pressure drop caused by the flow constriction. This appendix presents an analysis of the pressures across these devices.

The estimation of the pressure drop for the two-phase case is commonly analyzed estimating the two-phase pressure drop multiplier, ϕ^2, and then comparing the resulting values with the experimental results. This parameter refers to the pressure drop of the two phase flow as a function of the pressure drop that would occur if the liquid phase were flowing alone.

The pressure drop multiplier for two-phase flow, through a thin or thick plate, can be obtained from:

$$\phi^2 = \frac{\Delta P_{\mathrm{Two-Phase}}}{\Delta P_{\mathrm{Liquid}}} \tag{F.1}$$

The pressure change for liquid-phase flow can be expressed as follows:

$$\Delta P_{\mathrm{Liquid}} = K \rho_{\mathrm{L}} \frac{U_{\mathrm{L}}^2}{2} \tag{F.2}$$

Where ρ_L is the density of the liquid and U_L is the liquid velocity as a single-phase. The parameter K represents of the loss coefficient through the plate.

Combining both equations the parameter K resulted in:

$$K = \frac{\Delta P_{\mathrm{Two-Phase}}}{\phi^2 \rho_{\mathrm{L}} U_{\mathrm{L}}^2} \tag{F.3}$$

To estimate the value of the pressure drop multiplier, ϕ^2, the Lockart-Martinelli model suggests the equation

$$\phi^2 = 1 + \frac{C}{X} + \frac{1}{X^2} \tag{F.4}$$

where the factor X is given by:

$$X = \left(\frac{\Delta P_{\mathrm{SL}}}{\Delta P_{\mathrm{SG}}}\right)^{1/2} \tag{F.5}$$

here ΔP_{SL} is the single-phase liquid pressure loss and ΔP_{SG} is single-phase gas pressure loss, both in $\mathrm{N/m^2}$.

The factor C in Eq. (F.4) is a function of condition of the flow, laminar or turbulent, based on the superficial Reynolds numbers of each phase. The correspondent values of C are shown in Table **??**.

Table F.1: C values according to Locarkt-Martinelli Model.

Liquid	Gas	C value
Turbulent	Turbulent	20
Laminar	Turbulent	12
Turbulent	Laminar	10
Laminar	Laminar	5

To estimate the real velocity of each phase is needed to know the area occupied by each phase, or the local void fraction. See equation in Chapter 2.

Several models are used to predict void fraction, such as:

- Homogeneous Model, assumes both phases travel at the same velocity
- Non - homogeneous model
- Model considering the radial distribution of the local void fraction
- Empirical and semi-empirical model

In the homogeneous model the slip velocity is zero. Thus, both phases flow at the same velocity. This model has a reasonable accuracy for bubble and dispersed bubble flow, where the velocity of the entrained phase is nearly the velocity of the continuous phase. The liquid velocity and void fraction are obtained by Eq. (F.6) and Eq. (F.7), respectively.

$$U_{\mathrm{L}} = U_{\mathrm{m}} = U_{\mathrm{L}}^{\mathrm{S}} + U_{\mathrm{G}}^{\mathrm{S}} \tag{F.6}$$

$$\alpha_{\mathrm{HOM}} = \frac{\dfrac{x}{\alpha_{\mathrm{G}}}}{\dfrac{1-x}{\alpha_{\mathrm{L}}} + \dfrac{x}{\alpha_{\mathrm{G}}}} \tag{F.7}$$

For non-homogeneous, slip is considered and void fraction could be estimated according to Chisholm model reported by Kosasoy et al.(1997). For details refers to Appendix E, Eq. (E.8).

Figure F.1 shows the calculated values of the loss coefficient through the plate, K, considered the homogenous and non-homogenous models for two different the bubble breakers. The coefficient change with the water flow rate and the model used to estimate the liquid velocity. These values of K are over an arithmetic average for the gas flow rate. The changes of K as function of air to liquid ratio, γ, for 151 kg/min is shown in Figure **??**.

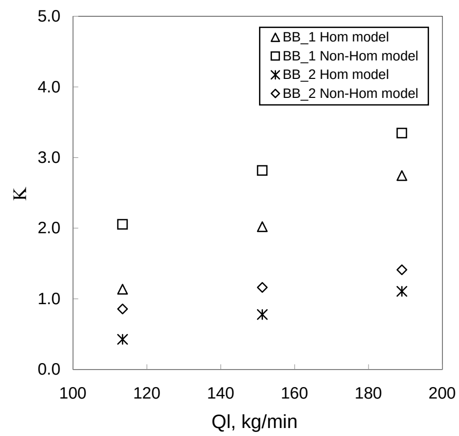

Figure F.1: Average loss coefficient through the plates calculated for homogeneous and non-homogeneous model.

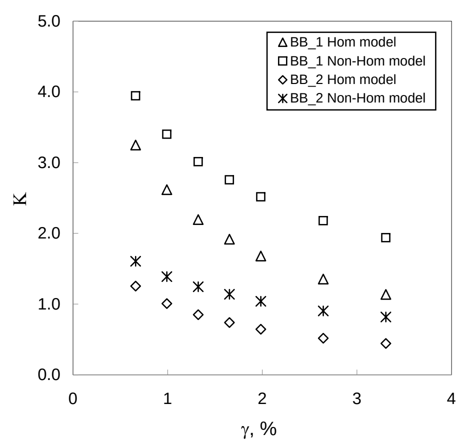

Figure F.2: Loss coefficient through the plates calculated for 151 kg/min, using to homogeneous and non-homogeneous model.

The empirical values of K for each bubble breaker are estimated to predict the pressure of the two-phase flow over them. Thus, the estimation of the Pressure Drop Multiplier, ϕ^2, calculated from Eq. (**??**) are shown in Figure **??**.

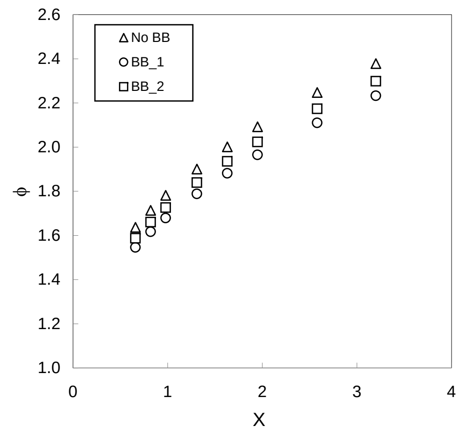

Figure F.3: Pressure Drop Multiplier as funcion of the quality of the flow for 151 kg/min.

Appendix G

Bubble images analysis

As indicated in the Section 3.2.1 bubbles were identified manually, indicating the largest and shortest diameter of each bubble, and then "sized" by the DaVis software.

In addition a routine was developed in MatLab, in the Images Processing module, to process each image, enhance the contrast of the intensity and transform it in a grey scale with the objective to intensity the bubbles boundaries. Later, the resulting images were processed in DaVis for the statistical results.

Comparisons indicate that the visual inspection does not generate a significant error, values differ in 4.46 % average for the compared conditions. Details are shown in Table G.1. However, a bigger difference may be induced by a manual detection of small bubbles.

Table G.1: Comparisons of the values of the Sauter mean diameter for bubbles from the manual sizing and Matlab routine.

Water flow (kg/min)	γ (%)	Manual sizing $D_{32,B}$ (μm)	MatLab Routine $D_{32,B}$ (μm)	Difference (%)
151.2	1.3	245.4	244.21	0.50
151.2	2.0	229.7	214.59	7.03
189.0	0.5	232.2	249.59	6.97
189.0	1.1	216.7	231.19	6.27
189.0	1.6	208.5	211.75	1.52

Appendix H

Reproducibility

To evaluate the reproducibility of the experimental data acquired, experiments for the same working conditions were performed on three different dates. All variables were measured for each test. Knowing that the injection pressure is the most important parameter in the determination of the droplet size in effervescent atomization, reproducibility was studied based on its variation, for the same configuration and same liquid and air flow rates. Given a configuration, if two or more runs have the same values for all three parameters, injection pressure injection, water flow rate and air flow, same characteristic sprays are produced.

Figure H.1 presents the injection pressure, P_i, for tests performed at different days for two configurations. It is observed, for all cases, that P_i has the same trends and the values measured are quite similar. Some discrepancies are found but in average the pressure varies by 0.85 % for two different runs without bubble breaker and in 3.00 % for bubble breaker 1, BB_1. To guarantee the reproducibility of the experiments, the same procedure was followed for each run allowing enough time to the control systems to reach the corresponding values of flow rates. Maximum differences were found at lower liquid flow rates.

Reproducibility of the P_i was evaluated with a t-Student test with a significance level of 95 %, for both configurations. A test of the variance of two sample provided information of the type of t-Test required, the t-Test for two-samples with equal variance or two-samples with unequal variance.

For both configurations, without and with bubble breaker, variances indicate that groups were not significatively difference, values are shown in Table H.1. Thus, a two-sample with equal variance test was performed.

Table H.1 provides the results for the t-test for two samples of each configuration. For no bubble breaker, since t statistic $<$ t-critical (-0.0572 $<$ 1.67) and p-value $> \alpha$ (0.9546 $>$ 0.05), null hypothesis is accepted and the mean of the sample are the same with 95 % confidence level. The same conclusion is drawn for the configuration with bubble breaker.

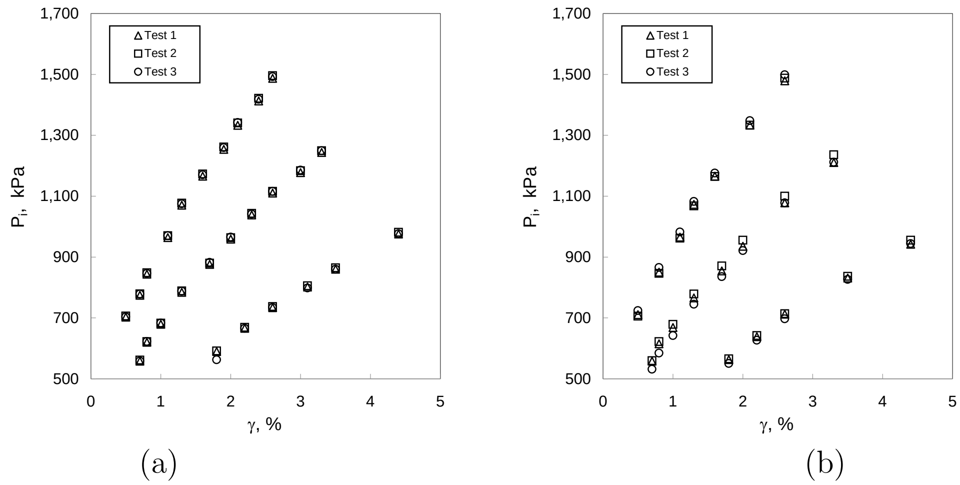

Figure H.1: Injection pressure for different test performed (a) without bubble breaker and (b) with bubble breaker 1, BB_1.

Table H.1: Variance analysis of two test for same configuration performed on different days.

	No BB Test1-Test2	BB_1 Test1-Test2
F-value	0.9824	0.99
p-value	0.48	0.49

Table H.2: t-Test for two different samples performed on different days.

	No BB Test1-Test2	BB_1 Test1-Test2
Observations	28	22
Pooled variance	84992	80604
Hypothesized mean difference	0	0
df	54	42
t-Stat	-0.0572	-0.0818
$P(T \leq t)$ one-tail	0.4773	0.4676
t critical one-tail	1.6736	1.6820
$P(T \leq t)$ two-tail	0.9546	0.9351
t critical two-tail	2.0049	2.0180

Appendix I

Regression analysis

In this appendix the detailed results of the Regression Analysis is provided. The analysis was done using Polymath software. The dependent variable was defined as the droplet size($D_{32,D}$) and as the independent variables the the bubble size ($D_{32,B}$), water flow rate (Q_L), air to liquid ratio (γ) and inlet pressure (P_i).

POLYMATH Report
Nonlinear Regression (L-M)

Model: D32D = A + B*(D32,B)^C + D*QL + F*γ^G + J*(Pi)^K

Variable	Initial guess	Value	95% confiden
A	-200.0	-893.79	1.2909
B	4.5	5.2169	0.0475
C	0.5	0.6168	0.0017
D	1.0	1.2134	0.0084
F	200.0	609.10	1.4141
G	-0.5	-0.2452	0.0037
J	50.0	5050.99	15.6644
K	-0.5	-0.3757	0.0005

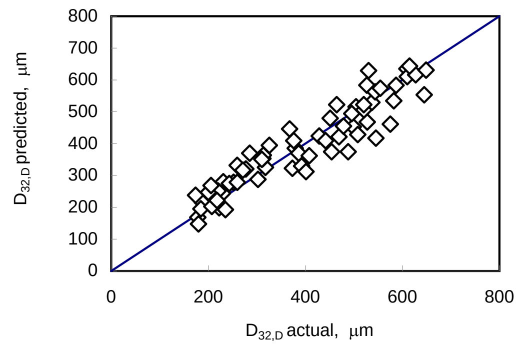

Nonlinear regression settings
Max # iterations = 64

Precision

R^2	0.879027
R^2adj	0.864427
Rmsd	6.202967
Variance	2889.74

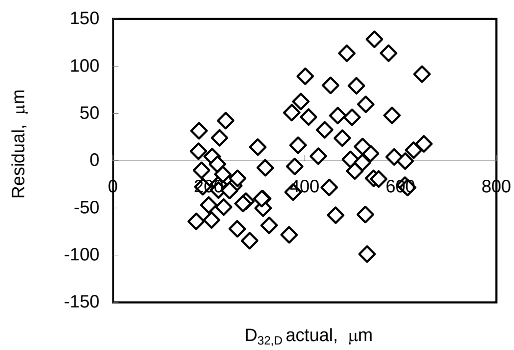

General

Sample size	66
Model vars	8
Indep vars	4
Iterations	47

Source data points and calculated data points

	D32, B	QL	γ	Pi	D32,D	D32D calc	Delta D32D
1	220.79	113.42	0.90	386.08	644.87	553.33	91.54
2	211.12	113.42	1.30	480.79	498.79	452.82	45.97
3	202.60	113.42	1.80	571.31	454.05	374.32	79.73
4	187.38	113.42	2.20	650.57	277.49	320.34	-42.85
5	177.38	113.42	2.60	716.02	231.02	280.14	-49.12
6	166.78	113.42	3.50	847.31	187.81	215.33	-27.52
7	156.78	113.42	4.40	956.02	178.55	168.52	10.03
8	251.04	113.42	0.90	354.54	586.84	582.86	3.98
9	213.58	113.42	1.30	446.34	527.59	467.90	59.69
10	196.09	113.42	1.80	529.05	379.17	385.19	-6.02
11	169.55	113.42	2.20	602.66	317.86	325.38	-7.52
12	150.56	113.42	2.60	670.13	252.07	278.67	-26.60
13	111.94	113.42	3.50	794.89	222.53	198.37	24.16
14	101.00	113.42	4.40	907.86	179.75	148.02	31.73
15	419.85	113.42	0.90	366.02	609.18	635.09	-25.91
16	354.53	113.42	1.30	457.72	504.60	515.45	-10.85
17	341.92	113.42	1.80	589.70	469.23	421.43	47.80
18	325.87	113.42	2.20	665.84	285.41	370.04	-84.63

19	318.65	113.42	2.60	733.71	259.53	331.62	-72.09
20	244.35	113.42	3.50	860.19	220.78	245.60	-24.82
21	225.00	113.42	4.40	975.81	184.84	195.01	-10.17
22	258.34	151.23	0.70	559.69	526.67	583.58	-56.91
23	222.13	151.23	0.80	622.15	537.30	529.63	7.67
24	218.76	151.23	1.00	678.51	451.24	479.56	-28.32
25	195.12	151.23	1.30	781.22	375.96	409.25	-33.29
26	188.34	151.23	1.70	874.07	312.55	352.89	-40.34
27	183.29	151.23	2.00	956.04	271.28	316.67	-45.39
28	137.49	151.23	2.60	1101.80	229.29	243.65	-14.36
29	120.81	151.23	3.30	1233.80	235.27	192.82	42.45
30	286.16	151.23	0.70	510.96	609.92	610.35	-0.43
31	261.25	151.23	0.80	562.18	543.79	562.50	-18.71
32	216.11	151.23	1.00	617.26	495.65	494.25	1.40
33	197.36	151.23	1.30	716.44	428.63	423.87	4.76
34	183.10	151.23	1.70	803.28	313.27	363.39	-50.12
35	170.93	151.23	2.00	885.72	373.22	322.36	50.86
36	135.84	151.23	2.60	1036.40	220.14	251.29	-31.15
37	125.64	151.23	3.30	1165.02	207.23	202.86	4.37
38	346.91	151.23	0.70	557.90	627.38	616.14	11.24
39	339.43	151.23	0.80	620.04	554.57	573.90	-19.33
40	287.14	151.23	1.00	679.49	520.73	505.77	14.96
41	244.21	151.23	1.30	784.39	507.92	428.66	79.27
42	229.50	151.23	1.70	875.98	386.13	369.68	16.45
43	214.59	151.23	2.00	958.68	392.18	329.53	62.65
44	209.25	151.23	2.60	1110.17	243.26	274.77	-31.51
45	184.35	151.23	3.30	1243.49	218.05	221.70	-3.65
46	218.80	189.04	0.50	710.15	648.69	630.92	17.77
47	215.60	189.04	0.80	852.99	464.74	522.49	-57.75
48	194.57	189.04	1.10	972.15	367.66	446.17	-78.51
49	165.45	189.04	1.30	1082.47	325.91	394.39	-68.48
50	155.39	189.04	1.60	1172.10	310.50	350.64	-40.14
51	115.00	189.04	2.10	1337.57	259.90	278.56	-18.66
52	112.34	189.04	2.60	1489.26	173.66	237.89	-64.23
53	207.12	189.04	0.50	696.36	530.38	629.27	-98.89
54	206.59	189.04	0.80	832.65	520.49	522.40	-1.91
55	204.90	189.04	1.10	944.57	478.50	454.68	23.82
56	186.34	189.04	1.30	1041.10	441.75	409.06	32.69
57	169.37	189.04	1.60	1130.73	408.07	361.86	46.21
58	125.15	189.04	2.10	1296.20	302.27	287.79	14.48
59	122.05	189.04	2.60	1440.99	200.05	246.97	-46.92
60	249.59	189.04	0.50	710.15	614.77	643.17	-28.40
61	246.07	189.04	0.80	854.94	582.29	534.33	47.96
62	231.19	189.04	1.10	972.15	575.14	461.29	113.85
63	218.00	189.04	1.30	1082.47	545.45	416.99	128.46
64	211.75	189.04	1.60	1178.99	488.13	374.52	113.61
65	188.66	189.04	2.10	1351.36	401.38	312.04	89.34
66	178.25	189.04	2.60	1503.04	205.65	268.39	-62.74